



UNIVERSITÀ DEGLI STUDI DI SALERNO



UNIVERSITÀ DEGLI STUDI DI SALERNO
Dipartimento di Farmacia

PhD Program
in **Drug Discovery and Development**
XXXI Cycle — Academic Year 2018/2019

PhD Thesis in

***Target-based study to identify new
bioactive diterpenes***

Candidate

Lorenzo Fiengo

Supervisors

Prof. *Nunziatina De Tommasi*

Prof. *Fabrizio Dal Piaz*

PhD Program Coordinator: Prof. Dr. *Gianluca Sbardella*

“Della vita non bisogna temere nulla. Bisogna solo capire”
(Marie Curie)

Ai miei genitori...

Index

Abstract.....	I
- Chapter 1 -	1
Introduction	3
1.1 Plant small molecules in drug discovery and development	3
1.2 Terpenes	7
1.3 Diterpenes in cancer	9
1.4 Drug discovery today: Chemical Genetics.....	12
1.5 Aim of the thesis	14
1.6 Cell-free and cell-based assays	14
1.7 Outline of the thesis	23
- Chapter 2 -	25
Introduction	27
2.1 Nucleolin: structure and localizations	27
2.1.1 Roles of Nucleolin in physiological and pathological pathways	34
2.1.2 Roles of Nucleolin in ribosome biogenesis.....	35
2.1.3 Nucleolin as shuttle between nucleus and cytoplasm	38
2.1.4 Nucleolin as receptor on the cell surface	39
2.1.5 Nucleolin as tumor marker: therapeutic strategies.....	39
2.1.6 Nucleolin Inhibitors	43
2.1.7 Aim of the project	46
Results and discussion.....	47
2.2 Screening of diterpenes by <i>Cellular Thermal Shift Assay</i> (CETSA)	47
2.2.1 Biological activity of 6,19-dihydroxy- <i>ent</i> -trachiloban-17-oic acid (12) in Jurkat and HeLa cells	52
2.2.2 Nucleolin- 12 interaction achieved by CETSA in HeLa cells	54

2.2.3 Study of Nucleolin/ 12 interaction by <i>Drug Affinity Responsive Target Stability</i> (DARTS) in HeLa cells	57
2.2.4 MS-based identification of further targets of 6,19-dihydroxy- <i>ent</i> -trachiloban-17-oic acid	60
2.2.5 Investigation of 6,19-dihydroxy- <i>ent</i> -trachiloban-17-oic acid activity in the cell migration: Wound Healing Assay	61
2.2.6 Biological effect of 6,19-dihydroxy- <i>ent</i> -trachiloban-17-oic acid on Nucleolin into the cell.....	62
2.2.7 6,19-dihydroxy- <i>ent</i> -trachiloban-17-oic acid activity in subcellular compartments.....	63
2.2.8 RTq-PCR and Western Blot analyses	65
2.2.9 Inhibition of Protein Synthesis	66
2.2.10 Nucleolin (RBD1-2) expression and purification.....	67
2.2.11 Screening of diterpenes against Nucleolin (RBD 1-2) by <i>Saturation Transfer Difference</i> NMR (STD-NMR).....	70
2.2.12 Screening of diterpenes against Nucleolin (RBD 1-2) by WaterLOGSY	74
2.2.13 Diterpenes/Nucleolin (RBD 1-2) interaction by SPR.....	77
2.2.14 Conclusions.....	78
Materials and methods	79
2.3 Determination of the apparent melting curve (T_m) of Nucleolin in HeLa cells by <i>Cellular Thermal Shift Assay</i> (CETSA).	79
2.3.1 Determination of the EC_{50} of the complex (ITDRF _{CETSA}).....	80
2.3.2 <i>Drug Affinity Responsive Target Stability</i> (DARTS) experiment	80
2.3.3 Wound Healing assay	82
2.3.4 RNA isolation and quantitative Real-Time-PCR (qRT-PCR).....	82
2.3.5 Protein Synthesis assay	83
2.3.6 Cell viability and cell cycle analysis.....	83
2.3.7 Determination of apoptosis	84

2.3.8 Expression and purification of recombinant NCL (RBD1-2)	84
2.3.9 Ligand-binding NMR experiments	85
2.3.10 Saturation Transfer Difference NMR (STD-NMR) analysis	85
2.3.11 WaterLOGSY experiment.....	86
2.3.12 Surface Plasmon Resonance (SPR).....	87
2.3.13 Western Blot analysis.....	87
2.3.14 Reagents and Antibodies	88
2.3.15 Cytosol and membrane extracts	88
2.3.16 Nuclear extracts.....	89
2.3.17 Statistical analysis	89
- Chapter 3 -	91
Introduction	93
3.1 Heat Shock Proteins (HSPs) family	93
3.1.1 Heat Shock Protein 70 (Hsp70): structure, localizations and roles.....	94
3.1.2 Hsp70 inhibitors	103
3.1.4 Aim of the project	104
Results and discussion.....	106
3.2 Identification of Hsp70 ligands by Surface Plasmon Resonance (SPR).....	106
3.2.1 Epoxysiderol	111
3.2.2 MS-based studies on the epoxysiderol-Hsp70 interaction	112
3.2.3 Cytotoxic activity of epoxysiderol	114
3.2.4 Validation study of epoxysiderol/Hsp70 interaction by DARTS	114
3.2.5 Western Blot of Hsp70, Hsp70 co-chaperones and client proteins.....	117
3.2.6 Evaluation of epoxysiderol biological activity in HeLa cells by flow cytometry and WB	119
3.2.7 Epoxysiderol effect on Hsp70 levels in subcellular compartments	122
3.2.8 Inhibition of Hsp70 ATPase activity mediated by epoxysiderol	123
3.2.9 Molecular docking experiment	125

3.2.10 Conclusions.....	126
Materials and Methods.....	128
3.3 Surface Plasmon Resonance (SPR)	128
3.3.1 Drug Affinity Responsive Target Stability on HeLa cells.....	128
3.3.2 Monodimensional electrophoresis SDS Page	129
3.3.3 LC/MS/MS Analysis	130
3.3.4 HSP70 peptide mapping	130
3.3.5 Cell culture and treatment.....	131
3.3.6 Cell viability and cell cycle analyses	131
3.3.7 Determination of apoptosis	132
3.3.8 Western Blot analysis	132
3.3.9 Cytosol and membrane extracts	133
3.3.10 Nuclear extracts	133
3.3.11 ATPase activity Assay	134
3.3.12 Reagents and Antibodies	134
3.3.13 Molecular Docking Studies	135
3.3.14 Statistical analysis.....	136
- Chapter 4 -	137
Introduction.....	139
4.1 Heat Shock Protein 90: isoforms and localizations	139
4.1.1 Hsp90 structure	140
4.1.2 Hsp90 ATPase activity and ATP binding Site.....	142
4.1.3 Hsp90 client proteins	146
4.1.4 Functions of Hsp90 in cancer	147
4.1.6 Hsp90 inhibitors: therapeutic targeting of Hsp90 ATPase activity	148
Results and discussion	150
4.2 Screening of fusicoccane and abietane diterpenes by SPR.....	150

4.2.1 Antiproliferative activity of fusicocanes and abietanes tested by MTT on Jurkat, HeLa and MCF7 cell lines.....	152
4.2.2 Evaluation of the biological activity of the selected diterpenes by flow cytometry and WB	154
4.2.3 Effect of 6 and 20 on Hsp90 α ATPase activity.....	157
4.2.4 Study of the interaction Hsp90 α / 6 by molecular docking.....	158
4.2.5 Conclusions	159
Materials and methods	161
4.3 Reagents and Antibodies.....	161
4.3.1 Surface Plasmon Resonance Analyses.....	161
4.3.2 ATP hydrolysis inhibition	162
4.3.3 Cell Culture and Treatment	163
4.3.5 Western Blot Analyses	164
4.3.6 Statistical Analysis	164
4.3.7 Molecular Docking Studies.....	164
4.3.8 Induced Fit Docking.....	165
Bibliography.....	166
Publications	187
Poster and oral presentations at international meetings	188

Abstract

Target identification and mechanism of action studies of plant-derived compounds play a critical role in drug discovery. The knowledge of the bioactivity of natural compounds can lead to a number of advantages: first of all, it is possible to understand their full therapeutic potential; in addition, it can allow the further identification of their side-effects, their toxicity and also structure-activity relationships studies.

This research project is focused on a *Reverse Chemical Genetics* approach, which relies on the screening of libraries of plant small molecules (provided by the Department of Pharmacy (DIFARMA)-Bioactive Natural Products, University of Salerno (UNISA), Fisciano, Italy) able to bind specific target proteins and on the validation of the ligand/protein interaction. In my PhD project I focused on three protein targets, over-expressed in cancer and identified as potential markers in several tumor cell lines: Nucleolin, Heat Shock Protein 70 (Hsp70) and Heat Shock Protein 90 (Hsp90).

Nucleolin (NCL) is a multifunctional protein involved in many process such as DNA transcription, ribosome biogenesis and regulation of mRNAs of anti-apoptotic and antiproliferative proteins such as AKT1, Bcl2, p53. Firstly, a screening of *ent*-kaurane and *ent*-trachilobane library by *Cellular Thermal Shift Assay* (CETSA) on Jurkat (leukemia T cells) and HeLa (cervical carcinoma) was performed, obtaining as main ligand of Nucleolin the 6,19-dihydroxy-*ent*-trachiloban-17-oic acid (**12**) from *Psiadia punctulata* ((Vatke) Asteraceae). Full length Nucleolin/**12** interaction was validated in HeLa (cervical carcinoma) cells by CETSA and *Drug Affinity Responsive Target Stability* (DARTS). Nucleolin RNA Binding Domains 1-2/**12** interaction was investigated by *Saturation Transfer Difference* NMR (STD-NMR), WaterLOGSY and *Surface Plasmon Resonance* (SPR): no interaction was

observed with these two domains of the protein. The mechanism of action of the selected diterpene was studied by Flow Cytometry (sub G₀/G₁ cell cycle arrest), WB analysis (reduction of intracellular AKT1 and Bcl2 levels and pNCL levels on the cell membrane), RTq-PCR (reduction of AKT1 and Bcl2 mRNAs), MTT (IC₅₀: 20 ± 1 μM), Protein Synthesis and Wound Healing assays in HeLa cells (reduction of 20% of migration). Therefore, the 6,19-dihydroxy-*ent*-trachiloban-17-oic acid (**12**) may be considered as a new promising modulator of Nucleolin.

The second target protein was the molecular chaperon Heat Shock Protein 70 (Hsp70). A diterpene library was screened by SPR assay, in order to select putative Hsp70 ligands. SPR results showed that the *ent*-7β-acetoxy,18-hydroxy-15α,16α-epoxikaurane (epoxysiderol or compound **27**) from *Sideritis* spp (Lamiaceae) interacts with Hsp70 (K_D: 54 ± 1.2 nM). Epoxysiderol ability to modulate Hsp70 activity was assessed through MS (no covalent binding), DARTS and WB experiments. Moreover, epoxysiderol was tested on HeLa cells by MTT (IC₅₀: 20 ± 0.9 μM), Flow Cytometry (G₂/M and subG₀/G₁ cell cycle arrest), WB for its effect on the intracellular levels of Hsp70, Hsp90, and Hsp70 client proteins (reduction of pAKT1, p-p38 and p-JNK1) in HeLa cells, and by WB also for Hsp70 cytosolic and cell membrane levels (reduction of Hsp70 levels). Finally, ATPase assay (50% of reduction in dose-dependent manner) and molecular docking studies (interaction with the Hsp70 Nucleolide Binding Domain) were carried out. Therefore, in this study epoxysiderol was identified as a new Hsp70 inhibitor through cell-free and cell-based assays.

Another target object of study in this PhD project was the Heat Shock Protein 90 (Hsp90). Fusicoccane diterpenes from *Hypoestes forsskaolii* ((Vahl) Acanthaceae), abietane diterpenes from *Zhumeria majdae* ((Rech.f. & Wendelbo) Lamiaceae) and from different *Salvia* spp (Lamiaceae) were

screened against Hsp90 by SPR and by MTT in HeLa, Jurkat and MCF7 cells, selecting the 18-hydroxyhypoestenone (**6**) and lanugon Q (**20**) as Hsp90 ligands. Subsequently, MTT assay was performed to investigate their cytotoxic and anti-proliferative activity: 18-hydroxyhypoestenone was the most cytotoxic in HeLa cells (IC_{50} : $18 \pm 1 \mu M$), whereas lanugon Q showed higher activity towards MCF7 (IC_{50} : $20 \pm 2 \mu M$). In addition, Flow Cytometry and WB analyses were carried out: G_2/M cell cycle arrest and reduction of p-Cdc2, pAKT1 and pERK1 levels were observed in HeLa cells after treatment with **6** ($10 \mu M$ and $20 \mu M$ for 48h); Decrease of pERK, pAKT, cyclin A was observed in MCF7 after 48h of treatment with **20** ($18 \mu M$). Selected diterpenes were also tested against Hsp90 by ATPase activity assay: dose-dependent reduction (40%) of hydrolysis was observed with compound **6** ($1,5, 10 \mu M$), while no inhibition was induced by **20**. Furthermore, molecular docking studies were implemented with compound **6**, and the computational analysis of the Hsp90/**6** interaction suggested a C-terminal domain. In conclusion, in this study 18-hydroxyhypoestenone and lanugon Q were identified as new Hsp90 interactors, able to modulate its activity and its client proteins levels.

- Chapter 1 -

Introduction

1.1 Plant small molecules in drug discovery and development

Natural compounds play a crucial role in drug discovery and drug development. This is particularly evident in the areas of cancer and infection diseases, whereas over 60% and 75% of therapeutic agents have to be considered of natural origin. This contribution seems impressive, but it can be easily explained in the light of the chemical and evolutionistic proprieties shown by natural products. First of all, they exhibit a wide range of pharmacophores and a high degree of stereochemistry. Therefore, they have been - and they are still - an invaluable source of inspiration for organic chemist to synthesize novel drug candidates,¹ since they provide a new starting point for new synthetic compounds with diverse structures and often with multiple stereocenters that can be challenging synthetically. Indeed, many structural features common to natural products (e.g., chiral center, aromatic rings, complex ring system, degree of molecule saturation and number and ratio of heteroatoms) are expected to contribute to the ability of natural products to provide hits even against the more difficult screening targets, such as protein-protein interactions.² Moreover, they may have the additional advantage of being natural molecules: compounds that are efficient as drugs have been suggested to have the propriety of 'metabolite-likeness'.³ Therefore, natural compounds are a good starting point for the setting up of libraries to test for drug discovery, not only for their complex and diversified chemical space but also for their ability to interact with biomolecules.

Although natural products have not been developed to bind to human proteins, they can do it. There are two main theories to explain this phenomenon: the first, widely accepted, is based on their ability to bind human proteins as a

result of a long-term co-evolution within biological communities; interacting organisms, that evolved in close proximity to one another, developed compounds that could influence the biological process of neighboring species.⁴ The second theory, advanced by Howitz and Sinclair and called xenohormesis, (Fig. 1) is based on the hypothesis that there have been common ancestors of plants and animals able to synthesize a large number of stress- induced secondary metabolites; animals and fungi, that feed on plants, gradually lost the capacity to synthesize these low-weight molecular compounds while plants retained this ability. Animals and fungi only retained the ability to sense these chemical cues in plants, possibly in order to detect when plants were stressed and gain an early warning of changing environmental condition.⁵

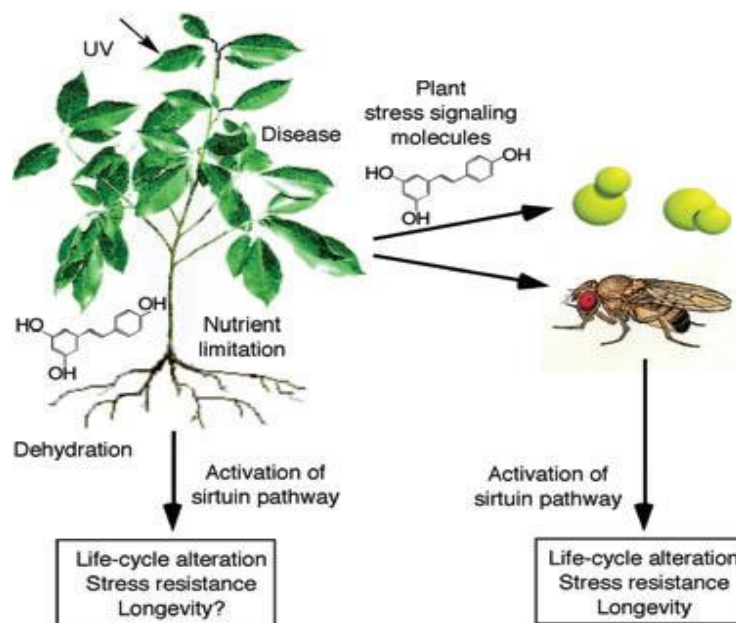


Figure 1. Xenohormesis hypothesis. Sirtuin enzymes evolved early in life’s history to increase somatic maintenance and survival during times of adversity. The xenohormesis hypothesis of Howitz and Sinclair proposes that primordial species synthesized polyphenolic molecules to stimulate sirtuins during times of stress. Only plants have retained this ability. Survival pathways in fungi and animals, instead, have retained the ability to respond to plant stress signalling molecules because they provide useful prediction about the state of the environment and/or food supply. This ability would allow organisms to prepare for and survive adversity when they might otherwise perish. Adopted from Lamming DW *et al.* 2004; *Molecular Microbiology*.

In fact, natural products are evolutionary preselected, owing structural requirements to be bound to proteins. Their structural scaffolds represent the biologically relevant fractions of chemical space explored by nature so far.⁶ Moreover, recently Stuart Schreiber, Paul Clemons and their colleagues at the Broad Institute in Boston, performed a bioinformatic analysis of natural product targets, thus demonstrating that natural molecules statically tend to target proteins with a high number of protein–protein interactions that are particularly essential for an organism.⁷ This observation is consistent with the common role played by natural products as chemical weapons against predators or competitors.

The long-lasting experience of traditional folk medicines may facilitate the identification of novel agents. Although in industrialized countries medicinal herbs gradually lost importance, replaced by the chemical progress during the 20th century, bioactive plant compounds are recently experiencing an impressive revival.

The plant world possesses an uncountable number of specialized metabolites, characterized by different chemical scaffolds and a wide range of biological properties such as protective agents against herbivores and various pathogens or growth regulators. The rationale in exploring plant-derived products relies on the assumption that their chemical scaffolds have been under a continuous co-evolutionary selection process to achieve interactions with biological macromolecules. Therefore, it is reasonable to assume that they might have more suitable structures to interact with cellular targets compared with chemicals.⁸ The use of plant small molecules to fight human diseases is a centuries old practice that has led to the discovery of more than half of the all “modern” pharmaceuticals, becoming an essential source of leads for drug discovery.⁹

Nowadays, researchers still focus on the identification and structural characterization of new plant compounds and on the discovery of their detailed mechanism of action. To have an idea of the significance of the ethnobotanic use of plant drugs, it is sufficient just to consider the wide consumption of medicinal plants in the traditional Chinese medicine to cure and prevent diseases.¹⁰

Despite the success of plant molecules as drugs and the large number of benefits they show, they are losing favor among drug developers. One reason is the perceived “dirtiness” of plant molecules: a molecule is considered “dirty” if it interacts with numerous endogenous proteins. Such compounds presumably are more likely to have negative “off target” effects than a molecule that specifically targets a single protein. Indeed, there are examples of plant molecules that, despite interacting with multiple human enzymes and receptors, are surprisingly safe:¹¹ for example, salicylic acid, capsaicin or curcumin are surprisingly powerful and nontoxic, although they are multi-target molecules. In fact, having multi-target molecules could be a winning strategy to face different diseases. It has been increasingly recognized that, in several pathologies, there is a large number of mutated genes and/or modified proteins that disrupt multiple pathways, which normally exhibit extensive biological cross-talk and redundancy. Therefore, the development of drugs that bind selectively to single protein targets also appears less clinically useful, since, interfering with a single target and/or pathway may not abrogate the disease. Moreover, a promising strategy for mitigating an acquired drug resistance or suppress disease, is to simultaneously inhibit multiple molecular pathways, either by using several agents in combination or by using a single agent that concurrently blocks multiple targets or pathways.

Even if natural products enjoy a privileged position in drug discovery, they can exhibit multiple behaviors that could interfere in assay redouts, such as

metal chelation, redox cycling and protein reactivity. For these reasons several natural molecules were termed Pan Assay INterference compoundS (PAINS).

¹² These compounds possess reactive moieties, such as:

- catechols (e.g. apomorphine, droxidopa): catechols have a high propensity to be redox active and can also variously chelate metals as well as being reactive in the oxidized form to nucleophiles present in the side chain of proteins such as cysteine and lysine.
- quinones (e.g. geldanamycin), because of the redox-active and reactive quinone moiety.
- phenolic Mannich bases and hydroxyphenylhydrazones (e.g. topotecan, rifampicin).

1.2 Terpenes

Among the plant specialized metabolites, terpenes are an important class which constitute a vast family of natural substances structurally different from each other, whose starting elements for the biosynthesis are the isoprene units. They are produced by diverse organisms to perform an assortment of biological functions in varying ecological contexts and they are derived biosynthetically from units of isoprene (2-methyl-1,3-butadiene). Isoprene itself does not undergo the building process, whereas the activated forms, isopentenyl pyrophosphate (IPP or also isopentenyl diphosphate) and dimethylallyl pyrophosphate (DMAPP or also dimethylallyl diphosphate), are the actual components in the biosynthetic pathway (Fig. 2). There are two metabolic pathways that create terpenes: mevalonic acid pathway (MVA) and the 2-C-methyl-D-erythritol 4-phosphate/1-deoxy-D-xylulose 5-phosphate pathway (MEP/DOXP pathway), also known as non-mevalonate pathway. In both MVA and MEP pathways, IPP is isomerized to DMAPP by the enzyme isopentenyl pyrophosphate isomerase. IPP and DMAPP condense to give

geranyl pyrophosphate, the precursor to monoterpenes and monoterpenoids. Geranyl pyrophosphate is also converted to farnesyl pyrophosphate and geranylgeranyl pyrophosphate, respectively C15 and C20 precursors to sesquiterpenes and diterpenes (as well as sesquiterpenoids and diterpenoids).¹³ Their biosynthesis is mediated by the terpene synthase.¹⁴

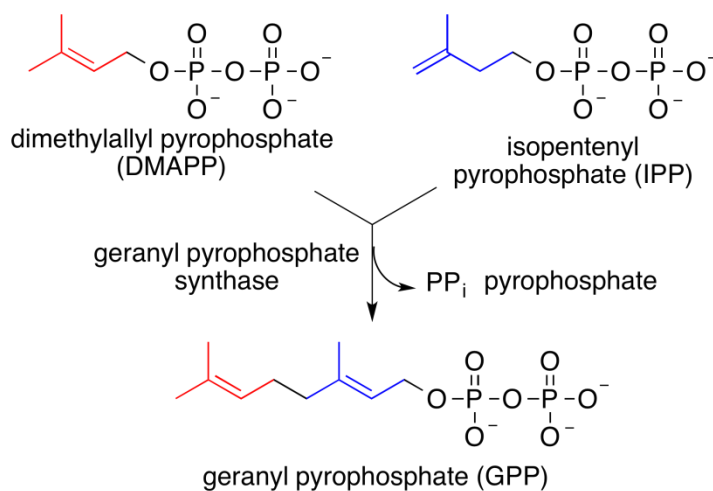


Figure 2. Isopentenyl pyrophosphate (IPP) and dimethylallyl pyrophosphate (DMAPP) condense to produce geranyl pyrophosphate, precursor to all terpenes and terpenoids.

Although all terpenes are synthesized from two five-carbon building blocks, the structures and functions vary widely. Many terpenes have shown several biological activities. Isoprenoids and derivatives play a critical role in all living systems: the cell structure, systems of electron transport in cell-cell signals (steroids, abscisic acid, gibberellic acid, phytol ecc.), in the structure of organisms and interactions between them. Some isoprenoids play a role in plant defense systems against attack by micro-organisms and insects, act as allelopathic compounds in plant-insect and plant-environment.¹⁵ They are also used for the treatment of human diseases. In fact, there is a wide spectrum of bioactivities for these types of substances such as antibacterial, antifungal, antiparasitic, anti-inflammatory, cytotoxic and antitumor.¹⁶ Although they show all of these activities, approximately 35,000 terpenes have been

identified and the majority of the possible functions or biological activity of these molecules are unknown. Then, it would be interesting to study this class of natural molecules to find out its potential biological effects and uses in therapy.

1.3 Diterpenes in cancer

Among plant terpenes, diterpenes form a vast class of more than 10000 structures (Fig.3). A number of potential anticancer diterpenes and their derivatives have been introduced already, such as taxanes (e.g. taxol and paclitaxel),^{17,18} kauranes (e.g. oridonin),¹⁹ andrographolide,²⁰ diterpenes from coffee (e.g. cafestol, cafeic acid and kahweol)²¹ and so on.

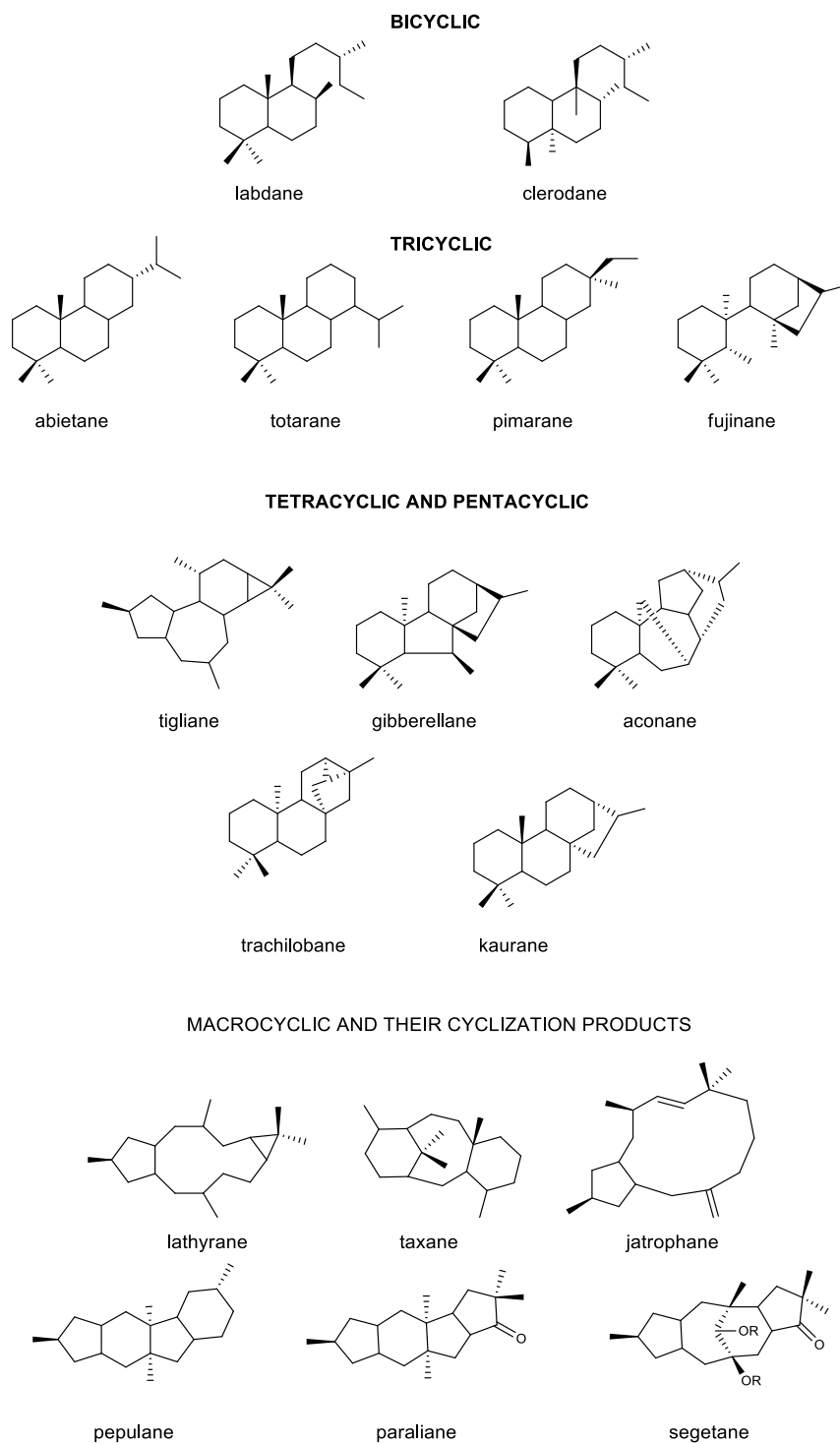


Figure 3. Structures of diterpene skeletons.

As we all know, cancers are considered one of the most lethal causes of death throughout the world.²² The use of medicinal preparations with plant-derived products is antique and, more recently, they have continued to enter in clinical trials or to provide leads for compounds in clinical trials, particularly as anticancer agents.²³

In Figure 4 most of the known diterpenes involved in anti-cancer pathways such as oxidative stress, ER stress, proliferation/differentiation, autophagy, cell cycle arrest and apoptosis, are reported.

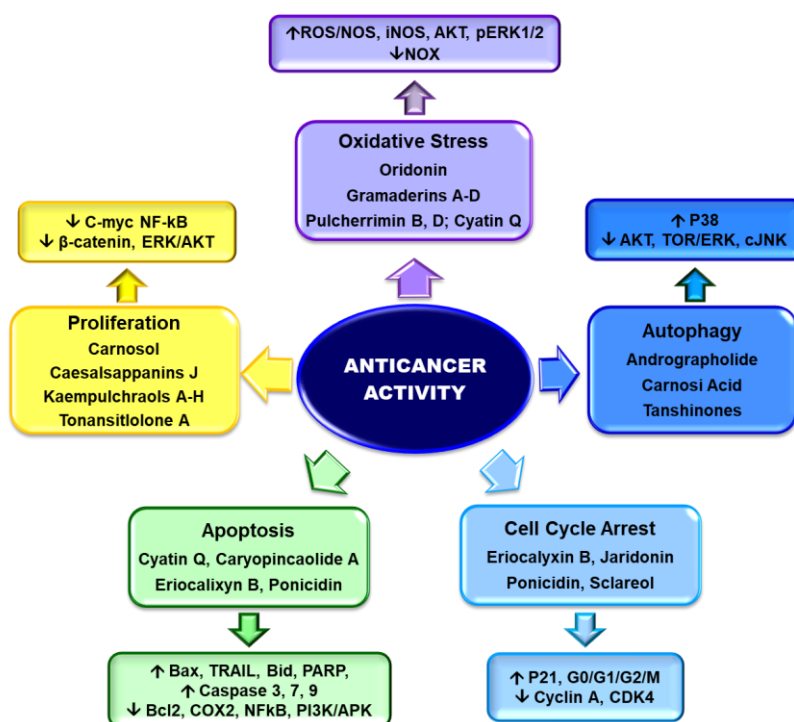


Figure 4. Anticancer pathways of diterpenes.

Several diterpenes are reported to act in a number of cancer cells such as T leukemia (Jurkat), cervical carcinoma (HeLa), breast cancer (MCF7), human embryonic kidney (HEK293) cell lines, while either alone or combined to other diterpenes or anticancer drug, have been found to work synergistically.

Altogether, we can conclude that diterpenes may be one of the leading therapeutic molecules in cancer.²⁴

1.4 Drug discovery today: Chemical Genetics

Chemical genetics is an emerging field that can be used to study the interactions of chemical compounds, including natural products, with proteins. Chemical genetics uses chemical compounds, including plant molecules, that may modulate the activity of target proteins.^{24, 25} This field comes from the classical genetics, widely used to study biology by manipulating the biological system at the level of the gene.

Chemical Genetics offers several advantages over its classical counterpart and allows the study of unexplored biological space. For example, genes essential for survival or development cannot be studied using classical genetics; this can only be done using chemical genetics. Thus, the instantaneous effects of small molecules can be characterized using chemical genetics. It also makes it possible to study mammals whereas classical genetic techniques are more complicated to apply due to their diploid genome, physical size and slow reproduction rate.²⁶ Other benefits of using chemical compounds are the temporal control and reversibility of the inhibition of protein function.²⁷

Classical genetics is divided into *forward genetics* (involving random mutations followed by phenotypic screening and gene identification) and *reverse genetics* (involving mutation of a specific gene and phenotype characterization). So, genetics in the 'forward' direction is from phenotype to gene; in the 'reverse' direction it is from gene to phenotype. As classical genetics, two approaches can be taken also to chemical genetics (Fig. 5): *Forward Chemical Genetics* (FCG) and *Reverse Chemical Genetics* (RCG).²⁷

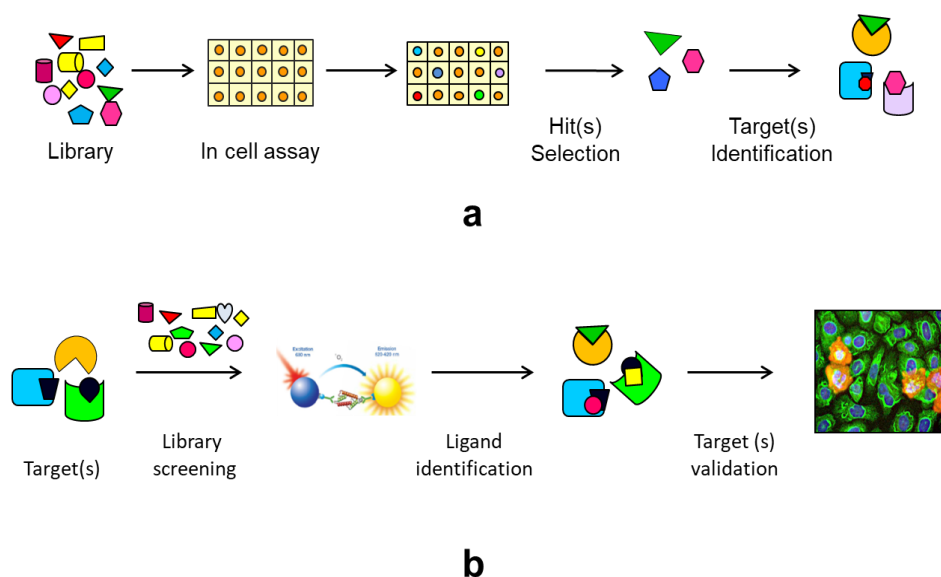


Figure 5. Chemical Genetics approaches: a) Forward chemical genetics;
b) Reverse Chemical Genetics

- 1) In FCG, typical random mutagenesis is replaced by a screening of a library of not targeted small molecules against multiple potential targets simultaneously. Compounds that induce a phenotype of interest can be selected and then the target protein of this compound is identified.²⁶ Forward chemical genetics requires three components: a) a collection or library of small molecules; b) a biological assay with a quantifiable phenotypic output, usually performed using living cells or complex cellular extracts and c) a strategy to join an active compound to its biological target. Therefore, the last goal of FCG is the target identification.
- 2) In RCG, a known target protein is screened using small molecule library to identify functional ligands that either stimulate or inhibit the target protein. Once a specific ligand that produces a change in the protein function is identified, it is introduced into a cell or organism and the resulting changes in

the phenotype are studied.²⁷ Also RCG requires three components: a) specific protein target; b) a library of small molecules; c) cell-free or cell-based assays to validate the interaction and to understand the mechanism of action of the target bound to the ligand. Therefore, the goal of RCG is the validation of the interaction and of the protein target functions.

1.5 Aim of the thesis

This PhD project was mainly focused on a RCG approach, starting from the screening of a library/collection of diterpenes able to bind a specific protein target. The molecules emerging from the screening were then studied to validate the screening results by cell-free and cell-based assays. In my PhD project were adopted:

- Cell-based techniques, such as: *Cellular Thermal Shift Assay* (CETSA), *Drug Affinity Responsive Target Stability* (DARTS), Western Blotting (WB), Flow Cytometry, RTq-PCR, Wound Healing, Apoptosis and Protein Synthesis assays.
- Cell-free techniques, such as: Mass Spectrometry (MS), Surface Plasmon Resonance (SPR), Saturation transfer difference NMR (STD-NMR), WaterLOGSY and ATPase activity assays.

1.6 Cell-free and cell-based assays

a) *Cellular Thermal Shift Assay* (CETSA)

CETSA allows to carry out qualitative and quantitative analyses of the direct interaction of a drug candidate to a target protein in the cells²⁸. In particular, this approach offers the opportunity to firmly link the observed phenotypic

response to a compound with a particular target engagement. CETSA, set up by Molina and coworkers in 2013, is based on the principle of thermodynamic stabilization inferred to the protein as a result of the ligand binding, which can be used for the estimation of binding free energies as well other thermodynamic properties for isolated systems at equilibrium. The shift in thermal stability is estimated by measuring the amount of remaining soluble target protein at different temperatures for treated and control samples.

CETSA protocol starts with the treatment of cells with either molecule of interest and vehicle as control, followed by cell heating (to denature and precipitate the protein of interest), cell lysis, removal of cell debris and aggregates through centrifugation and, finally, detection of the protein by WB studies (Fig. 6).

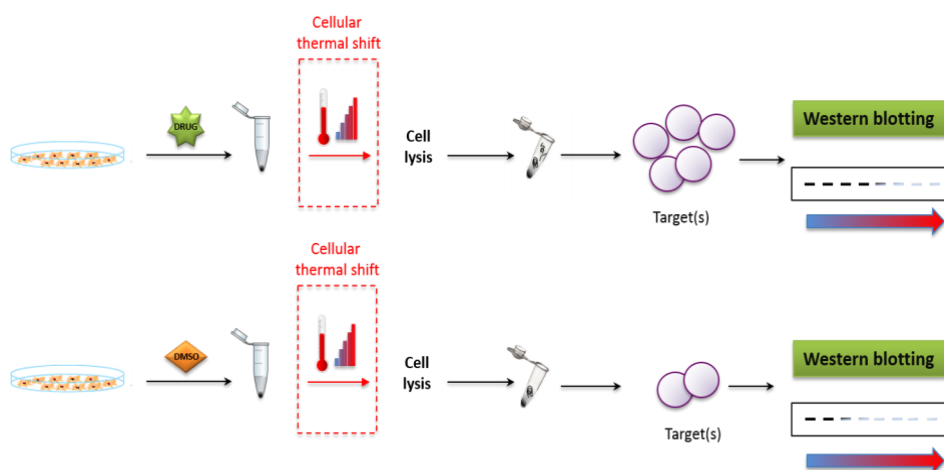


Figure 6. Schematic illustration of CETSA approach.

The apparent aggregation temperature (T_{agg} or T_m) observed in the presence or in the absence of the drug can be compared; the occurrence of significant shifts in these parameters following cells treatment with the drug, demonstrate the actual stabilization of the target protein by the molecule. Therefore, a typical output form CETSA experiment is a comparison between apparent melting curves (or, more accurately, temperature-induced aggregation curves)

measured in treated and control cells; these curves report the amount of residual target protein detected at different temperatures and a potential thermal stabilization can be assessed and identified as a shift of the melting curve on the right side of the graphic (Fig. 7, in purple).

Alternatively, an isothermal dose-response fingerprints CETSA (ITDRF_{CETSA}) could be generated, in which the stabilization of the protein can be followed as a function of increasing ligand concentration. This latter experiment requires knowledge of the temperature at which the protein denatures and precipitates (T_{agg} or T_m).

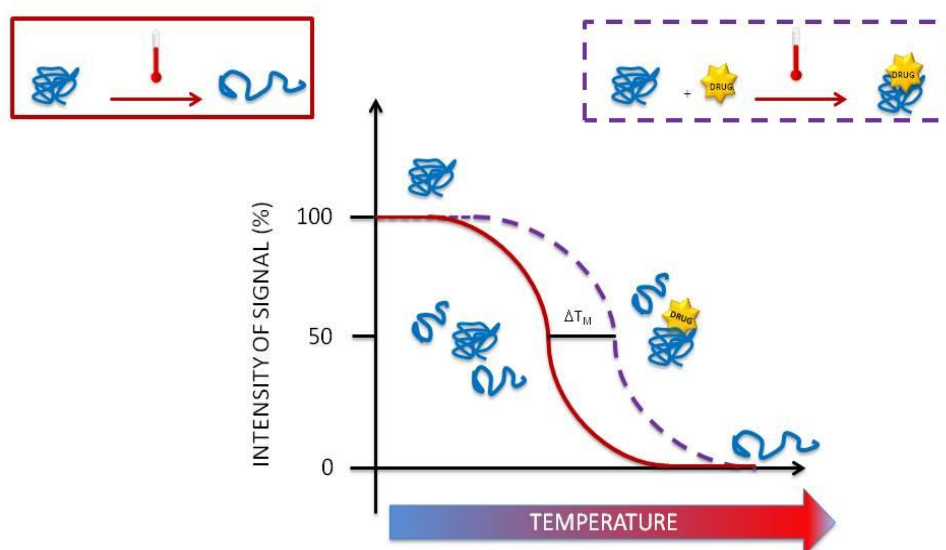


Figure 7. Principle of *Cellular Thermal Shift Assay* (CETSA)

b) Drug Affinity Responsive Target Stability (DARTS)

DARTS is a chemical proteomic technology performed to identify and study protein-ligand interactions.²⁹ It is based on the idea that small molecule binding its target protein may induce a protein stabilization, resulting in the resistance of a proteolytic enzyme (Fig. 8). This enhanced stability is postulated to result into a shift of the thermodynamic landscape of the protein

to favor the ligand-bound state, which prevents much of the protein's innate flexibility and movement from being realized. Therefore, DARTS can be applied to the initial identification of the target proteins of small molecules (*Forward Chemical Genetics*), but can also be used to validate potential protein-ligand interactions predicted or identified by other means and to estimate the affinity of interactions. This approach can be performed using intact cells, crude cell lysates and other complex protein mixtures (without requiring purified proteins), and in addition, it uses native and unmodified small molecules.

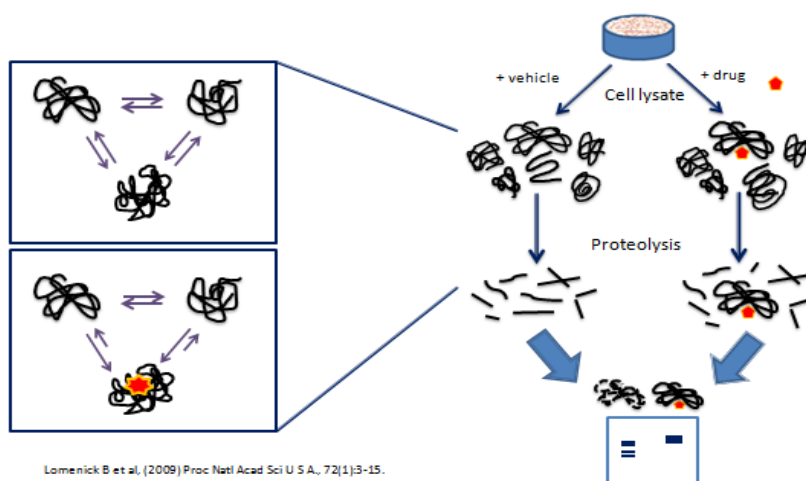


Figure 8. Principle of *Drug Affinity Responsive Target Stability* (DARTS).

As shown in Figure 8, DARTS protocol starts from the incubation of cell lysates or of intact cells (which will be lysated after the incubation) with only vehicle (DMSO) and with the compound of interest. Subsequently, the samples undergo limited enzymatic digestion using a non specific protease (such as subtilisin), followed by electrophoresis 1D SDS-PAGE. Digested proteins will be then investigated by WB and/or MS. Finally, if the drug interacts with the protein of interest, the final output will be higher levels of the protein in the treated sample than the control. There are different proteases that can be used for DARTS (e.g subtilisin, thermolysin and so on); in our

experiments subtilisin was selected, since we needed a rapid kinetic of hydrolysis and a protease with a broad specificity; thermolysin, another enzyme widely used for this technique, is not very stable and there is a significant proportion of the proteome that is not highly resistant to its proteolytic activity.²⁹

c) *Surface Plasmon Resonance (SPR)*

SPR is a non-invasive optical technique, based on the evanescent wave phenomenon, used to study the interactions of proteins with small molecules, protein conjugates, nucleic acids, lipid micelles and even larger particles such as viruses and whole cells.³⁰ The binding between a compound in solution and its ligand immobilized on the surface of a sensor chip results in a change of the refractive index, that could be monitored in real time allowing the measurement of association and dissociation rates. Different concentrations of the compound in solution are used against the putative protein target, singularly immobilized on sensor chips.³¹

A glass prism is coated with a thin layer of a noble metal (usually gold) to create a biosensor surface (Fig. 9A). The biomolecule (named “ligand”) is immobilized on the sensor surface. The metal layer possesses surface mobile electrons. At certain incidence angle the incoming beam of light disturbs these electrons causing changes in surface plasmon waves. Electrons “resonate” giving a name to SPR phenomena, this particular incidence angle is called SPR angle. At the SPR angle, reflectivity drops to a minimum. However, the binding of the protein to a free compound in solution onto sensor’s surface affects SPR conditions: refractive index increases and a shift of SPR angle occurs (Fig. 9B). The process is shown in real time by sensorgrams, where association (k_{on}) and dissociation (k_{off}) phases can be observed (Fig. 9C). The responsive units (RU) can be used to measure the binding affinity (K_D).

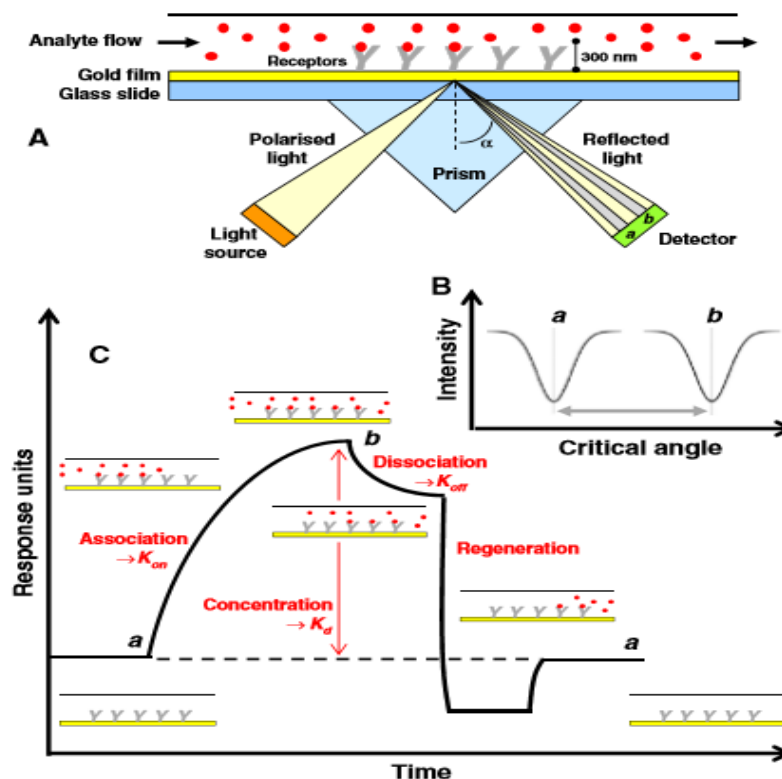


Figure 9. Surface Plasmon Resonance (SPR)-based instrument. A) SPR- biosensor surface; B) shift of SPR angle; C) SPR Sensorgram.

d) Saturation Transfer Difference NMR (STD-NMR)

The STD NMR experiment, at first described by Mayer & Meyer in 1999, is a spectroscopic technique used to study interactions, in solution, between a large molecule (protein) and a medium-small sized molecule (ligand).³² It is based on the Nuclear Overhauser Effect (NOE) and on the observation and analysis of the resonances of the ligand protons.

The experiment is carried out by first registering a reference spectrum under conditions of thermal equilibrium with the irradiation frequency set at a value that is far from any ligand or protein signal (e.g. 40 ppm), i.e, the so-called

off-resonance spectrum (Fig. 10, top), which is used as reference with signal intensities I_0 .

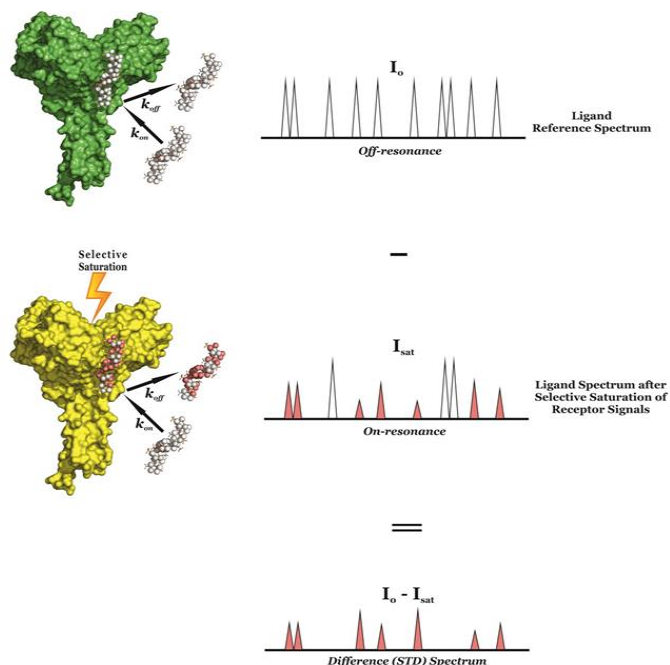


Figure 10. Scheme of the STD-NMR experiment showing the protein in surface representation and the non-exchangeable protons of the ligand as spheres. (Top) A 1D standard NMR experiments show only equilibrium intensities of the ligand in the free state (I_0). (Middle) Upon selective saturation of some receptor signals, this is efficiently spread throughout the protein (yellow surface) by spin diffusion (intra-molecular NOEs). The fast exchange (transient binding) between the free and bound ligand states allows the transfer of magnetization (inter-molecular NOEs) from the receptor to the ligand protons in contact with the protein surface (salmon spheres, on-resonance spectrum). (Bottom) The difference spectrum ($I_0 - I_{sat}$) only contains the ligand signals perturbed upon binding, whose intensities reflect the proximity of each proton to the protein surface. Adopted from Doctoral thesis of Garcia JCM, Alvarez JA, Nieto Mesa PM, insights on the structure and dynamics of glycosaminoglycans and their interactions with langerin: NMR and computational studies. 2013.

A second experiment is then recorded, in which the protein is selectively saturated (on-resonance spectrum; Fig. 10, middle), giving rise to ligand signals with I_{sat} intensities. In general, the selective irradiation consists of a cascade of Gaussian or Adiabatic-shaped pulses (low power) that saturate only a region of the spectrum that contains a few protein resonances (but not ligand signals), e.g., the aliphatic (from 0 to -1 ppm) or aromatic region (around 7

ppm), for a specific period of time (saturation time; typically from 0.5 to 5-6 seconds). The selective saturation is transferred to the whole protein via spin diffusion through the vast network of intra-molecular ^1H - ^1H cross-relaxation pathways (intra-molecular NOE; see Fig. 10, middle), being a quite efficient processes due to the typical large molecular weight of the receptor. Also, saturation is transferred from the protein to the bound ligand via spin diffusion through inter-molecular NOEs. The dissociation of the ligand will then transfer this saturation into the bulk solution where it accumulates during the saturation time of the experiment, as a result of the much slower relaxation in the unbound than the bound state. In particular, as in fast-exchanging protein-ligand systems the enthalpic relaxation (R_1) of fast-tumbling molecules (small) in the free state is much slower than the kinetic off-rate constant of binding ($k_{\text{off}} \gg R_1$), the accumulation of ligands molecules containing some of their resonances perturbed (NOE of large molecule) results in the macroscopic detection of transferred saturation on the ligand signals in the saturated STD NMR spectrum (I_{sat} ; Fig.10, middle). Furthermore, for those hydrogen atoms of the ligand establishing close contacts to the protein surface (4-5 Å) these I_{sat} values will be lower than the I_0 intensities, negative inter-molecular NOE, due to the transfer of the relaxation properties of the macromolecule to the small ligand in the bound state (Fig. 10, middle). By subtracting the off-resonance from the on-resonance spectrum ($I_0 - I_{\text{sat}}$) the difference or STD spectrum is obtained, which will just contain the proton signals of the ligand in close contact to the protein surface (Fig. 10, bottom), and where any signal coming from non-binding compounds is cancelled out. So, if a non-binder is present in solution, its resonances will not appear in the STD spectrum. Therefore, the difference spectrum, or the STD spectrum ($I_{\text{STD}} = I_0 - I_{\text{SAT}}$) yields only those resonances that experienced saturation in the *on-resonance* experiment, the receptor resonances and the ones from the binding ligands.³²

e) WaterLOGSY

WaterLOGSY is a widely applied 1D ligand-observation technique for the detection of protein–ligand interactions. As the STD-NMR approach, WaterLOGSY is based on the NOESY experiment, and implies transfer of magnetization via a intermolecular NOE and spin diffusion. The originality of WaterLOGSY comes from the intervention of water molecules in the transfer pathway.³³ (Fig. 11a)

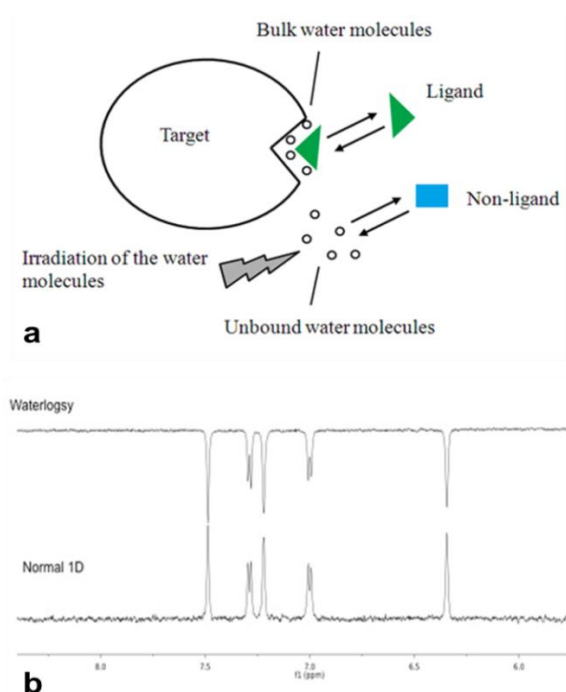


Figure 11. a) WaterLOGSY principle; b) WaterLOGSY spectrum in comparison with Normal 1D ^1H -NMR spectrum. Adopted from FragmentTech.univ-lyon1.fr

The bulk water magnetization is excited and transferred during the NOESY mixing time to the bound ligand via different mechanisms. The WaterLOGSY spectrum, which is recorded for the free ligand, contains the bound-state perturbed magnetization as long as the relaxation time T_1 of the ligand is

greater than the dissociation rate constant k_{off} . The inverted water magnetization can be transferred via different pathways to the bound ligand:

- a) direct transfer from water molecules immobilized in the protein binding site (water residence times greater than nanoseconds);
- b) chemical exchange between excited water and protein labile protons (amide, hydroxyl, amino, etc.) and propagation of the inverted magnetization to the ligand by intermolecular dipole–dipole crossrelaxation as well as spin diffusion via the protein–ligand complex;
- c) transfer from the water molecules found in the protein surface via the protein–ligand complex;

In all the pathways, the ligands interact with water via water–ligand–protein or protein–ligand complexes, whose rotational correlation times yield negative cross-relaxation rates and exhibit a negative NOE with water (Fig. 11b waterlogsy spectrum). By contrast, small molecules that only interact with bulk water (non-binders) will experience much faster tumbling, which translates into a positive NOE (Fig. 11b Normal 1D spectrum). Therefore, opposite signs for signals from free versus protein-bound ligands are observed in a WaterLOGSY spectrum, which enables one to easily discriminate binders and non-binders.³³

1.7 Outline of the thesis

The PhD thesis is organized in three chapters:

- in **Chapter 2**, a screening by CETSA of a collection of *ent*-kaurane and *ent*-trachilobane diterpenes against Nucleolin is described. Once identified a diterpene ligand of Nucleolin, cell-free and cell-based assays were implemented to validate the interaction and to study the diterpene biological activity in cancer cells;
- in **Chapter 3**, *ent*-kaurane, *ent*-trachilobane, fusicoccane, labdane and clerodane diterpenes were screened by SPR against Heat Shock Protein

70 (Hsp70). Aiming to expand and validate our knowledge about the selected compound, multidisciplinary approaches were adopted, either to validate Hsp70/diterpene binding, carried out by MS, DARTS and molecular docking or to identify its biological activity, proved by WB, Flow Cytometry and ATPase assay;

- in **Chapter 4**, the target protein is the Heat Shock Protein 90 (Hsp90). A collection of fusicoccane and abietane diterpenes was double screened by SPR against Hsp90 and by MTT. The compounds emerging from the screening were investigated for their biological activity by Flow Cytometry, WB, ATPase activity assays and molecular docking experiments.

- Chapter 2 -

Introduction

2.1 Nucleolin: structure and localizations

Nucleolin (Fig. 1) is a protein encoded in humans by the *NCL* gene. The human *NCL* gene is located on chromosome 2 and consists of 14 exons, 13 introns and is long approximately 11kb. The intron 11 of the *NCL* gene encodes a small nucleolar RNA (U20).³⁴

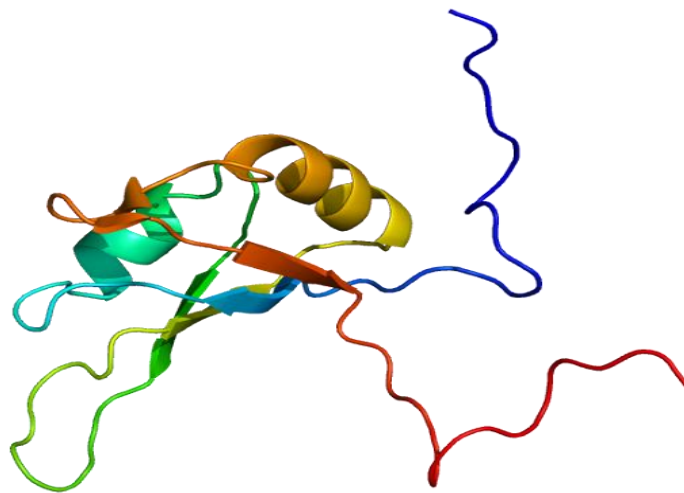


Figure 1. Structure of RNA Binding Domain 1 (RBD1) of Nucleolin. Adopted from Allain FH *et al.* 2000; *J Mol Biol.* 303(2):227-41.

Firstly, Nucleolin was described by Orrick *et al.* (1973) and called C23 because of its mobility on a two dimensional gel.³⁵ The name Nucleolin is now widely used for this protein, which can represent as much as 10% of total nucleolar proteins.³⁶ This protein is also often described as a 100-110 kDa protein; however, cloning of the cDNA of hamster Nucleolin revealed that it contained 713 amino acids, giving rise to a predicted molecular mass of 77 kDa. This difference was attributed to the amino acid composition of the N-terminal domain of Nucleolin.³⁷

Proteins homologous to human NCL were identified in rat, mouse, chicken and *Xenopus laevis*.³⁸ Nucleolin is highly phosphorylated, methylated, and can also be ADP-ribosylated.^{39,40} Analysis of its amino acid sequence revealed the presence of three different structural domains (Fig. 2):

- 1) The N-terminal domain, showing highly acidic regions interspaced with basic sequences and containing multiple phosphorylation sites.
- 2) The central domain, called RNA Binding Domain (RBD) or RNA Recognition Motif (RRM), where four RNA binding domains are localized.
- 3) The C-terminal domain, called GAR or RGG domain, rich in glycine, arginine and phenylalanine residues. This domain contains high levels of *NG,NG*-dimethylarginines.⁴¹

Several nucleolar proteins of different eukaryotic species exhibit a similar tripartite structural organization (Table 1).

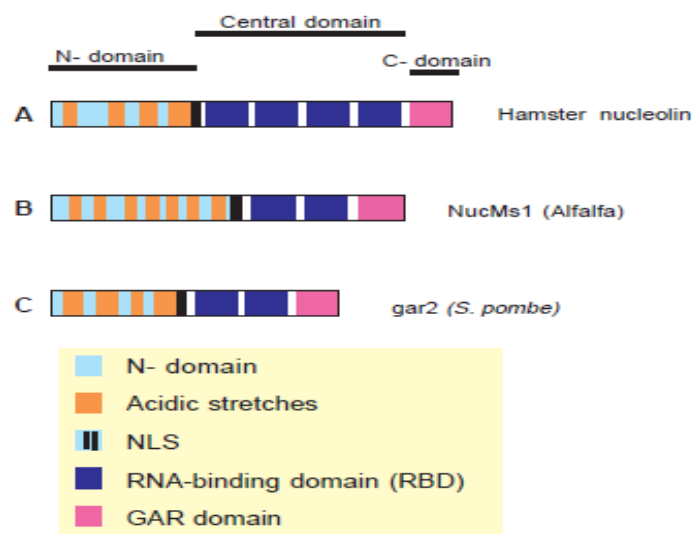


Figure 2. Schematic representation of the organization of three Nucleolin and ‘Nucleolin-like proteins’. RBDs are defined from the $\beta 1$ and $\beta 4$ strand. (A) Organization of hamster Nucleolin: mouse, rat chicken, human and *Xenopus laevis* Nucleolin have the same organization. (B) Alfalfa and pea ‘Nucleolin-like protein’ have the same organization. (C) Organization of gar2. Nsr1p possesses only 3 long acidic stretches. N-, N-terminal; C-, C-terminal.

Adopted from Ginisty H, Sicard H, Roger B, Bouvet P, structure and functions of Nucleolin. 1999; *Journal of Cell Science* 112: 761-772.

1) The N-terminal domain

The length of this domain is highly variable among the different Nucleolin-like proteins (Fig. 2). Highly acidic regions separated from each other by basic sequences represent a typical feature of this domain. Acidic domains have been proposed to bind histone H1, and could be responsible for a displacement of H1 from its interaction with linker DNA, thus inducing chromatin decondensation. Indeed, the presence of the basic and repeated octapeptide motifs (XTPXKKXX, X being a non-polar residue) bears strong similarity to an analogous sequence of histone H1 and could be responsible for the ability of Nucleolin to modulate DNA condensation in chromatin.⁴² Besides, the N-terminal domain of Nucleolin has been involved in many other protein-protein interactions, such as those with some ribosomal proteins.⁴³

The N-terminal domain of Nucleolin is highly phosphorylated,³⁸ being this protein a substrate for several kinases such as casein kinase II (CK2),⁴⁴ p34^{cdc2}⁴⁵ and protein kinase C- ζ .⁴⁶ CK2 catalyzes *in vitro* and *in vivo* phosphorylation of some Nucleolin serine residues in the acidic regions,⁴⁴ whereas p34^{cdc2} phosphorylation occurs on threonine residues within the basic TPXKK repeat. Phosphorylation of Nucleolin by CK2 and p34^{cdc2} is highly regulated during the cell cycle. Extensive phosphorylation by CK2 occurs in interphase and by p34^{cdc2} in mitosis. This regulated phosphorylation of Nucleolin probably regulates its function during the cell cycle.⁴⁵

2) The RNA-binding domains

Nucleolins from hamster, mouse, rat, human, chicken and *Xenopus laevis* possess four RNA-binding domains RBDs, also known as RRM (Fig. 2 and Table 1). These domains, found in a large number of proteins implicated in various functions, are known to confer an RNA-binding specificity to the

protein they belong to.⁴⁷ According to their RBDs sequence identity, Nucleolins and Nucleolin-like proteins can be divided in three groups. The first group includes Nucleolin from hamster, mouse, rat, human, chicken, *Xenopus laevis* and fish; in the second group there are yeast proteins such as gar2 and Nsr1p, and in the third group plant proteins such as NucMs1 and Nucleolin from pea.⁴⁸ RNAs associated with Nucleolin possess a small stem-loop structure composed of a short stem (5 base pairs) and a 7-10 nt loop containing the motif U/G CCCGA, obtaining a minimal RNA-binding site named Nucleolin Recognition Element (NRE).⁴⁹ The factors responsible for the binding affinity difference are not identified. Taken separately, none of the four individual RBDs interact significantly with RNA targets, but a peptide that contains the first two RBDs (RBD 1-2) is sufficient to account for Nucleolin/RNA binding specificity and affinity.⁵⁰ Both domains participate in a joint interaction with the NRE using a different surface to contact the RNA. The determination of the structure of this RNA/protein complex has been investigated by NMR and X-ray high-resolution crystallography. The presence of several RBDs in Nucleolin structure suggests that Nucleolin could interact with multiple RNA targets.

Table 1. Percentage of sequence identity of the RBD domain of Nucleolin from different species

	Hamster	Mouse	Human	Chicken	<i>Xenopus laevis</i>	Carp
RBD 1	100	96	85	62	53	ND
RBD 2	100	99	83	64	53	51
RBD 3	100	93	96	70	67	64
RBD 4	100	100	99	89	85	85

3) The C-terminal GAR/RGG domain

The C-terminal domain is defined as Arg-Gly-Gly (RGG) repeats interspaced with other - often aromatic - amino acids; the motif RGG is particularly frequent in nucleolar proteins. The length of the GAR/RGG domain is variable among Nucleolins, with its sequence and arrangement of the repeats not well conserved. For example, plant Nucleolin-like proteins have a longer GAR domain than mammalian Nucleolins.⁵¹ The presence of this domain in a protein is associated with the presence of an RNA-binding domain (RBD or others). The presence of this GAR domain does not influence the binding affinity and specificity for the NRE sequence, but it could be involved in the interaction of Nucleolin RBD domains with targets located within large and complex RNA, such as rRNA.^{49, 50} The GAR domain protein-protein interactions are not well defined. It is not known how the GAR domain mediates protein-protein interactions, but since the GAR domain of Nucleolin interacts with only a subset of ribosomal proteins, these interactions seem to be specific.⁴³ After its discovery, it was found that Nucleolin contained high levels of *NG,NG*-dimethylarginines; this post-translational modification is found on arginines located in the GAR domain.^{37,41} This modification could be an important signal for the regulation of GAR/RNA interactions, the stability of the protein, or its localization. It is not known if this post-translational modification is reversible.^{43, 50}

The intracellular localization of Nucleolin has been extensively studied by electron microscopy analysis and/or immunofluorescence ultrastructural localization in vertebrates,⁴¹ plants,⁵² and yeast cells.⁵³ It is localized in the nucleolus, in the cytoplasm⁵⁴ and on the cell membrane⁵⁵(Fig. 3). This different localizations are linked to changes in Nucleolin isoelectric point and/or post-translational modifications, such as glycosylation, ADP-ribosylation, acetylation and most importantly phosphorylation.^{39, 40} In fact,

Nucleolin translocation into the nucleus improves when it is dephosphorylated whereas phosphorylated nucleolin is mainly moved into the cytoplasm.

Biochemical fractionation of the nucleoli has shown that the nucleolar fraction of Nucleolin represents more than 90% of the Nucleolin cellular pool, while the nucleoplasmic compartment does not represent more than 5% of the protein.⁵⁶ The cytoplasmic fraction of Nucleolin is difficult to estimate as it depends on the quality of the fractionation, or sensibility of the detection techniques that are used; however, it probably does not represent more than a few % of the total protein. In specific cytoplasmic structures, such as the centrosomes, centrosomal Nucleolin represents less than 0.1% of the total protein.⁵⁷ S. Nisole *et al.* determined that the cell surface Nucleolin is less than 20% of the nuclear-free cytoplasmic fraction.⁵⁸ In the different cell compartments, Nucleolin has different molecular targets that confer distinct functions (Fig. 3).

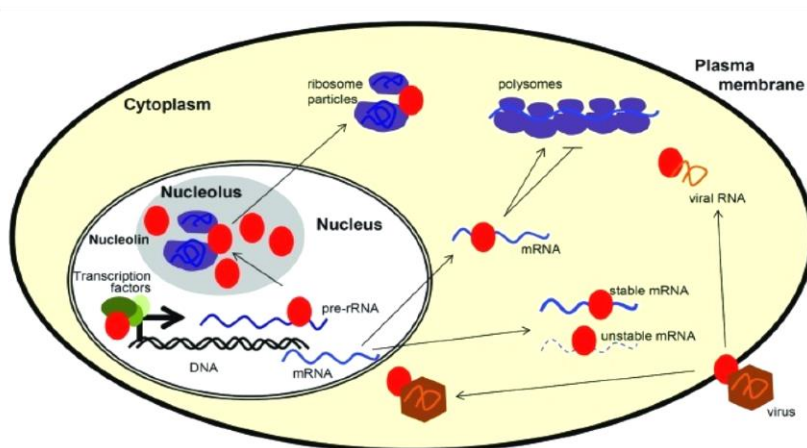


Figure 3: localizations of Nucleolin (in red).

Adopted from Kotb Abdelmohsen & Myriam Gorospe RNA-binding protein nucleolin in disease. 2012; *RNA Biology*. 9:799-808.

The predominant localization in the nucleolus represent an important aspect of Nucleolin profiling of its functions.^{59, 60} Nucleolin is mainly observed in the Dense Fibrillar Compartment (DFC), whereas it is less abundant in the

Granular Compartment (GC), and almost absent in the Fibrillar Center (FC).⁶¹ How Nucleolin accumulates in the nucleolus remains an important question: several studies were performed to identify the Nucleolin domains responsible for the nucleolar localization⁶² but, the obtained results showed that Nucleolin does not contain a single, linear nucleolar targeting signal. The well-defined bipartite nuclear localization signal (NLS) of Nucleolin (KRRKEMANKSAPEAKKKK) is used to enter in the nucleus and then the protein probably accumulates within the nucleolus as a consequence of its binding to other nucleolar components (probably rRNA) via the RNA binding domains and the C-terminal RGG domain. The RNA-binding domains of nucleolin are crucial for its nucleolar localization, but are unable by themselves to target hybrid proteins to the nucleolus. The C-terminal GAR domain allows total nucleolar accumulation when it is associated with at least one RBD.⁶³

Nucleolin has also been observed in the plasma membrane of several cell lines, using immunofluorescence and electron microscopy. This localization is surprising, because Nucleolin neither possesses a transmembrane hydrophobic domain nor a plasma membrane targeting sequence.⁶⁴ Ding *et al.* demonstrated that Nucleolin translocation to the cell membrane is mediated by Heat Shock Protein 70 (Hsp70). This chaperon interacts with Nucleolin in endothelial cells via its peptide-binding domain and the RNA-binding domain 3 and 4 of Nucleolin. Phosphorylation of Nucleolin by either protein kinase C- ξ or casein kinase 2 mediates Nucleolin interaction with Hsp70 and the surface expression. Moreover, Hsp70 regulates Nucleolin translocation via stabilizing it and enhancing its interaction with nonmuscle myosin heavy chain 9. On the plasma membrane, Nucleolin interacts with several proteins involved in cell proliferation, apoptosis and angiogenesis.⁶⁵

2.1.1 Roles of Nucleolin in physiological and pathological pathways

The multiple sub-cellular localizations of Nucleolin are directly connected to its physiological and pathological functions (Fig. 4):

- in the nucleolus, it is directly involved in ribosome biogenesis,⁶⁶ chromatin remodeling,⁶⁷ transcriptional regulation⁶⁸ and telomerase activity;⁶⁹
- in the nucleoplasm, Nucleolin interacts with several RNAs and proteins (such as transcription factors) and it is involved in regulation of the cellular response to stress;⁷⁰
- in the cytoplasm; Nucleolin constantly shuttles between nucleus and cytoplasm where it is involved in many non nucleolar functions, e.g. import/export of ribosomal proteins, centrosome duplication⁵⁹ as well as post-transcriptional and translational regulation of various mRNAs⁷¹ including p53⁷², Bcl2⁷³ and AKT;⁷⁴
- on the cell surface Nucleolin behaves as receptor, binding to several proteins, thus inducing tumorigenesis (cell migration, adhesion, angiogenesis), and mediating inflammation and viral infections;⁷⁵

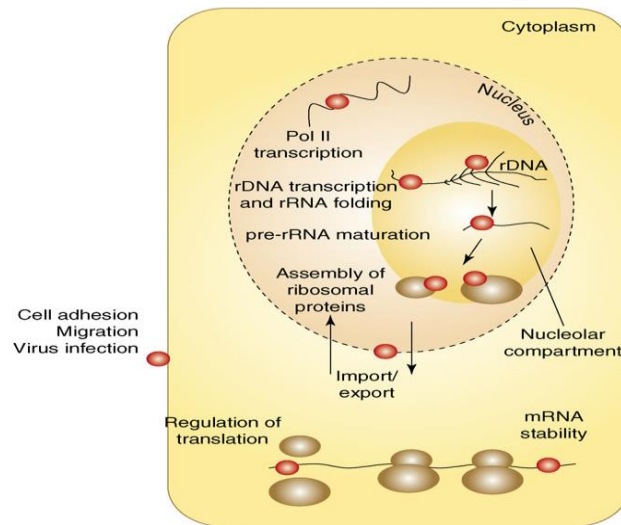


Figure 4. The cellular compartment locations of Nucleolin (red dots). (a) In the nucleolus, association of Nucleolin with nucleolar chromatin (rDNA) could be involved in the regulation of Pol I transcription. (b) Nucleolin has been seen on nascent pre-rRNA transcripts and is believed to participate in co-transcriptional pre-rRNA folding, (c) maturation at the first processing site and (d) assembly of pre-rRNA with ribosomal proteins. (e) The shuttling of Nucleolin between the nucleus and the cytoplasm might participate in the import and/or export of several nucleolar components or proteins, such as ribosomal proteins. (f) In the nucleoplasm, Nucleolin has been also found associated with several genes transcribed by Pol II and with mRNAs, with functions from (g) the regulation of translation to (h) mRNA stability. (i) A large number of reports have identified nucleolin on the cell membrane, with potential roles in cell migration and adhesion and virus infection. Adopted from Fabien Mongelard and Philippe Bouvet. Nucleolin: a multiFACeTed protein. *TRENDS in Cell Biology*. 2007; 17: 80-86.

2.1.2 Roles of Nucleolin in ribosome biogenesis

In the nucleolus, Nucleolin plays many functions, specially in ribosome biogenesis (Fig. 4):

- it is a chromatin co-remodeler, as it facilitates the interaction between nucleosomes and the remodeling complex of chromatin;⁶⁷
- it is a histone chaperone, with functional similarity to the “facilitates chromatin transcription” complex (FACT);⁶⁷
- it is involved in the regulation of RNA polymerase I transcription and RNA polymerase II activity;⁷⁶

- it is involved in the proper folding and maturation of the preribosomal RNA (pre-rRNA);

- it participates in the ribosome assembly;⁷⁷

According to its histone chaperone activity, Nucleolin promotes RNA transcription through nucleosomes. Histone chaperones are key factors for the dynamic organization of chromatin template. They mediate:

- histone storage;

- translocation of histones to the nucleus;

- exchange and deposition of histones onto the DNA during replication-dependent chromatin assembly;

- chromatin reorganization not only during elongation, but also during initiation of RNA transcription;

Chromatin assembly is a two-step process: deposition of a H3–H4 tetramer on DNA followed by the deposition of two H2A–H2B dimers. Various histone chaperones and ATPdependent chromatin remodeling factors facilitate the organization of nucleosomes into a regularly spaced array. Nucleolin directly binds to H2A–H2B dimers⁷⁶ and facilitates the assembly of nucleosomes on naked DNA, presumably by incorporating H2A–H2B dimers into auto-assembled tetrasomes ((H3–H4)₂ tetramer acceptor). This effect of Nucleolin on the dynamics of H2A–H2B dimers facilitates the passage of the RNA polymerase II through nucleosomes. The ability of Nucleolin in increasing H2A–H2B turnover is a key factor to understand its co-remodeling activity. The spontaneous or Nucleolin-induced disassembly of one H2A–H2B unit would be expected to lead to a destabilization of the histone octamer particles. Nucleolin also shows FACT-like activities (Fig. 5).

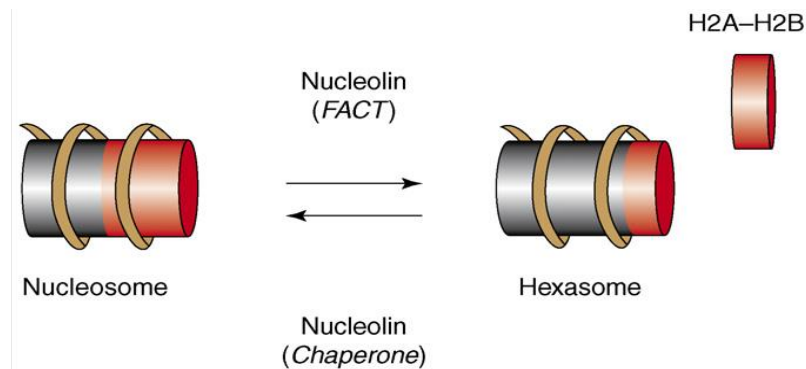


Figure 5. The histone chaperone and FACT-like activities of Nucleolin. In vitro, Nucleolin can, similar to FACT, destabilize nucleosomes to promote the formation of hexasomes (loss of one H2A–H2B dimer). This helps the passage of polymerase II through chromatin templates. The histone chaperone activity of Nucleolin helps the reformation of nucleosomal structures after the passage of the polymerase.

Adopted from Fabien Mongelard and Philippe Bouvet. Nucleolin: a multiFACeTed protein. *TRENDS in Cell Biology*. 2007; 17: 80-86.

The “facilitates chromatin transcription” (FACT) complex is required to overcome the nucleosomal barrier and to promote a modest but significant level of transcription elongation. Therefore, FACT is also itself a histone chaperone and facilitates the loss of an H2A–H2B dimer upon polymerase II transcription, enabling the passage of the polymerase through the nucleosomal particle.⁷⁸

Nucleolin is also involved in the regulation of rRNA transcription. Indeed, following inhibition of rRNA transcription, a rapid release of Nucleolin from the dense fibrillar zone of the nucleolus is observed,⁷⁹ demonstrating that its presence in this subnucleolar compartment is dependant upon rRNA transcription. A model related to Nucleolin ability to interact with rRNA has been proposed by Bouche *et al.*, where Nucleolin is involved in the regulation of rRNA transcription elongation through the binding of its RNA-binding domains with the nascent rRNA transcript. The N-terminal domain, instead, interacts with the polymerase I machinery, which would block transcription elongation. In this model, the phosphorylation of Nucleolin by CK2 during interphase would be required to proteolyse Nucleolin (between the N- and

central domains) and to release the transcription complex, while the central and C-terminal domains of Nucleolin could remain bound to the rRNA and participate in the pre-ribosome assembly.⁸⁰

The ability of Nucleolin *in vitro* to promote the formation of secondary structures in complex RNAs,⁸¹ and its association with preribosomal particles *in vivo*,⁸² suggest that Nucleolin could be required for the correct assembly of these particles. Therefore, Nucleolin can play a role as an assembly factor, bringing together a correctly folded rRNA and the other components necessary for rRNA maturation and/or assembly of the ribosome. The GAR domain of Nucleolin is implicated in some of these interactions.⁴³ The interaction of Nucleolin with these ribosomal proteins further supports its role at an early step of ribosome assembly.

2.1.3 Nucleolin as shuttle between nucleus and cytoplasm

Despite Nucleolin is found almost exclusively into the nucleolus, assays based on interspecies heterokaryons have shown that Nucleolin shuttles between nucleus and cytoplasm. However, a very small amount of Nucleolin is able to migrate to the cytoplasm. In the heterokaryon system, the N-terminal domain of Nucleolin is required for efficient shuttling, but it is unable to increase the nuclear export of an heterologous protein, indicating that Nucleolin does not contain a positively acting export signal.⁸³ In addition, its cytoplasmic localization is related to its phosphorylation by p34^{cdc2}, whereas the nuclear translocation is correlated with a dephosphorylation of Nucleolin. These data show that phosphorylation of its N-terminal domain can regulate the function of Nucleolin NLS.⁶³ Regarding to the C-terminal domain, it was shown that the GAR domain of Nucleolin reduced slightly the export process.⁸³ The discovery that this protein is able to shuttle, even under specific conditions, has raised the possibility that it can be involved in the nuclear import of

ribosomal components (like ribosomal proteins), or in the nuclear export of the ribosomal particles.

2.1.4 Nucleolin as receptor on the cell surface

Nucleolin has been observed at the plasma membrane of several cell lines using immunofluorescence and electron microscopy.⁸⁴ The expression of Nucleolin at the plasma membrane is increased in several tumor cells⁸⁵ and in endothelial cells during angiogenesis.⁸⁶ There are several evidences indicating that Nucleolin located in plasma membrane can facilitate the binding of HIV on host cell surface, and its entrance. Moreover, Nucleolin has been shown to promote inflammation, enhancing the internalization of lipopolysaccharides from the cell membrane to the cytosol.⁷⁵ Therefore, Nucleolin is believed to be a useful signature for cancer, inflammation and viral infection diagnostics and can be an interesting target for the development of new drugs.

2.1.5 Nucleolin as tumor marker: therapeutic strategies

An altered expression and function of Nucleolin has been observed in several cancers. For instance:

- an increase of Nucleolin expression is observed in tumor tissue from colorectal cancer human patients;⁸⁷
- it is also over-expressed in tumor tissues from gastric cancer, and a high cytoplasmic amount of Nucleolin is associated with worse prognosis for the patients;⁸⁸
- in human breast cancer tumors, Nucleolin is over-expressed (from 3 to 6 fold increase in human breast cancer cell lines compared to normal breast cells);⁸⁹
- higher Nucleolin mRNA or protein levels are also observed in leukemia cells as studied in different patients cohort;⁹⁰

- Nucleolin expression is also increased in lung cancer tissues from human patients and associated with largest tumors;⁹¹
- in glioblastoma cells, the presence of glycosylated Nucleolin at the cell surface increases with the malignancy of the human tumor;⁸⁵
- in human melanoma cells, a specific glycosylated form of Nucleolin is observed and the inhibition of cell surface Nucleolin in a mouse model, delays the emerging of melanoma and significantly prevents subsequent visceral metastasis;⁹²
- in cervical cancer, Nucleolin expression is directly linked to human papillomavirus type 18 induced carcinogenesis by favoring the expression of viral oncoproteins;⁹³

A major challenge is to understand the contribution of Nucleolin to the development of these cancers. In some cases, Nucleolin deregulation may just be the consequences of the pathological state, whereas in other situations the deregulation of Nucleolin may contribute to the initiation or the progression of the disease.

As shown in figure 6, Nucleolin can play several functions in cancer progression:

- in the nucleoplasm, Nucleolin binds promoters of genes that are over-expressed in cancer (such as c-myc) and promotes their transcription;
- in the cytoplasm, Nucleolin affects mRNA turnover by interacting with the 3'-untranslated region of several target mRNAs of proteins important for cancer development (p53, Bcl2 or AKT1 mRNAs). Particularly, binding to Bcl2 mRNA,⁷³ Nucleolin prevents its proteolysis inferred by exosomes, increasing Bcl2 levels and improving anti-apoptosis. In addition, interacting with AKT1 mRNA,⁷⁴ Nucleolin enhances its translation increasing cell proliferation. Nucleolin also interacts with miRNAs to affect the expression of oncogenes and tumor suppressor genes;

- at the plasma membrane, Nucleolin interacts with several proteins involved in cell proliferation, apoptosis and angiogenesis;
- Nucleolin interacts with Fas, member of the tumor necrosis factor superfamily of apoptosis receptors, inhibiting apoptosis;⁹⁴
- Nucleolin interaction with ErbB1⁹⁵ and Ras⁹⁶ at the plasma membrane favors cell proliferation;
- it can bind to the growth factors Pleiotrophin (PTN)⁹⁷ (inducing cell migration) and midkine⁹⁸ (promoting cell survival);
- numerous other key proteins involved in tumorigenesis and angiogenesis have been shown to interact with Nucleolin and act through cell surface Nucleolin as for instance Hepatocyte Growth Factor (HGF),⁹⁹ Vascular Endothelial Growth Factor (VEGF)¹⁰⁰ and tumor necrosis factor alpha inducing protein (Tip α);¹⁰¹

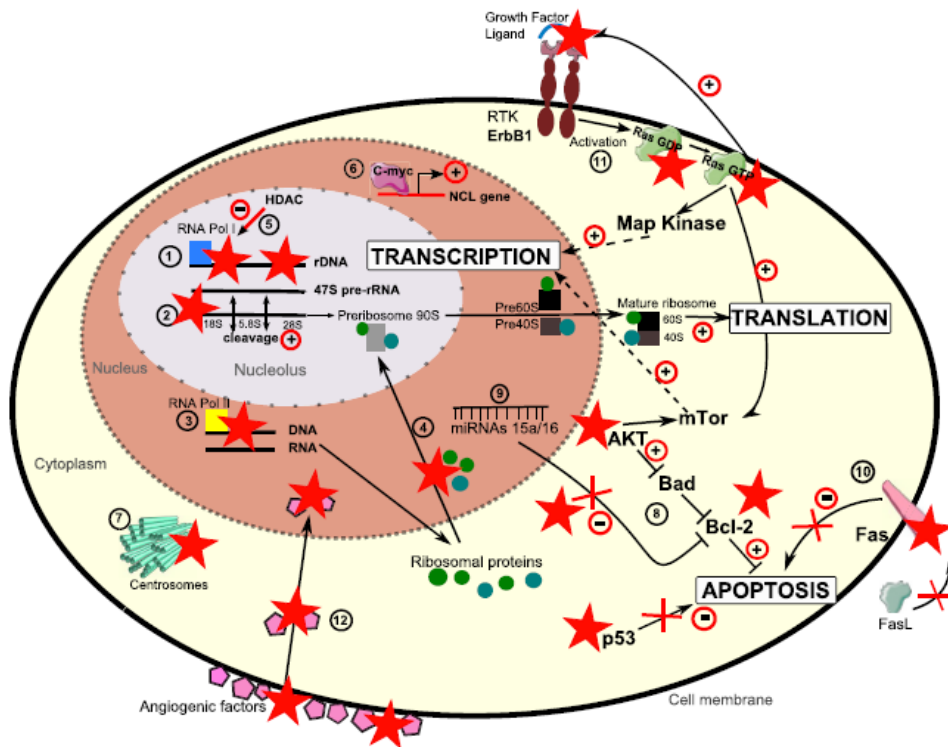


Figure 6. Nucleolin (represented by the red star) mediates cancer development in all cell compartments. In the nucleus and nucleolus, Nucleolin modulates the quantity of synthesized ribosomes. Firstly, RNA Polymerase I transcription and ribosomes synthesis are increased by Nucleolin (1). By binding unmethylated rDNA, it allows the maintenance of a euchromatin active state (5). Nucleolin helps the rRNA maturation and the cleavage of pre-rRNA (2). It is required for RNA polymerase II transcription (3) and ribosomal proteins synthesis (4). These ribosomal proteins can be imported by Nucleolin from the cytoplasm to the nucleus and to the nucleolus (4). Nucleoplasmatic Nucleolin binds also several promoters of genes that are overexpressed in cancer, like c-myc and promotes their transcription (6). Cytosolic Nucleolin is important for centrosome function (7) and binds to several mRNAs to promote their translation (8) like for example mRNAs coding for proteins important for cancer progression (p53, Bcl2 or AKT mRNAs). Nucleolin also interacts with miRNAs to affect the expression of oncogenes and tumor suppressor genes (9). On cell surface, Nucleolin interacts with the apoptosis pathway protein Fas, blocking cell death (10). Nucleolin can also bind to Ras GDP and RasGTP, increasing proliferation, migration, resistance to apoptosis through the Map Kinase/AKT pathways. Nucleolin/RasGTP interaction increases NCL/ErbB1 binding (11). Cell surface Nucleolin can also participate to the translocation of several entities such as virus and angiogenic factors from the cell surface to the nuclear compartment (12).
 Adopted from: C. M. Berger, X. Gaume, P. Bouvet, The roles of Nucleolin subcellular localization in cancer. 2015; *Biochimie*. 113: 78-85.

2.1.6 Nucleolin Inhibitors

Some compounds able to block Nucleolin activity have been reported. Unfortunately, this protein is involved in so many pathways that achieving its selective inhibition is quite hard.

One interesting Nucleolin-inhibitory molecule is the aptamer AS1411 (figure 7).¹⁰² This 26-base guanine-rich oligodeoxynucleotide quadruplex-forming aptamer is promising for therapy as it can target various Nucleolin pathways:

- AS1411 induces relocalization of the protein arginine methyltransferase 5-Nucleolin complex from the nucleolus to the cytoplasm,^{73,103} probably altering ribosome synthesis;
- AS1411 is internalized via binding to cell surface Nucleolin; inside the cell it may prevent Nucleolin from binding to and stabilizing mRNA of the anti-apoptotic Bcl2, thereby destabilizing Bcl2 mRNA and leading to a reduction in Bcl2 protein synthesis. This may lead to the induction of apoptosis;¹⁰²
- this aptamer also modulates the interaction between Nucleolin and the microprocessor complex involved in miRNA synthesis. Thus, AS1411 can reduce the level of Nucleolin-dependant miRNAs, such as miR-21, miR-221, miR-222 and miR-103, leading to the upregulation of genes involved in apoptosis.¹⁰⁴

Phase I and II human clinical trials to treat acute myeloid leukemia have confirmed anti-cancer activity of AS1411, actually named ACT-GRO-77.¹⁰²

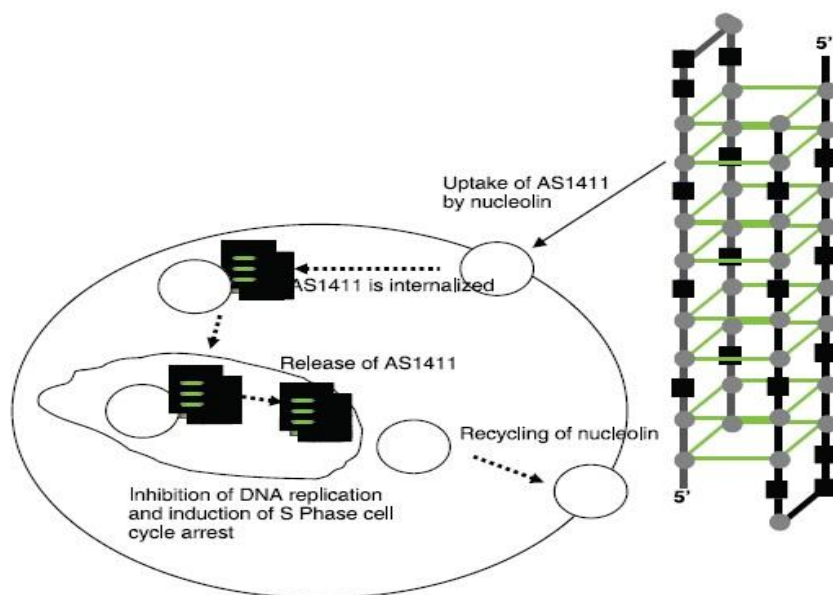


Figure 7. Structure and mechanism of action of AS1411. AS1411 self-anneals into a dimer and adapts a three-dimensional structure conferred by eight guanosine-quarters (gray circles). The black squares are the thymidine bases. AS1411 is internalized into the cell by binding cell surface Nucleolin. Into the cytoplasm it prevents Nucleolin from binding and stabilizing the mRNA of the anti-apoptotic Bcl2, thereby destabilizing its mRNA and leading to a reduction of Bcl2 protein synthesis. Into the nucleus, AS1411 inhibits DNA replication and induces S-phase cell cycle arrest.

Adopted from R. C. Ireson and L. R. Kelland, Discovery and development of anticancer aptamers. 2006; *Molecular Cancer Therapeutics*. 5: 2957-2962.

A small molecule quarfloxin (also known as CX-3543, figure 8), which selectively disrupt Nucleolin-rDNA interaction thereby inhibiting RNA polymerase I transcription, was found to induce apoptosis in cancer cells. Phase II of clinical trials was also performed in patient having carcinoid/neuroendocrine tumors.¹⁰⁵

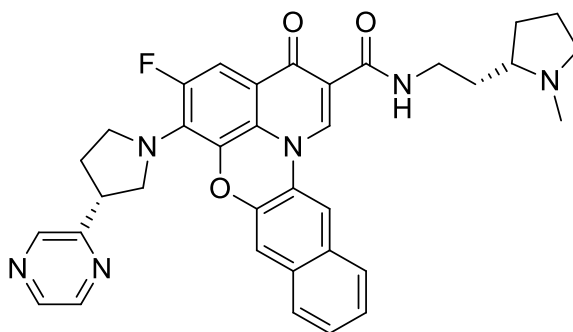


Figure 8. Structure of quarfloxin.

The cell surface Nucleolin is probably the most promising target for cancer therapy. Indeed, Nucleolin is over expressed on the membrane of cancer cells, compared to normal cells. Thus, chemotherapy may be less toxic since a drug would easily target the cell surface Nucleolin of tumor cells without altering it in the nucleus. For example, the HB-19 pseudo-peptide binds surface Nucleolin without interacting with nuclear Nucleolin.¹⁰⁶ Recent studies show how HB-19 can inhibit its oncogenic action *in vitro* and *in vivo*, by binding to the C-terminal domain of cell surface Nucleolin. Although additional evaluations of these Nucleolin aptamers are required, these preliminary studies suggest that such molecules could be relevant for both cancer therapy and diagnostic.

Another inhibitor of Nucleolin, identified by our research group, is the ent-kaurane diterpene Oridonin.¹⁹ Oridonin is the first identified plant small molecule inhibiting Nucleolin. After demonstrating its interaction with Nucleolin in cancer cells (Jurkat and HeLa) by cell-free and cell based assays (SPR, CETSA, DARTS), its cytotoxic effect in Jurkat cells after 24h and a cell cycle arrest in G₂/M phase were proved. In addition, Oridonin shows inhibition of protein synthesis and reduction of the levels of the proteins AKT and Bcl2 and of the respective mRNAs. There is also another interesting result emerging from our studies: Oridonin can inhibit simultaneously two proteins crucial for cancer development and progression: Hsp70 and Nucleolin. This

finding could actually explain the efficiency of Oridonin as antitumor agent and its ability in interfere with many different pathways.¹⁹ The two proteins are functionally related, as Hsp70 has been shown to prevent degradation and cleavage of Nucleolin in cancer cells following exogenous stresses,^{107,108} and to regulate Nucleolin translocation to cell surface.¹⁰⁶ Taken together, our results suggested Oridonin as an interesting starting point to obtain small-molecules able to modulate Nucleolin activity. Furthermore, the present discovery of the first plant small-molecule interactor of Nucleolin provides a proof-of-principle evidence of modulation of Nucleolin activity induced by a small-molecule.

2.1.7 Aim of the project

In this frame, our aim was to to set-up, optimize, develop, and apply cell-free and cell-based techniques to identify new bioactive diterpene as Nucleolin inhibitors and to elucidate their molecular mechanism of action. Our project started from a screening of several plant diterpenes against Nucleolin in order to find a potential binder; to achieve this goal, a Cellular Thermal Shift Assay (CETSA) was performed. This screening led us to obtain the diterpene 6,19-dihydroxy-*ent*-trachiloban-17-oic acid (**12**) as a promising ligand of Nucleolin. To validate the interaction and to investigate more in detail the mechanism of action of **12**, several cell-free, cell-based and chemical proteomic approaches were carried out: WB, MTT, Flow Citometry, RTq-PCR, LC-MS/MS, DARTS, SPR, STD-NMR and WaterLOGSY experiments were performed.

Results and discussion

2.2 Screening of diterpenes by *Cellular Thermal Shift Assay* (CETSA)

Our study started from a *Reverse Chemical Genetics* (RCG) approach, selecting Nucleolin as target. The choice of this target derived from previous studies performed by our research group, where Nucleolin was identified, by a *Forward Chemical Genetics* (FCG) strategy, as target of Oridonin, a bioactive diterpene isolated from *Isodon rubescens* (Lamiaceae) with interesting antitumoral properties. Oridonin is the first reported plant small molecule ligand for Nucleolin.¹⁹

In order to find further diterpenes able to inhibit Nucleolin, a small library based on structural similarity with Oridonin scaffold, was screened by performing *Cellular Thermal Shift Assay* (CETSA) in Jurkat cells (leukemia T cells). CETSA allows to carry out a qualitative and quantitative analyses of the direct interaction of a drug candidate to a target protein inside a cell.²⁸ In particular, this approach offers the opportunity to firmly link the observed phenotypic response to a compound with a particular target engagement. CETSA, set up by Molina and coworkers in 2013, relies on the principle of thermodynamic stabilization inferred to the protein as a result of ligand binding, which can be used for the estimation of binding free energies as well other thermodynamic properties for isolated systems at equilibrium. Basically, the shift in thermal stability is estimated by measuring the amount of remaining soluble target protein in treated and control experiments at different temperatures. CESTA protocol starts with the treatment of cells with the molecule of interest and vehicle (DMSO) as control, followed by cell heating (to denaturate and precipitate the protein of interest), cell lysis, removal of cell

debris and aggregates through centrifugation and, finally, detection of the residual target protein by western blot (Fig. 9).

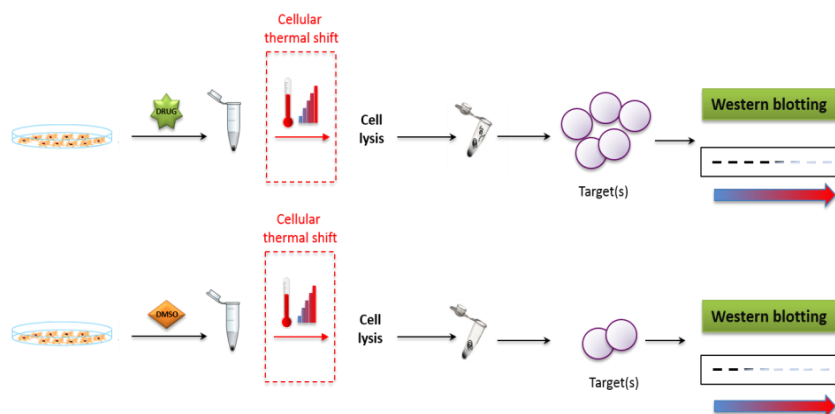


Figure 9: Schematic illustration of CETSA approach.

The apparent aggregation temperature (T_{agg} or T_m) observed in the presence or in the absence of the drug can be evaluated; the occurrence of significant shifts in these parameters following cells treatment with the drug, demonstrate the actual stabilization of the target protein by the drug. Therefore, a typical output form CESTA experiment is a comparison between apparent melting curves (or, more accurately, temperature-induced aggregation curves) measured in treated and control cells; these curves report the amount of residual target protein detected at different temperatures and a potential thermal stabilization can be assessed and identified as a shift of the melting curve on the right side of the graphic (Fig. 10, in purple).

Alternatively, an isothermal dose-response fingerprints CETSA (ITDRF_{CETSA}) is generated, in which the stabilization of the protein can be evaluated as a function of increasing ligand concentration. This latter experiment requires knowledge of the temperature at which the protein denatures and precipitates (T_{agg} or T_m).

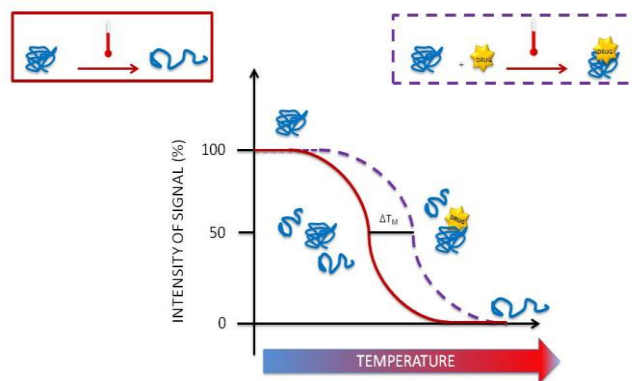
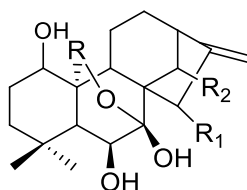
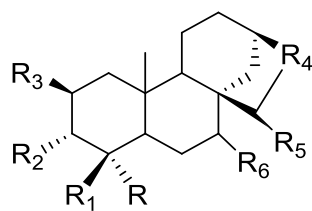


Figure 10: Cellular Thermal Shift Assay (CETSA)

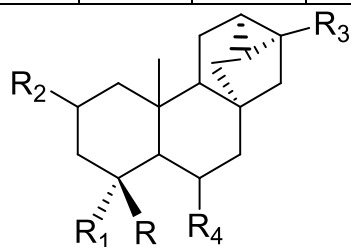
Nucleolin was confirmed as oridonin target by CETSA experiments in Jurkat cells,¹⁹ and the stabilization of Nucleolin was inferred by oridonin at 55°C, T_{agg} of Nucleolin. On these bases, we performed a screening of several diterpenes as Nucleolin binders at this T_{agg} in Jurkat cells. We screened 16 diterpenes, with *ent*-kaurane and some *ent*-trachilobane skeletons (Fig. 11); Most of these diterpenes were isolated from aerial parts of *Psiadia punctulata* (DC) Vatke (Asteraceae), and oridonin was used as positive control. The choice of these diterpenes was due to their similarity in terms of chemical scaffold in comparison with oridonin.



Compound	R	R ₁	R ₂
1		$=O$	H
2	$=O$	$\blacktriangleleft OH$	$\blacktriangleleft OH$
3		$=O$	$\blacktriangleleft OH$
Oridonin		$=O$	$\blacktriangleleft OH$



Compound	R	R ₁	R ₂	R ₃	R ₄	R ₅	R ₆
4	-COOCH ₃	H	H	OH		=O	H ₂
5	-CH ₃	-CH ₃	H	=O		H ₂	H ₂
6	-CH ₃	-CH ₃	=O	H		H ₂	H ₂
9	-CH ₃	-COOH	H	H		H ₂	=O
14	-CH ₂ OH	-CH ₂ OH	H	OH		H ₂	H ₂
16	-CH ₂ OH	-CH ₂ OH	H	=O		H ₂	H ₂



Compound	R	R ₁	R ₂	R ₃	R ₄
7	-CH ₂ OH	-CH ₂ OH	=O	-CH ₃	◀OH
10	-CH ₂ OH	-CH ₂ OH	◀OH	-CH ₃	H
11	-CH ₂ OH	-CH ₂ OH	=O	-CH ₃	H
12	-CH ₃	-CH ₂ OH	H	-COOH	◀OH
13	-CH ₃	-CH ₂ OH	=O	-CH ₃	◀OH

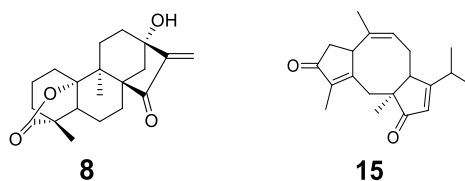


Figure 11. Structures of diterpenes screened against Nucleolin by CETSA.

As shown in figure 12, WB results indicated that the main ligands for Nucleolin stabilization at 55 °C were compounds **1**, **5**, **6**, **7**, **12**, **13** and **15**. Compound **1** shares with oridonin the presence of an α,β -unsaturated carbonyl group and an the methylene group in R. They seem to be important for the interaction with Nucleolin. For the other compounds was not possible to predict structure-activity relations.

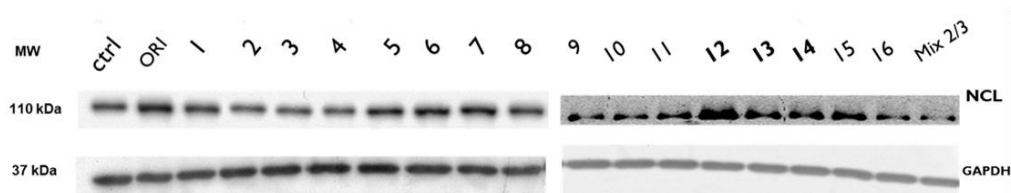


Figure 12: Screening of diterpenes in Jurkat cells monitored by WB using CETSA.

Our attention was focused on **12**, the 6,19-dihydroxy-*ent*-trachiloban-17-oic acid, a diterpene with trachilobanic scaffold isolated from *Psiadia punctulata* (Vatke) Asteraceae, which was found as the compound that showed the higher stabilization of Nucleolin at its T_{agg} (Fig. 13).

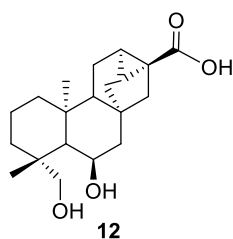


Figure 13: Structure of 6,19-dihydroxy-*ent*-trachiloban-17-oic acid (**12**)

2.2.1 Biological activity of 6,19-dihydroxy-*ent*-trachiloban-17-oic acid in Jurkat and HeLa cells

The biological activity of N-**12** was investigated by MTT assay in liquid and solid cancer cells, respectively Jurkat (leukemia T cells) and HeLa cells (cervical carcinoma cells), and also on nontumor human peripheral blood mononuclear cell line (PBMC). After treatment of the cells with **12** (10 μ M, 30 μ M and 70 μ M for 48h), higher cytotoxicity in HeLa cells (IC₅₀= 25 \pm 0.5 μ M) than Jurkat cells (IC₅₀= 50 \pm 1.2 μ M) was observed (table 2). Therefore, HeLa cells were selected for our cell-based studies. On PBMC cells **12** did not show cytotoxic activity (IC₅₀ up to 100 μ M).

Table 2. IC₅₀ (μ M) in HeLa and Jurkat cells by MTT assay. HeLa and Jurkat cells were treated with DMSO (ctrl) or **12** (10 μ M, 30 μ M e 70 μ M) for 48h.

Compound	Jurkat	HeLa	PBMC
12	50 \pm 1.2 μ M	25 \pm 0.5 μ M	>100 μ M

Data represent the mean \pm SD of 3 different experiment.

Moreover, to study more in detail the biological activity of **12** on HeLa cells, a cytofluorimetric analysis was performed. Particularly, HeLa cells were incubated with **12** (20 μ M and 40 μ M) for 48h. Compound **12** was found to arrest HeLa cell cycle at subG₀/G₁ phase (Fig. 14).

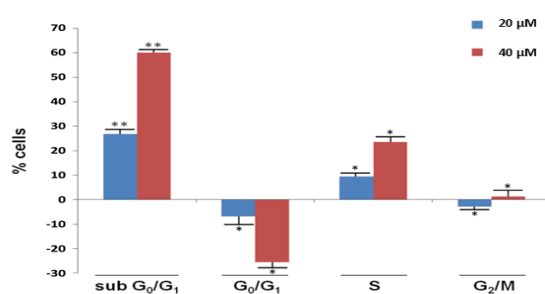


Figure 14. Effect of **12** on cell cycle progression. Flow cytometric evaluation of DNA content in HeLa cells treated with DMSO (control) or **12** (20 μ M and 40 μ M) for 48h. On the Y axis: the percentages of cells in subG₀/G₁ (hypodiploida) and in each cell cycle phase of **12**-treated cells subtracted for the corresponding percentages of control cells. Results are expressed as means \pm SD of three experiments performed in duplicate (**p<0.005, *p<0.05).

In order to understand if the subG₀/G₁ cell cycle arrest was due to apoptosis or necrosis events, Annexin V, FITC Coniugate/PI protocol was implemented.¹⁰⁹ The results, analyzed by flow cytometry, showed HeLa cells in late (9.67%) and early (8.01%) apoptosis after treatment with **12** 10 μM for 48h and in late (11.3%) and early (28.5%) apoptosis with **12** 20μM for 48h (Fig. 15a, b and c). No significant necrosis effects were observed. Apoptosis results were also confirmed by cleavage of PARP, increased after treatment of HeLa with **12** 10 μM and 20μM for 48h (Fig. 15d).

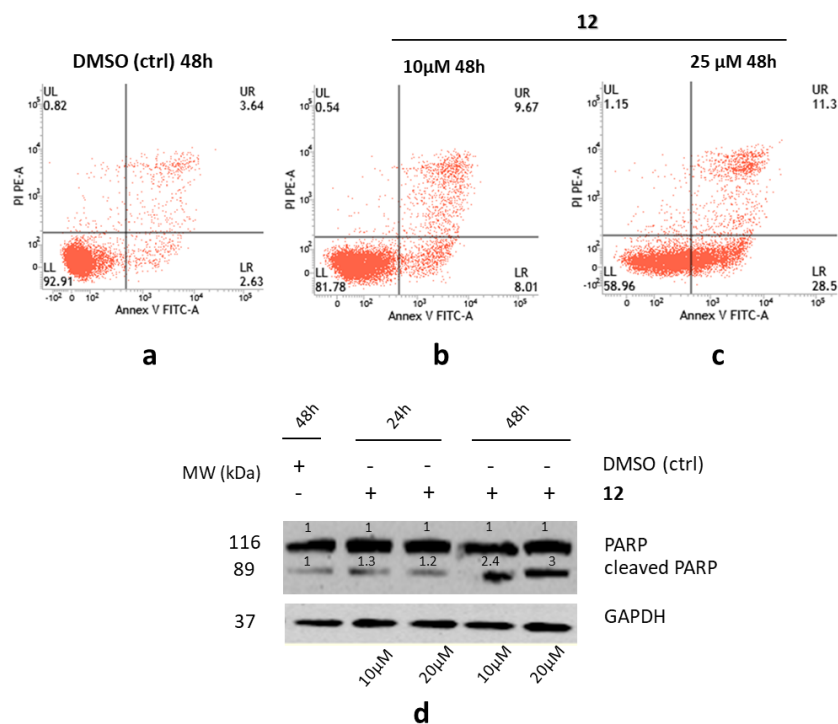


Figure 15. Flow cytometry experiment using Annexin V-FITC/PI protocol. a) HeLa cells treated with DMSO (control) for 48h. b) HeLa cells treated with **12** 20 μM for 48h. c) HeLa cells treated with PEITC (positive control) 10 μM for 24h. d) WB of HeLa treated with **12** 10 μM and 20 μM for 24h and 48h. GAPDH was used as loading control. The blots are representative of at least two different experiments with similar results.

2.2.2 Nucleolin-12 interaction achieved by CETSA in HeLa cells

The next step of our study was to demonstrate Nucleolin-**12** interaction by CETSA also in HeLa cells. Firstly, we had to identify the T_{agg} of Nucleolin also for this cell line: HeLa cells were incubated with **12** (20 μ M), DMSO (control), and oridonin (5 μ M) as positive control for 2h at 37 °C. Afterwards, the samples were divided in 8 aliquots, and each of those was subjected to a 5 minute incubation at a specific temperature, in the range from 38.4 °C up to 61.3 °C. Samples were then lysated and centrifuged, in attempt to separate the soluble proteins from the aggregated and precipitated ones, and Nucleolin levels were evaluated by WB analysis. In Fig. 16 we can observe a gradual decrease of the soluble portion of the protein in the control and an increase of its levels in the treated samples, due to the thermal stabilization inferred by oridonin and **12** in the range of temperatures 52.8-55.6 °C. In our experiments, 55.5 °C was the appropriate temperature to appreciate thermal stabilization of Nucleolin, as the amount of soluble protein at this temperature in **12** and oridonin-treated cells was about 2 or 3 times higher than that observed in the control (Fig. 16).

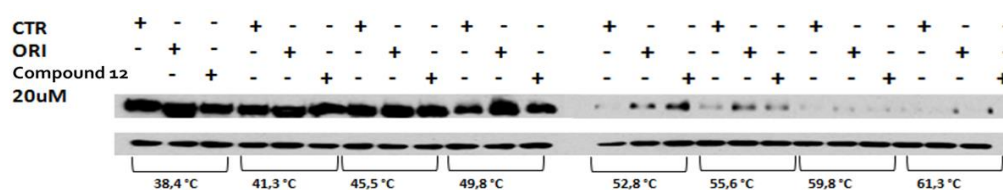


Figure 16. T_{agg} of Nucleolin monitored by CETSA. WB on Nucleolin levels after treatment of HeLa cells with DMSO (control), oridonin 5 μ M (positive control) and **12** 20 μ M. Therefore, treated and untreated HeLa cells were heated and then the soluble amount of Nucleolin by WB was evaluated.

In Figure 17, densitometry-based quantification of western blot signals (ratio Nucleolin/GAPDH depending on the temperature) was graphed and melting

curves of Nucleolin for control (DMSO), positive control (Oridonin) and treated samples with **12** were reported.

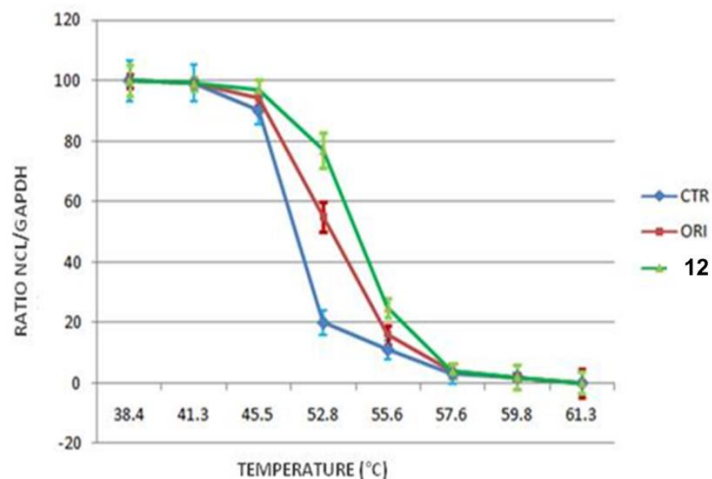


Figure 17. Apparent melting curves of Nucleolin in HeLa cells. Densitometry-based quantification of WB signals was graphed (Nucleolin intensities normalized to GAPDH intensities for each data point). Results are expressed as means \pm SD of three experiment performed in duplicate.

Comparing the treated curves with the control, a shift of the curves of treated with **12** and oridonin on the right side of the graphic can be observed, indicating that the T_{agg} of Nucleolin is higher due to its interaction with the compounds which protect Nucleolin from the denaturation under heating conditions.

In order to investigate the kinetic profile of the engagement of Nucleolin in the cell, HeLa cells were treated with DMSO (control), 15-ketoatractyligenin methyl ester (SR2017), used as negative control since from previous studies in our research group it was identified as a non-binder of Nucleolin¹⁹ (Fig. 18) and **12** (5 μ M and 20 μ M) for 1h up to 4h.

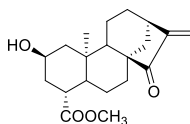


Figure 18. Structure of 15- ketoatractyligenin methyl ester (SR2017)

The time-course experiment revealed that the maximum binding was observed after 2h of incubation with **12** (5 μ M) (Fig. 19, highlighted in blue); after that, the difference between treated and control samples decreased, and it became negligible after 4 h of incubation.

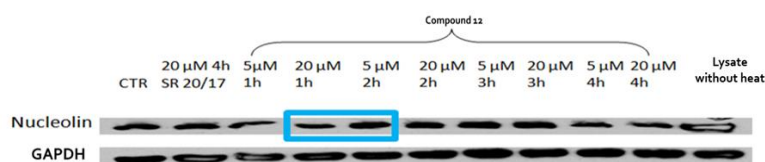


Figure 19: Kinetic profile of the engagement of Nucleolin by **12** in cells using CETSA. HeLa cells were treated with **12** (5 μ M and 20 μ M) for 1h up to 4h. Each samples was heated and then the soluble amount of Nucleolin was evaluated by WB analysis. 15-chetoatractiligenin methyl ester (SR2017) was used as negative control.

Taking advantage of the defined T_{agg} of Nucleolin, we carried out an ITDF_{CETSA} experiment to establish the half-maximal effective dose (EC_{50}) of Nucleolin/**12** complex. Therefore, HeLa cells were treated with a wide range of concentrations of **12**, from 0.1 to 20 μ M (Figure 20a), while incubation time (2h) and temperature ($T_{agg} = 55.3$ °C) were kept constant. Increased stabilization of Nucleolin in a dose-dependent manner was observed, and the obtained EC_{50} was 5 μ M (Figure 20b).

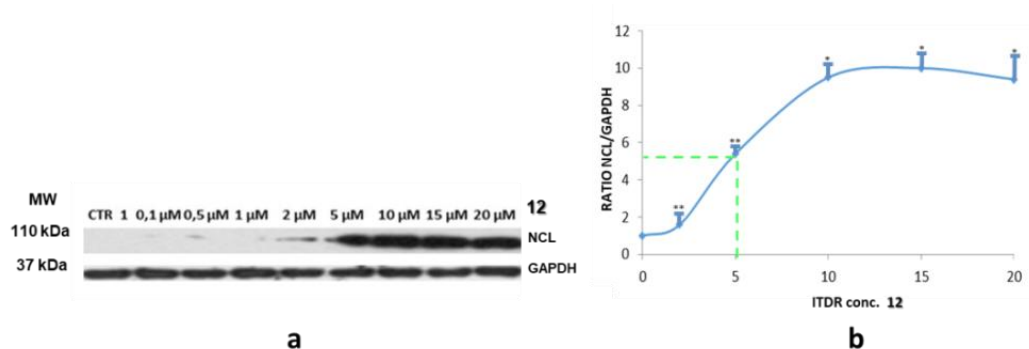


Figure 20. a) CETSA in HeLa cells in presence of DMSO or **12** (from 0,1 to 20 μ M) at 55.3 °C. **b)** densitometry-based quantification of western blot signals.

2.2.3 Study of Nucleolin/12 interaction by DARTS in HeLa cells

Nucleolin/12 interaction was studied by *Drug Affinity Responsive Target Stability* (DARTS)²⁹ in HeLa cells. Firstly, a preliminar optimization of the DARTS protocol had to be set up to select the best limited proteolysis condition with subtilisin. Thus, lysates from human HeLa cells were split into different aliquots which underwent digestion with different concentrations of subtilisin for 30 min and 60 min at 25°C and 37°C. The digestion was stopped by adding sample loading buffer and boiling immediately. Each sample was then loaded onto 10% SDS/PAGE gels, stained with Fixing solution for 30min and Brilliant Blue G-Colloidal over-night, and finally washed with water. Achieved results showed that ratio of 1:6000 enzyme:lysate (w:w) at 25°C for 30 min resulted as the best experimental condition (figure 21b).

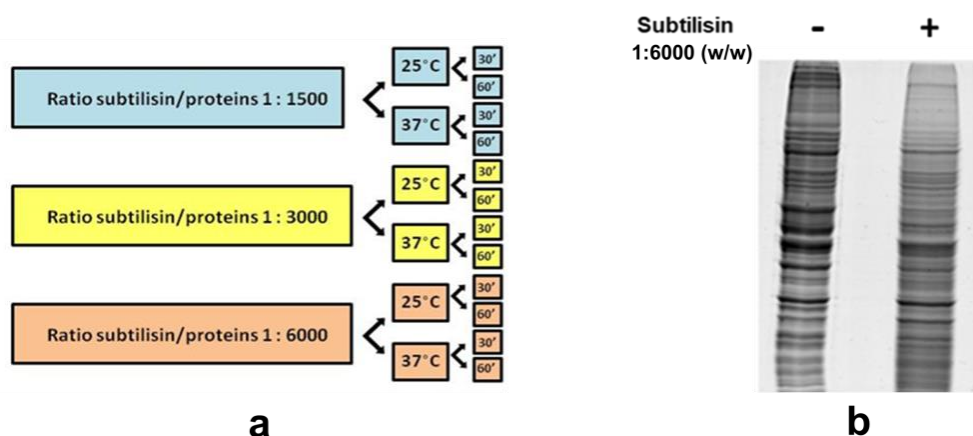


Figure 21: Optimization of DARTS protocol. a) Scheme of different conditions used for DARTS optimization; b) HeLa lysates with and without subtilisin (1:6000 w:w).

Hence, HeLa cells were treated with **12** (20 μ M) for 2h; after the incubation, the cells underwent lysis with RIPA buffer, and the resulting protein extract was subjected to enzymatic digestion, carried out by adding subtilisin (1:6000 w/w) for 30 minutes at 25 °C. Subsequently, the partially digested proteins were fractionated by SDS-PAGE; each sample was divided in two aliquots,

each loaded on a gel: in the first gel, the proteins were transferred into nitrocellulose membranes to perform a WB analysis. As shown in Figure 22b, in the sample treated with subtilisin and **12** there was an enrichment of Nucleolin in comparison with the sample treated with only subtilisin, meaning that the diterpene interacted with Nucleolin protecting it from the enzymatic proteolysis.

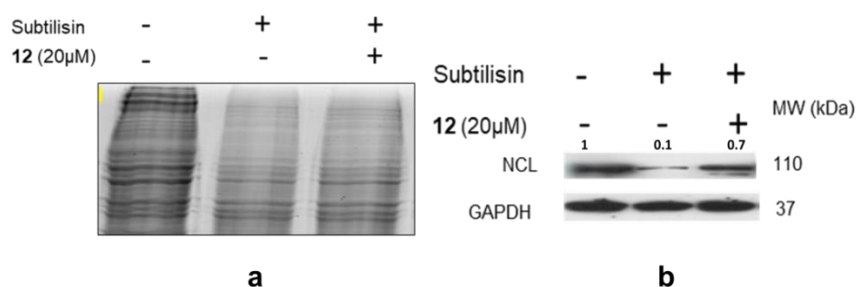


Figura 22: a) 1D SDS PAGE after digestion with subtilisin 1:6000 w:w using **12** 20µM b) WB analysis of DARTS results. GAPDH was included as a loading control. The blots are representative of at least two different experiments with similar results.

The second gel was treated with Fixing Solution for 30 min, stained with Comassie Blue Colloidal, and each lane of control and treated samples was cut into five pieces, digested with trypsin and analyzed by LC-MS/MS.

In order to evaluate the relative abundance of Nucleolin in treated and control samples, we carried out further data analyses by Mass Spectrometry. Bands of each lane underwent a digestion protocol with trypsin and then analyzed by LC-MS/MS. Subsequently, each raw file was analyzed using Max Quant software, using a label-free quantification (LFQ) “within groups” method (each band of the same lane was united). In Table 3, Nucleolin intensities in the samples treated with DMSO (control) and with 20 µM **12** for 2h are shown.

Achieved results were in agreement with DARTS data obtained by WB, since the LFQ total intensity of treated samples is higher than the LFQ total intensity of control samples.

Table 3. Max Quant software data. Control (DMSO) and treated (**12** 20 μ M) samples.

Protein name	Mr	LFQ Intensity CTRL (DMSO)	LFQ Intensity TR (12)	mean	ratio
Nucleolin	76,613	$2.22 \cdot 10^7$	$6.79 \cdot 10^9$	$3.50 \cdot 10^8$	30.5

Data are representative of at least two different experiments with similar results. According to our previous Isothermal Dose Response Fingerprint CETSA (ITDRF_{CETSA}) results, where the EC₅₀ for Nucleolin/**12** was 5 μ M, we carried out further DARTS experiments using this concentration. Therefore, different proteolytic profiles among the lane of control (only DMSO), the lane of treated with subtilisin and the lane treated with subtilisin and **12** were observed (Fig 23a).

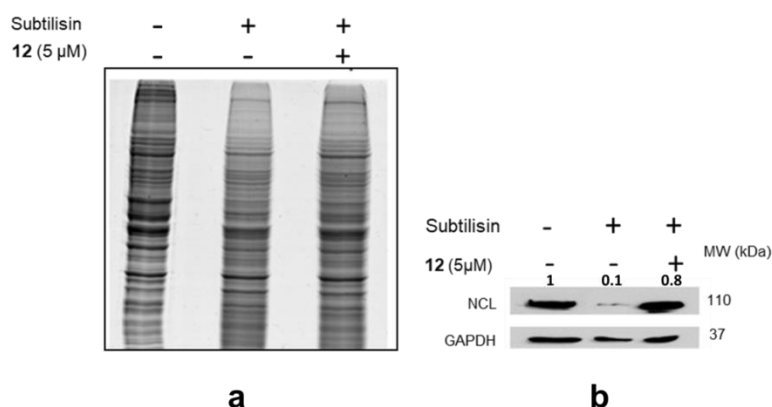


Figura 23: a) 1D SDS PAGE after digestion with subtilisin 1:6000 w:w using 5 μ M **12**; b) WB analysis of DARTS results. GAPDH was included as a loading control. The blots are representative of at least two different experiments with similar results.

WB and MS results, showed in figure 23b and in table 4 respectively, allowed us to confirm Nucleolin/**12** interaction.

Table 4. Max Quant-based data analysis. Control and treated (5 μ M **12**) samples.*

Protein name	Mr	LFQ Intensity CTRL (DMSO)	LFQ Intensity TR (12)	mean	ratio
Nucleolin	76,613	$9.32 \cdot 10^6$	$2.33 \cdot 10^8$	$1.21 \cdot 10^8$	25

*Data are representative of at least two different experiments with similar results.

2.2.4 MS-based identification of further targets of 6,19-dihydroxy-*ent*-trachiloban-17-oic acid

In order to further investigate the mechanism of action of **12**, a detailed analysis of DARTS results analyzed by MS was implemented. Particularly, by analyzing results from several DARTS experiments (five in total) by Mascot Daemon Matrix Science software, we identified Nucleolin as main target, and also ezrin and alpha-catenin (Table 5). These two targets are mainly involved in cell migration and cell adhesion, and have been described as potential markers for metastatic cancer progression.¹¹⁰ In addition, Nucleolin takes part of cancer cells migration events as well. Indeed, there are several studies in literature that show the roles of Nucleolin in cell migration and invasion. Nevertheless, nowadays there is no evidence in literature that there could be a possible interaction or cooperation among Nucleolin, Ezrin and α -Catenin in this process. Some studies implied that the reduction of Nucleolin levels (transfecting cells with nucleolin-targeted small interfering RNA) in cancer cells could inhibit the process of epithelial mesenchymal transition (EMT) which enhances their metastatic potential. Yang *et al* showed that si-Nucleolin treatment attenuated the expression of p-Erk1/2, p-Akt, vimentin, N-cadherin, and MMP2, leading to decreased migration and invasion of gastric cancer cells.¹¹¹ Therefore, since Nucleolin is involved in cell migration and it is able to interact with **12**, these informations prompted us to investigate a possible modulation of compound **12** in these Nucleolin-mediated process.

Table 5: Putative targets identified for 6,19-dihydroxy-*ent*-trachiloban-17-oic acid. DARTS experiment were performed at least five times, and the number of times each protein was identified is reported.

Protein name	number of times
Nucleolin OS=Homo sapiens GN=NCL	4
Ezrin OS=Homo sapiens GN=EZR	3
Catenin alpha-1 OS=Homo sapiens GN=CTNNA1	3

Data are representative of at least five different experiments with similar results.

2.2.5 Investigation of 6,19-dihydroxy-*ent*-trachiloban-17-oic acid activity in the cell migration: Wound Healing Assay

On these bases, the involvement of **12** in cancer cell migration by Wound Healing Assay was evaluated. After treatment of HeLa cells with **12** (20 μ M for 48h), a 1-mm wide scratch was made across the cell layer using a sterile pipette tip. After washing with PBS, DMEM medium was added to replace matrix depleted with the scratch. Using LAS-EZ software, each plate was photographed immediately after scratching, and the healing process was monitored at the electronic microscope each hour up to 24h at the identical location of initial image. The distance between each side of the scratch was measured in pixels. As shown in figure 24, at 24h the cell migration for HeLa treated with **12** increased only for 25%, whereas for the control the migration increased up to 45%. Therefore, achieved results demonstrated a reduction of migration (20%) of HeLa cells induced by the treatment with the diterpene.

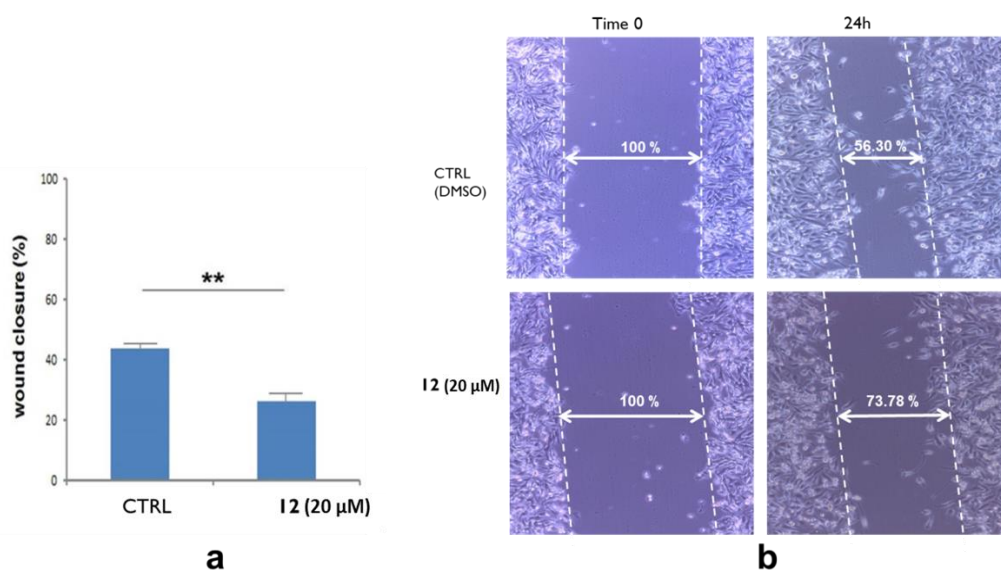


Figure 24: Wound Healing assay on HeLa cells. a) Percentage of wound closure induced after treatment of HeLa cells with DMSO (control) and 20 μ M **12**. b) Photographic monitor at time 0 and after 24h from the scratch. Data are representative of at least two different experiments with similar results.

2.2.6 Biological effect of 6,19-dihydroxy-*ent*-trachiloban-17-oic acid on Nucleolin into the cell

The evidence that **12** binds Nucleolin allowed us to further investigate the role of this diterpene in the modulation of Nucleolin-mediated processes in the cells. Most of them are mediated by Nucleolin in its phosphorylated form. In fact, phosphorylation is one of the most important post-translational modifications of Nucleolin, playing a crucial role in its translocation from the nucleolus to the plasma membrane.^{39,40} In this frame, we decided to verify the biological relevance of the binding of **12** to Nucleolin and p-Nucleolin. Firstly, we evaluated the levels of this protein, its fragmentation and phosphorylation in cell lysates following incubation of HeLa cells with DMSO (control), oridonin 5 μM (used as negative control because from previous results we demonstrated that oridonin does not modulate Nucleolin and p-Nucleolin levels¹⁹) and 20 μM **12** for 4h, 8h and 16h and then underwent protein extraction procedure using RIPA buffer. WB results (Fig. 25) showed a moderate reduction of Nucleolin levels; in addition, a time-dependent reduction of p-Nucleolin was observed. This result led us to seek for further Nucleolin functions which our compound could modulate.

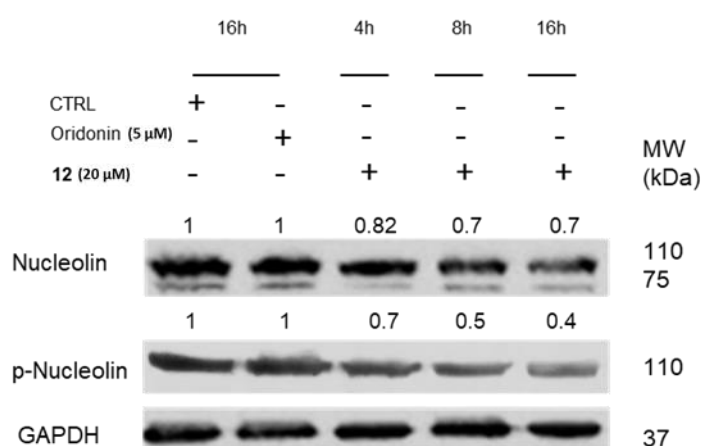


Figure 25: Treatment of HeLa cells with oridonin (5 μM , negative control) and **12** (20 μM) up to 16h and evaluation of proteolytic fragments of Nucleolin in cell. The blots are representative of at least two different experiments with similar results.

2.2.7 6,19-dihydroxy-*ent*-trachiloban-17-oic acid activity in subcellular compartments

As mentioned above, Nucleolin is not only located in the nucleolus, but also in the cytoplasm and on the cell membrane.^{54, 55} These different localizations are due to changes in Nucleolin post-translational modifications, specially phosphorylation.^{39,40} In fact, Nucleolin translocates into the nucleus when it is dephosphorylated and enhances into the cytoplasm when phosphorylated. These results therefore indicate that the changes in the phosphorylation state of Nucleolin during the cell cycle might be a possible regulatory element of Nucleolin localization.⁴⁰ Moreover, Hsp70 has been shown to regulate the phospho-Nucleolin translocation (through its RNA binding domains 3 and 4) to the cell surface (Fig. 26),⁶⁵ where it becomes tumor receptor. According to this, the simultaneous inhibition of Hsp70 and Nucleolin functions by Oridonin and **12** in different cell compartments could lead to the decrease of several anti-apoptotic and proliferation signal pathways, crucial for cancer cell survival.

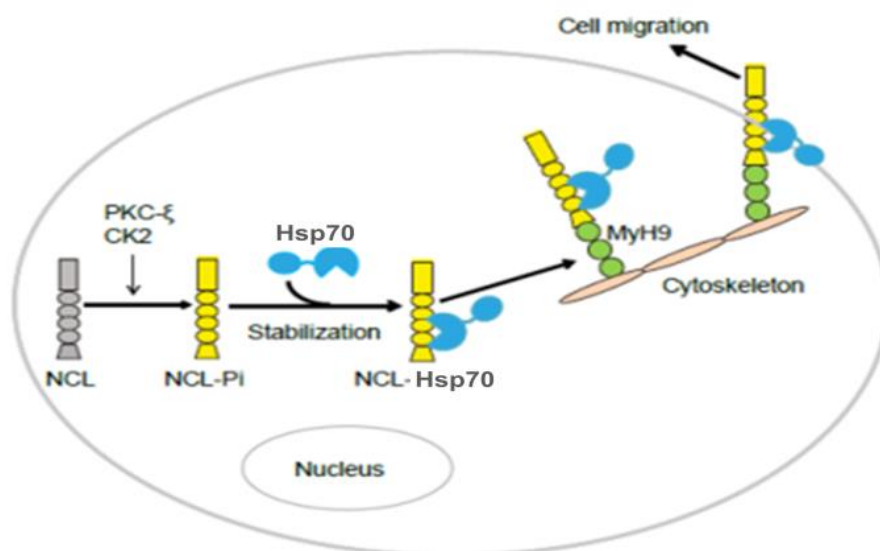


Figure 26. Illustration of Nucleolin phosphorylation and translocation to the plasma membrane mediated by Heat Shock Protein 70.

To obtain the subcellular compartments, HeLa cells were incubated with DMSO (control), oridonin 5 μ M and 20 μ M **12** for 4h at 37 °C. After obtaining nucleus, cytosolic and plasma membrane extracts, each lysate was fractionated by SDS-PAGE and the proteins were immunoblotted on a nitrocellulose membrane with antibodies specific for each cell compartment.

As shown in figure 27, after 4h we can observe:

- no modulation of nucleolar Hsp70, Nucleolin and phospho-Nucleolin levels;
- reduction of cytoplasmatic phospho-Nucleolin and Hsp70 levels induced by **12**;
- high reduction of cell-membrane Hsp70 and phospho-Nucleolin levels induced by oridonin and **12**;

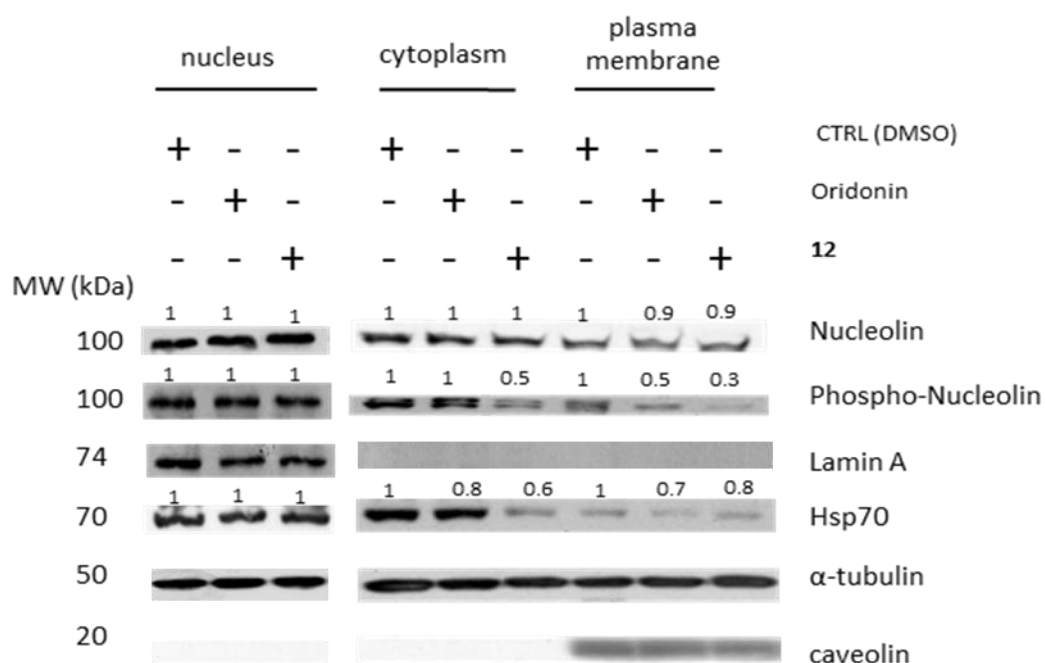


Figure 27. Effect of oridonin and **12** on Nucleolin, p-Nucleolin and Hsp70 levels in nucleus, cytosol and plasma membrane. Western Blot analysis in HeLa cells treated with DMSO (ctrl), oridonin (5 μ M) and **12** (20 μ M) for 4h. For each immunoblot, band intensity was quantified by densitometry (numbers above each lane). α -Tubulin was included as a loading control for cytosol extracts, Lamin A for the nucleus extracts, Caveolin for plasma membrane extracts. The blots are representative of at least two different experiments with similar results.

2.2.8 RTq-PCR and Western Blot analyses

Nucleolin is highly expressed in proliferating cells, including stem cells and cancer cells. Cancer cells acquire a number of features in order to become malignant, including the abilities to grow and proliferate, overcome senescence, evade apoptosis and the immune system, invade and metastasize other tissues and promote angiogenesis.¹⁹ Nucleolin through its RNA binding activity, conferred by its four RNA binding domains, could affect these traits. In fact, the expression of several proteins involved in the survival of malignant cells during cell damage are modulated by Nucleolin. Specifically, this protein affects mRNA turnover by interacting with the 3'-untranslated region of several target mRNAs. In particular, we paid attention on the anti-apoptotic proto-oncogene Bcl2, and on the pro-survival protein AKT1. Indeed, Nucleolin binds to Bcl2 mRNA and promotes the expression of Bcl2, increasing apoptosis in cancer cells, and also interacts with AKT1 mRNA, enhancing the translation of AKT1^{73, 74} On this basis, we decided to verify the effects of **12** on the levels of these specific mRNAs.

HeLa cells were treated with DMSO (control), oridonin (5 μ M, positive control) and **12** (20 μ M) for 4h and 8h and the stabilization of Bcl2 and AKT1 mRNAs by Real-Time Quantitative Polymerase Chain Reaction (rtq-PCR) was evaluated. In figure 28a (left side, treatment with **12**) we can observe a reduction in a time-dependent manner (22% of Bcl2 mRNA after 4h and 26% after 8h and 40% of AKT mRNA after 8h). Our WB results (figure 28b) confirmed the effect of **12**, showing moderate decrease of AKT1 levels at 4h and 8h and Bcl2 at 8h.

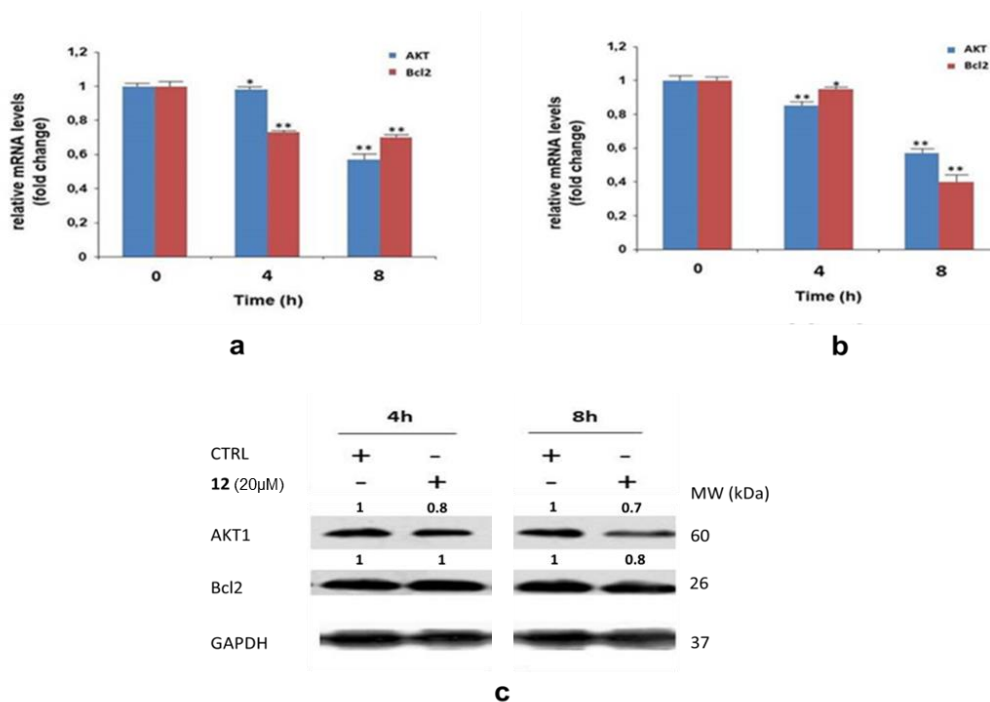


Figure 28: RTq-PCR of AKT1 and Bcl2 mRNAs HeLa cells, treated with **12** 20 μ M (a) and oridonin 5 μ M (b) at 4h and 8h; c). WB of AKT1 and Bcl2 levels HeLa cells treated with **12** 20 μ M.

2.2.9 Inhibition of Protein Synthesis

Nucleolin plays a critical role in several steps of ribosome biosynthesis;⁶⁶ this protein is indeed involved in rDNA transcription,⁶⁸ is associated with nascent pre-rRNAs, helps assembly, and transport of ribosomal particles,⁷⁷ as reported in paragraph 2.1.2. Consequently, Nucleolin interaction with compound **12** could have dramatic effects on protein synthesis. On this basis, we monitored protein neo-synthesis in control cells and in cells after incubation with **12** (20 μ M) for 5h. Cycloheximide, a well-known inhibitor of the protein synthesis, was used as positive control, whereas DMSO was the negative one. Following incubation, the samples were treated with Click-iT® OPP (O-Propargyl Puromycin), a puromycin analog readily taken up by actively growing cells, which inhibits protein synthesis by disrupting peptide transfer on ribosomes

and causing premature chain termination during translation. Addition of the 5-fluorescein azide and the click reaction reagents led to a chemoselective ligation between the azide dye and the alkyne OPP, allowing the modified proteins to be detected. Finally, all the samples were analyzed by flow cytometry. As depicted in Figure 29, cells treatment with the compound (highlighted in green) was comparable with the treatment with DMSO (control). This result demonstrated that 6,19-dihydroxy-*ent*-trachiloban-17-oic acid did not affect the protein synthesis.

Therefore, we could speculate on the involvement of **12** in Nucleolin-mRNA interaction pathways, whereas it is not involved in Nucleolin-mediated ribosome biogenesis pathways.

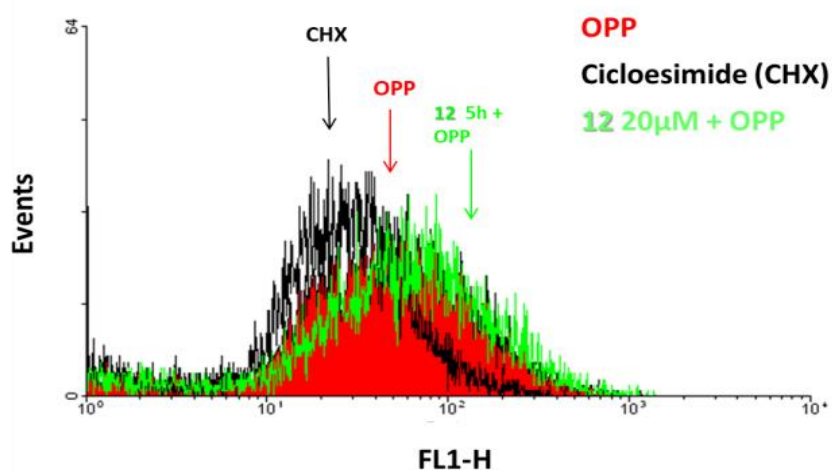


Figure 29: Compound **12** effects on protein synthesis and cell cycle progression. HeLa cells were treated with vehicle (red), 50 µg/mL cycloheximide for 30 min (black), or **12** (20 µM) for 5 h (green). Cells were then incubated with OPP.

2.2.10 Nucleolin(RBD1-2) expression and purification

Once identified the biological effect of 6,19-dihydroxy-*ent*-trachiloban-17-oic acid in HeLa cells on Nucleolin, Bcl2 and AKT1 levels, our next goal was to study more in detail the Nucleolin/**12** complex, in particular the binding site of the interaction. Serin *et al.* in 1999 studied the molecular mechanism of action

of Nucleolin when bound to mRNAs with its RNA-binding domains.¹¹² As mentioned in paragraph 2.1, they discovered that the presence of the first two RNA binding domains of Nucleolin (called RBD1-2) was crucial for the interaction with RNAs; in fact, if one of them is missing, no interaction with RNAs is observed. Furthermore, their activity could be cooperated by the GAR C-terminal domain.⁷⁷ In addition, RBD 3 and 4 are not necessary for the binding with RNAs, since they are mostly specialized in Nucleolin translocation to the cell membrane.⁶⁵ Based on this report, our next goal was to validate our results of reduction of ATK1 and Bcl2 mRNAs. In fact, a possible binding between **12** and Nucleolin (RBD1-2) could prevent its interaction with AKT1 and Bcl2 mRNAs, allowing us to link our data. Therefore, during my six months exchange PhD training at the Biomolekulares Wirkstoffzentrum (BMWZ), Leibniz University (Hannover, Germany) in the research group of Prof. Teresa Carlomagno and in collaboration with Prof. Anna Maria D'Ursi, an expression and purification protocol specific for Nucleolin (RBD1-2) was adopted.¹¹³ A stab culture of BL21 (DE) pLysS cells, containing the plasmid encoding for Nucleolin (RBD1-2), was provided. As shown in figure 30, Tuner cells showed better expression conditions than BL21 without mutation, indeed Tuner cells were selected for Nucleolin purification.

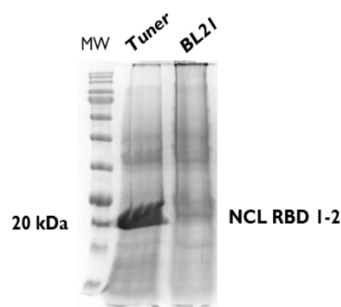


Figure 30. Optimization of Nucleolin (RBD1-2) expression conditions.

Therefore, Tumor cells were lysed by sonication for 20min. After centrifugation (1h at 19,000 g), the supernatant was filtered, added to a superloop connected to a His-trap FF Column (5mL) and analyzed by GE ÄKTA FPLC™ (Figure 31).

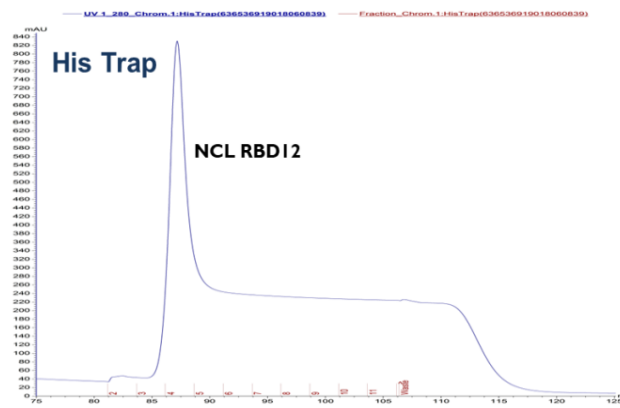


Figure 31. His-Trap purification of Nucleolin (RBD1-2).

Subsequently, protein fractions were collected, concentrated and analyzed by Gel Filtration using a S75 column (figure 32a). The final concentration (28mg/L of LB) was estimated with Bradford reagent (Bio-Rad protein assay) and checked by SDS-polyacrylamide gel electrophoresis (Figure 32b).

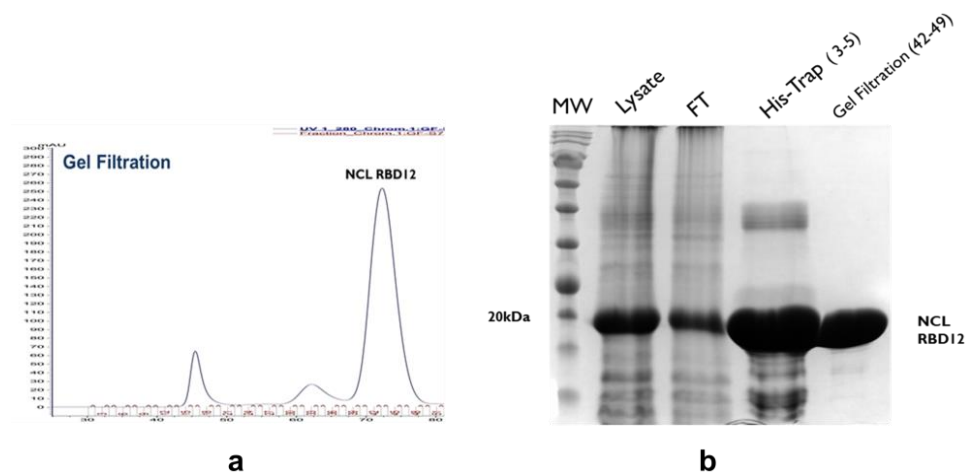
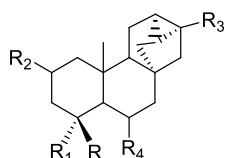


Figure 32. a) Size Exclusion purification of Nucleolin (RBD1-2); b) Final SDS-PAGE of purification steps.

Once expressed and purified Nucleolin (RBD1-2), the next step was to test on these two domains oridonin and **12**, and to perform a screening of diterpenes with similar scaffold to oridonin and **12**. The screening was implemented by different cell-free techniques: Saturation Transfer Difference NMR (STD-NMR), WaterLOGSY and Surface Plasmon Resonance (SPR).

2.2.11 Screening of diterpenes against Nucleolin (RBD 1-2) by Saturation Transfer Difference NMR (STD-NMR)

The first screening was performed by STD-NMR against Nucleolin (RBD1-2), using a small library of thirteen diterpenes, most of them with the same trachilobanic scaffold of compound **12** (figure 33).



Compound	R	R ₁	R ₂	R ₃	R ₄
1	-CH ₃	-CH ₂ OH	H	-CH ₂ OH	OH
2	-CH ₂ OH	-CH ₂ OH	H	-CH ₃	OH
3	-CH ₂ OH	-CH ₂ OH	≡O	-CH ₃	H
4	-CH ₃	-CH ₂ OH	≡O	-CH ₂ OH	OH
5	-CH ₃	-CH ₂ OH	≡O	-CH ₃	OH
6	-CH ₂ OH	-CH ₂ OH	≡O	-CH ₃	OH
7	-CH ₃	-CH ₂ OH	◀OH	-CH ₃	OH

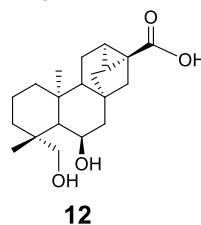
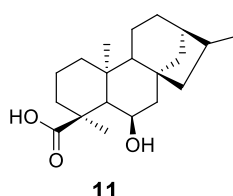
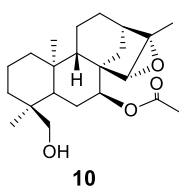
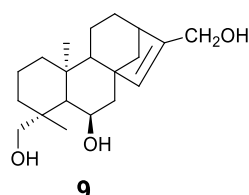
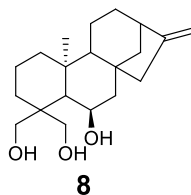
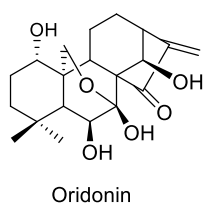


Figure 33. Structures of diterpenes screened against Nucleolin RBD 1-2 by STD-NMR.

The STD-NMR experiment is a spectroscopic technique used to study interactions, in solution, between a large molecule (protein) and a medium-small sized molecule (ligand).³² It is based on the Nuclear Overhauser effect and on the observation and analysis of the resonances of the ligand protons.

In order to start our screening by STD-NMR, the best conditions of saturation for Nucleolin RBD1-2 were set up. Therefore, we recorded a ¹H-NMR spectrum with only Nucleolin (RBD1-2) at high concentration (150 μM, figure 34a) in order to see protonic signals. Subsequently, at the protein sample oridonin 1mM was added (figure 34b). As shown in figure 34b, we decided to irradiate the protein signals at 8.4 ppm, because of the lack of the ligand signals which could not undergo saturation. In fact, we could not irradiate the protein signals from 0 to 1ppm because they were overlapped with the ligand signals. In addition, irradiations with Gaussian and Adiabatic shape pulses were carried out (figure 34c and d). Particularly, the Adiabatic pulse was chosen, allowing us to obtain the best saturation conditions for the protein.

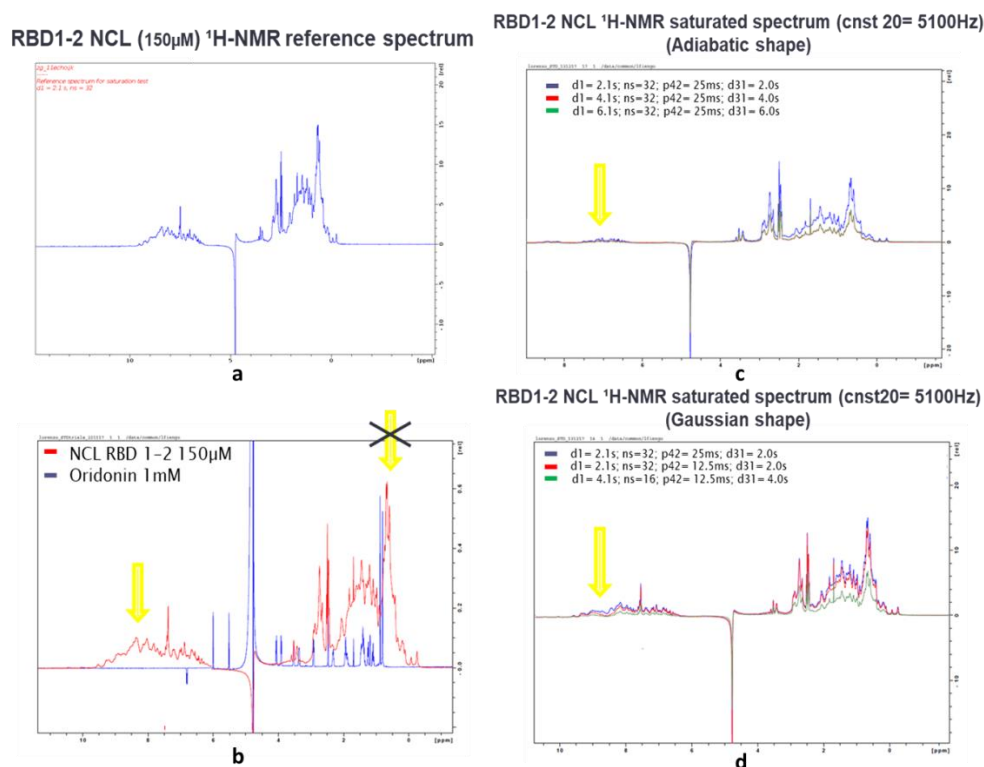


Figure 34. Optimization of STD-NMR. a) $^1\text{H-NMR}$ spectrum of Nucleolin (RBD 1-2) 150 μM . b) $^1\text{H-NMR}$ spectrum of Nucleolin (RBD 1-2) 150 μM and oridonin 1mM. c) $^1\text{H-NMR}$ spectrum of Nucleolin (RBD 1-2) 150 μM saturated in Adiabatic-shape. d) $^1\text{H-NMR}$ spectrum of Nucleolin (RBD 1-2) 150 μM saturated in Gaussian-shape.

Once optimizing the best conditions of saturation for Nucleolin (RBD1-2), samples in ratio ligand:protein 100:1 (1mM:10 μM) were prepared. Achieved spectra led us to assert that compounds **5**, **7** and **8** showed STD effect (figure 35a, b and c respectively). In fact, in the STD spectra (in figure 35a in green, 35b in red, 35c in blue) we could observe intense STD signals (highlighted with green circles) in the range from 0 to 2 ppm. Oridonin and **12** did not show interaction by STD-NMR. This could depend on two reasons:

- it was not possible to see STD-signals because there was a stable interaction (K_D in the nM range or covalent interaction);

- there was interaction but the signals of the protons of the ligand undergo saturation such as the ones of the protein, causing no NOE effect and no transfer of magnetization.

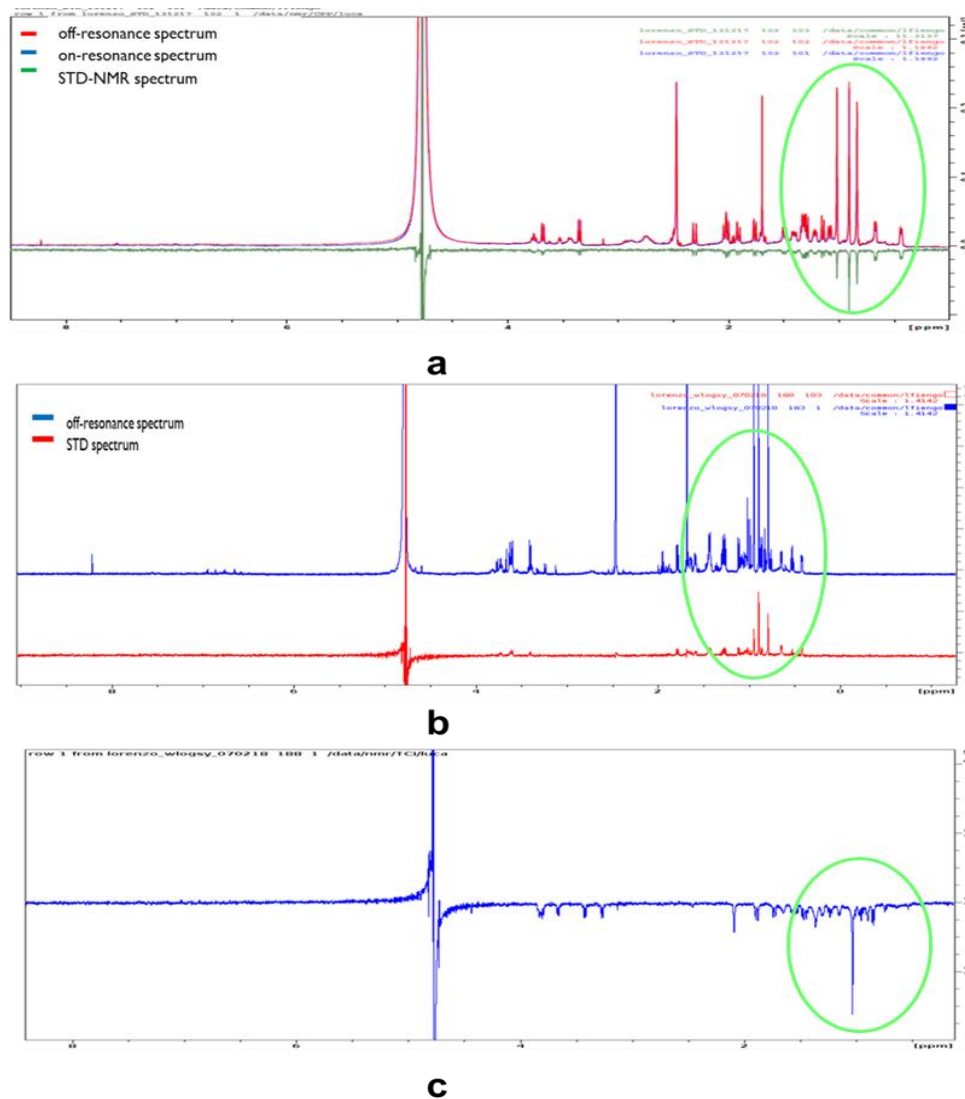


Figure 35. a) 1H-NMR *off-resonance* (in red), *on-resonance* (in blue) and STD-NMR spectrum (in green) of Nucleolin (RBD1-2):5 in comparison; b) 1H-NMR *off-resonance* (in blue) and STD-NMR spectrum (in red) of Nucleolin (RBD1-2):7; c) STD-NMR spectrum (in blue) of Nucleolin (RBD1-2):8.

2.2.12 Screening of diterpenes against Nucleolin (RBD 1-2) by WaterLOGSY

In order to validate and elucidate our STD results, we performed a second screening on the same collection of diterpenes. We decided to perform also WaterLOGSY experiments because STD-NMR can show some limitations, such as the effect of saturation which can be inferred not only on the protons of the protein, but also on the protons of the ligand, resulting in lack of STD-NMR signals. This problem can be overcome using WaterLOGSY (figure 36).³³

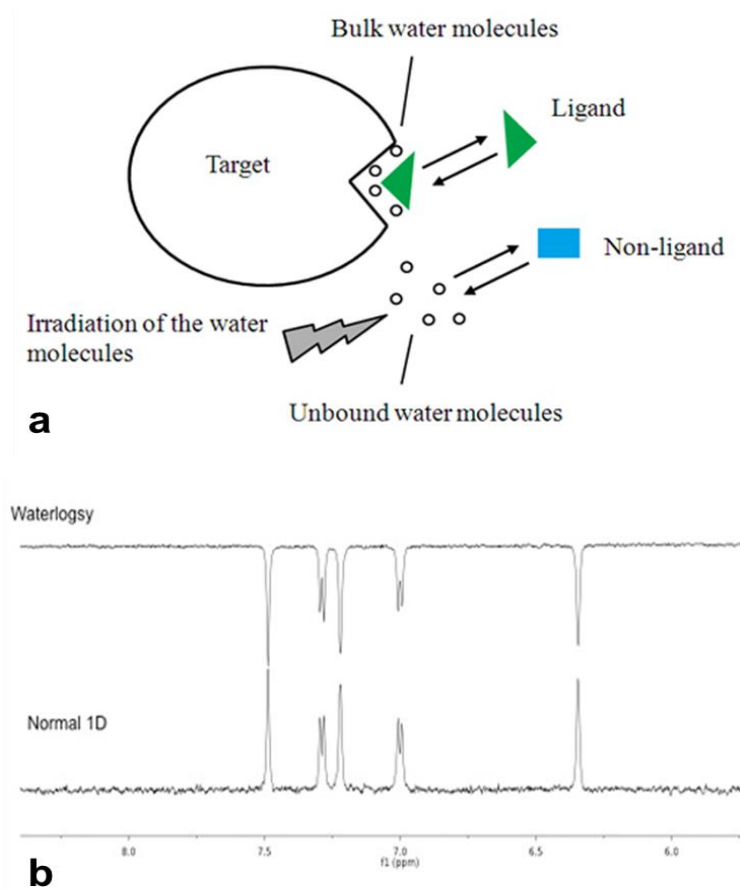


Figure 36. a) WaterLOGSY principle; b) WaterLOGSY spectrum in comparison with Normal 1D ^1H -NMR spectrum. Adopted from FragmentTech.univ-lyon1.fr

WaterLOGSY is a widely applied 1D ligand-observation technique for the detection of protein–ligand interactions. As the STD approach, WaterLOGSY is based on the NOESY experiment, and implies transfer of magnetization via a intermolecular NOE and spin diffusion. The originality of WaterLOGSY comes from the intervention of water molecules in the transfer pathway (Fig. 36a). The bulk water magnetization is excited and transferred during the NOESY mixing time to the bound ligand.

Small molecules that only interact with bulk water (non-binders) will experience much faster tumbling, which translates into a positive NOE (Fig 36b Normal 1D spectrum). Therefore, opposite signs for signals from free versus protein-bound ligands are observed in a WaterLOGSY spectrum, which enables one to easily discriminate binders and non-binders.

In our experimental conditions, a ratio ligand/protein 100:1 was set up for each sample. The WaterLOGSY results allowed us to confirm compounds **5**, **7** and **8** interaction with (RBD1-2) Nucleolin domains (figure 37 a,b and c). Indeed, intense negative NOE signals can be observed in the range 0-2 ppm, whereas for **8** also in the range 3-4 ppm.

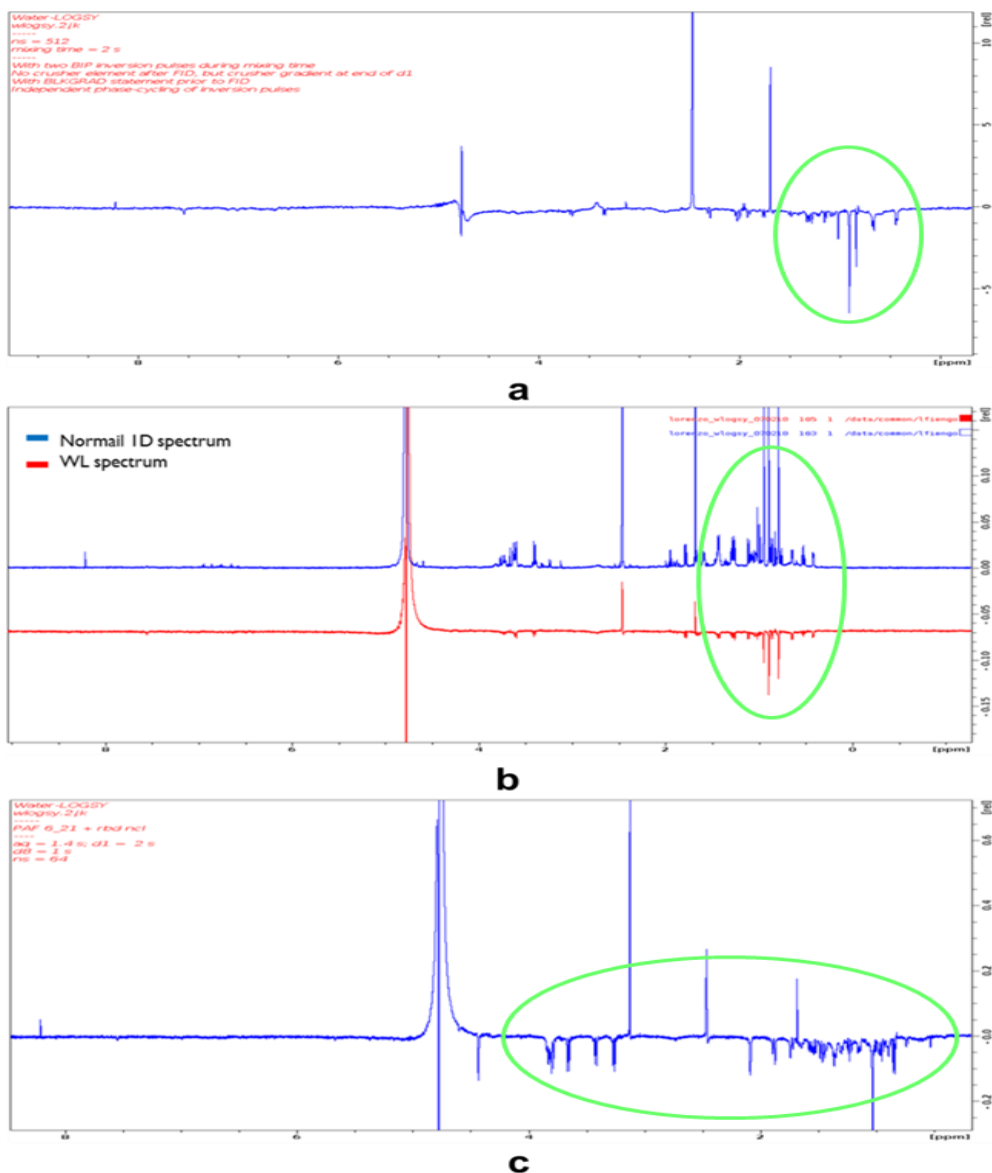
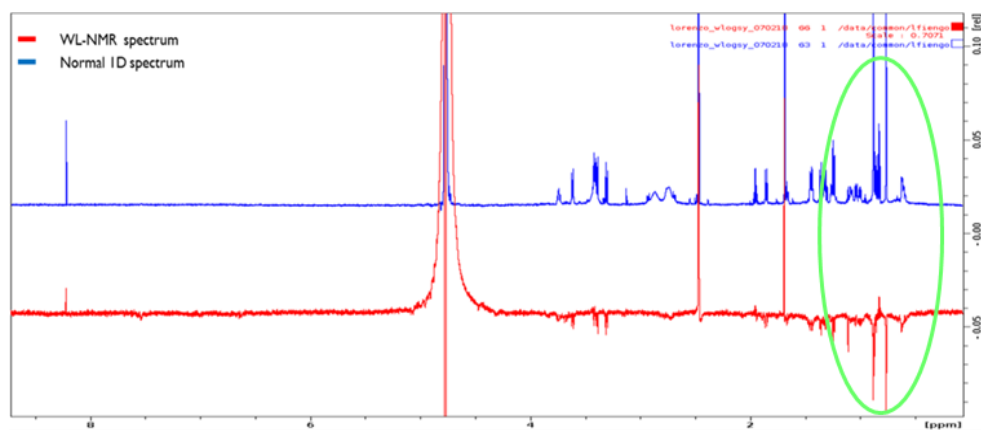


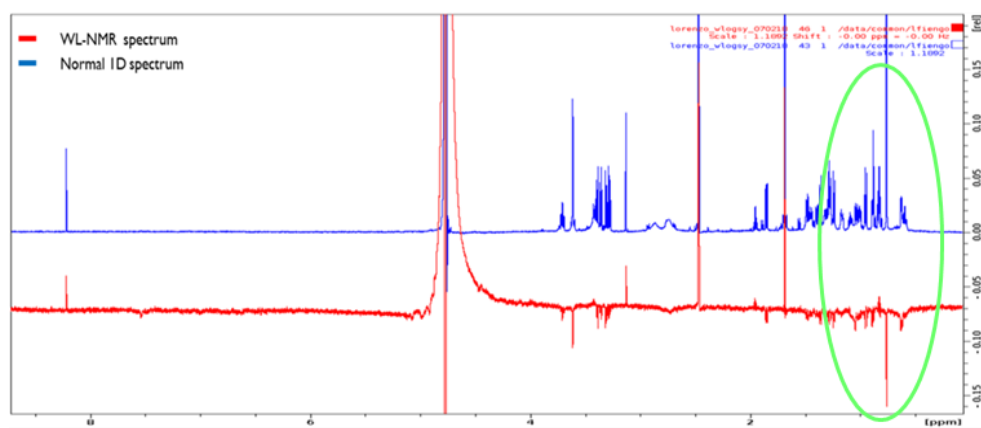
Figure 37. Water-LOGSY experiment. a) Water-LOGSY spectrum of Nucleolin (RBD1-2)/5 (10 μM:1mM). b) Comparison between ¹H NMR spectrum of **7** (in blue) and Water-LOGSY spectrum of Nucleolin (RBD1-2)/7 (10 μM:1mM) (in red). c) Water-LOGSY spectrum of Nucleolin (RBD1-2)/8 (10 μM:1mM).

Interestingly, also **1** and **2** showed Water-LOGSY effect, observing intense negative NOE signals always in the window 0-2 ppm (figure 38a and b, respectively). The reason why no STD effect for these compounds was observed, can be explained with the effect of saturation inferred on the protons

of the ligand whose signals are close to 8 ppm. In Water-LOGSY experiment this problem is overcome, since there is no saturation process on the protein. No interaction was observed with oridonin or **12**: this result led us to suppose a possible covalent binding between these two diterpenes and Nucleolin.



a



b

Figure 38. Water-LOGSY experiment. a) Comparison between ^1H NMR spectrum of **1** (in blue) and Water-LOGSY spectrum of Nucleolin (RBD1-2)/**1** ($10\mu\text{M}:1\text{mM}$) (in red). b) Comparison between ^1H NMR spectrum of **2** (in blue) and Water-LOGSY spectrum of Nucleolin (RBD1-2)/**2** ($10\mu\text{M}:1\text{mM}$) (in red).

2.2.13 Diterpenes/Nucleolin (RBD 1-2) interaction by SPR

To further investigate on a possible diterpenes/Nucleolin (RBD 1-2) covalent interaction, SPR experiments by Biacore technology were implemented.

Therefore, 1 μ M Nucleolin (RBD1-2) in sodium acetate 50 mM, pH 4.16 was opportunely immobilized on a CM5-sensor chip, and the diterpenes were dissolved in PBS buffer in concentrations ranging from 10nM up to 4000nM and injected over the enzyme-modified chip. Compounds **1**, **2**, **5**, **7** and **8** showed interaction with Nucleolin (RBD1-2) with thermodynamic constants lower than 1 μ M. Achieved SPR results were in agreement with previously described WaterLOGSY results (Table 6).

Table 6. Thermodynamic constants measured by SPR for the interaction between tested compounds and immobilized Nucleolin (RBD1-2).

Compound	K_D (nM) \pm SD	k_a [1/(nMxs)]	k_d (1/s)x10 ⁻³
1	660 \pm 0.5	10 \pm 2	6,6 \pm 0.1
2	487 \pm 0.3	82 \pm 7	40 \pm 1
5	308 \pm 0.1	39 \pm 5	120 \pm 3
7	570 \pm 1	100 \pm 11	57 \pm 0.5
8	3750 \pm 2	20 \pm 6	750 \pm 2

According to our last results, for compound **12** and oridonin no interaction with Nucleolin (RBD1-2) was observed by SPR. This result allow us to assert that these two diterpenes probably esplicate their inhibition by binding to other domains of Nucleolin, such as the C-terminal GAR domain. Indeed, as mentioned above, one function of the GAR domain could be to facilitate the interaction of Nucleolin RBD domains with targets located within large and complex RNA.^{49,50} For these reasons, our next goal will be to test our compounds against other domains of Nucleolin.

2.2.14 Conclusions

Taken together, our results suggest 6,19-dihydroxy-*ent*-trachiloban-17-oic acid as a reasonable starting point to obtain small-molecules able to modulate Nucleolin activity. The present discovery might lead to new pharmacological tools to study Nucleolin and Nucleolin-mediated pathologic pathways.

Finally, this compound might represent a promising probe to study more in depth the biology of this protein in cancer cells.

Materials and methods

2.3 Determination of the apparent melting curve (T_m) of Nucleolin in HeLa cells by *Cellular Thermal Shift Assay (CETSA)*.

Approximately 5×10^6 of HeLa cells in a final volume of 10 mL of growth media were used for each condition (DMSO, positive control and treated) in a p100 Petri plate. A stock solution of oridonin (positive control) and of **12** (10 μ L of a 20 mM in DMSO) were added to each Petri plate to get a final concentration of 20 μ M (0.1% DMSO); 10 μ L DMSO was used as control. Cells were gently mixed by pipetting up and down at least 3 times and were incubated for 1 h up to 2 h in the CO₂ incubator at 37 °C. Afterwards, the cell suspensions were collected and centrifuged in 15 mL conical tubes. Cell pellets were washed with PBS and gently suspended each pellet in 1 mL of PBS supplemented with protease inhibitors. Each cell suspension (DMSO, positive control and treated) was divided into 8 different tubes and heated in a PCR machine (Invitrogen Life Science Technologies) at different temperatures (38.4, 41.3, 45.5, 49.8, 52.8, 55.6, 59.8, 61.3 °C) for 3 min. After heating, tubes were kept at R.T. for 3 min and then immediately snap-frozen in liquid nitrogen. After that, cell lysate-containing tubes were centrifuged at 20,000 g for 20 min at 4 °C to pellet cell debris together with precipitated and aggregated proteins. Each supernatant (10 μ L) underwent WB analysis using anti-Nucleolin (rabbit polyclonal, ab22758; Abcam, Cambridge, UK) and anti-GAPDH (rabbit polyclonal, sc-25778; Santa Cruz Biotechnology, Santa Cruz, CA, USA) antibodies. Cell whole lysates for immune-blotting analysis were prepared according to the standard protocol. Protein concentration was

determined by DC Protein Assay (Bio-Rad, Berkeley, CA, USA), using BSA as a standard. Proteins were fractionated on SDS-PAGE, transferred into nitrocellulose membranes, and immune-blotted with appropriate primary antibodies. Signals were visualized with appropriate horseradish peroxidase-conjugated secondary antibodies and enhanced chemiluminescence (Amersham Biosciences-GE Healthcare, NY, USA). Densitometry of bands was performed with ImageJ software. The achieved results were plotted on graphs reporting the ratio between the density measured for each Nucleolin band and the density measured for the corresponding GAPDH band. The density measured for cells kept at 38.4 °C was set as 100%.

2.3.1 Determination of the EC₅₀ of the complex (ITDRF_{CETSA})

Equal number of HeLa cells (5×10^5 cells/well) were seeded in 12 well cell culture plates in 1 mL of growth media and exposed to different concentrations of **12** (0.1, 0.5, 1, 2, 5, 10, 15 and 20 μ M) for 2 h. Following the incubation, the drug-containing media were removed by centrifugation; cells were washed with PBS and prepared for CETSA experiment. In this case cells were heated at 55.5 °C (T_m of Nucleolin) for 3 min, and the experiment was performed as described above. In this case, the density ratio Nucleolin/GAPDH measured at Nucleolin concentration producing the maximum stabilizing effect (20 μ M) was set as 100%.

2.3.2 Drug Affinity Responsive Target Stability (DARTS) experiment

HeLa cells were lysed in RIPA buffer (10 mM Tris-Cl pH 7.6, 1 mM EDTA, 1% Triton X-100, 0.1% sodium deoxycholate, 0.1% SDS, 140 mM NaCl, 1 mM PMSF) supplemented with protease and phosphatase inhibitors. Protein concentration was determined by DC Protein Assay (Bio-Rad, Berkeley, CA, USA), using BSA as a standard. Lysates (30 μ g) were incubated with DMSO (control), or **12** 20 μ M and 5 μ M (to obtain the final concentration of 20 μ M and

5 μ M and 0.1% DMSO). The samples were incubated for 2h at R.T. After that, the samples underwent proteolysis with subtilisin (enzyme: lysate 1:6000 w/w) for 30 min; hydrolysis was stopped adding Laemmli buffer 4X and incubating the mixture at 100 °C for 5 min. Finally, the samples were loaded in duplicate in two 10% mono dimensional SDS-PAGE gels, in order to perform at the same time MS and WB analyses.

The first gel was treated with Fixing solution (MeOH:CH₃COOH:H₂O 4:1:5) for 30 min and then stained with Brilliant Blue G-Colloidal (Sigma-Aldrich) overnight. After washing with water, Bands appearing more intense in the treated samples than in the control ones were excised from both the gel lanes and subjected to classical in gel digestion procedure by trypsin (Promega, Milano, Italy). The resulting fragments were extracted and analyzed by LC/MS/MS. MS and MS/MS data were used by Max Quant and Mascot Daemon Matrix Science softwares. The proteins detected in treated samples but not in controls were taken into account as possible **12** targets. This DARTS experiment was performed in triplicate.

The proteins on the second gel were transferred into a nitrocellulose membrane, and immunoblotted with the appropriate primary antibody (1:1000). Signals were visualized with the appropriate horseradish peroxidase-conjugated secondary antibody and enhanced chemiluminescence (Amersham Biosciences-GE Healthcare, NY, USA). Densitometry of bands was performed with ImageJ software.

A similar procedure was performed to carry out DARTS on living cells. HeLa cells (5 \times 10⁶ cells/well) were treated with **12** (5 or 20 μ M) or 0.1% DMSO for 2 h at 37 °C. Cells were lysed with RIPA buffer (10 mM Tris-Cl pH 7.6, 1 mM EDTA, 1% Triton X-100, 0.1% sodium deoxycholate, 0.1% SDS, 140 mM NaCl, 1 mM PMSF) supplemented with protease and phosphatase inhibitors (P8340, Sigma-Aldrich, St. Louis, MO, USA). After centrifugation

and determination of protein concentration, each lysate (30 µg) was diluted with PBS, quickly warmed to R.T. and proteolysed with subtilisin (enzyme: lysate 1:6000 w/w) for 30 min. Reaction mixture was then analyzed as described above. Also in this case, DARTS experiment was performed in triplicate, and the proteins identified in all the experiments were considered putative **12** targets.

2.3.3 Wound Healing assay

Equal number of HeLa cells (3×10^5 cells/points) were seeded in a 6 well cell culture plates in 1 mL of growth media (DMEM high glucose with glutamine, 10% FBS, 1% pen/strep). After 24h they were treated with **12** 20 µM or 0.1% DMSO (control). After incubation for 72h at 37°C, a 1-mm wide scratch was made across the cell layer using a sterile pipette tip. After washing with PBS, DMEM medium was added to replace matrix depleted with the scratch. Using LAS-EZ software, each plate was photographed immediately after scratching, and the healing process was monitored at the electronic microscope each hour up to 24h at the identical location of initial image. For each scratch 4 measurements (distance between two sides of the scratch measured in pixels) were carried out, and the difference between the cell migrations after 1h and 24h of incubation with DMSO (control) or **12** was calculated. All experiments were performed at least two times in triplicates.

2.3.4 RNA isolation and quantitative Real-Time-PCR (qRT-PCR)

Total RNA was isolated using Trizol Reagent (Life Technologies, Grand Island, NY, USA) according to the manufacturer's instructions and spectrophotometrically quantified. RNA integrity was assessed by agarose gel electrophoresis. RNA (3 µg) was reverse transcribed, and real-time PCR was performed with Light-Cycler® 480 (Roche Diagnostics GmbH, Mannheim, Germany) using SYBR Green detection in a total volume of 20 µL with 1 µL

of forward and reverse primers (10 mM) and 10 µL of SYBR Green I Master Mix (Life Technologies). Reactions included an initial cycle at 95 °C for 10 min, followed by 40 cycles of denaturation at 95 °C for 10 sec, annealing at 56 °C for 5 sec, extension at 72 °C for 15 sec. The 18S RNA was used as an internal standard. The following primer sets were used for real-time PCR to assay specific mRNAs:

forward Akt 5'-TCT ACA CCC ACA GAT GAC AG-3'

reverse Akt 5'-CTC AAA TGC ACC CGA GAA AT-3'

forward Bcl-2 5'-GGA AGT GAA CAT TTC GGT GAC-3'

reverse Bcl-2 5'-CTC CAT CAG CTT CCA GAC AT-3'

forward 18S 5'-CGA TGC TCT TAG CTG AGT GT-3'

reverse 18S 5'-GGT CCA AGA ATT TCA CCT CT-3'

2.3.5 Protein Synthesis assay

HeLa cells (4×10^5 cells/well) were incubated with **12** (20 µM for 5h), respectively, or with 50 µg/mL cycloheximide (CHX) for 30 minutes, in a cell culture incubator. Cells were then processed for detection of protein synthesis according to the protocol described in the Protein Synthesis Assay Kit (Cayman Chemical, Michigan, USA). Following incubation, the samples were treated with Click-iT® OPP (O-Propargyl-Puromycin), and added of 5-fluorescein azide, the click reaction reagents leading to a chemoselective ligation between the azide dye and the alkyne OPP, allows the modified proteins to be detected. Finally, all the samples were analyzed by flow cytometry.

2.3.6 Cell viability and cell cycle analysis

The number of viable cells was quantified by MTT [3-(4,5-dimethylthiazol-2-yl)-2,5-diphenyl tetrazolium bromide] assay. Absorption at 550 nm was

assessed using a microplate reader (LabSystems, Vienna, VA, USA). Cell viability was also checked by Trypan Blue exclusion assay using a Bürker counting chamber.

Cell cycle was evaluated by propidium iodide (PI) staining of permeabilized cells according to the available protocol,¹⁰⁹ and flow cytometry (BD FACSCalibur *flow cytometer*, Becton Dickinson, San Jose, CA, USA). Data from 5000 events per sample were collected. The percentages of the elements in the hypodiploid region and in G₀/G₁, S and G₂/M phases of the cell cycle were calculated using the CellQuest and MODFIT software, respectively.

2.3.7 Determination of apoptosis

HeLa cells (3x10⁵ cells/well) were incubated with DMSO (control), (phenethyl isothiocyanate (PEITC, positive control) 10µM for 24h and **12** 20µM for 48h in a cell culture incubator. Cells were then processed for detection of apoptosis according to the protocol described in the Annexin V, FITC Apoptosis Detection Kit (Dojindo EU GmbH, Munich (Germany)). Following incubation, HeLa pellets were washed twice with PBS and suspended in 100µL of Annexin V Binding Solution; subsequently, 5µL of Annexin V, FITC conjugate and 5µL of PI Solution were added in each sample and incubated for 15 min at room temperature with protection from light. After adding 400µL of Annexin V Binding Solution, samples were detected by Flow Cytometry (BD FACSCalibur *flow cytometer*, Becton Dickinson, San Jose, CA, USA) and analyzed by BD Facsuite software.

2.3.8 Expression and purification of recombinant NCL (RBD1-2)

Tuner cells (BL21 (DE3) with a mutation in the lac permease (lacZY) gene) were transformed with recombinant pET15b plasmid containing the gene for Nucleolin (RBD1-2). Cells were grown at 37 °C in LB (100 mg/liter

ampicillin) at 200 rpm and induced with 0.1 mM isopropyl-1-thio- β -D-galactopyranoside. After induction the cells were incubated overnight at 16 °C at 200rpm. The cells were harvested and resuspended in buffer A (Tris 50 mM, NaCl 100 mM, 50% Glycerol, imidazole 10mM, β -mercaptoethanol 5mM, pH 7,6) with DNase I (5 mg/ml), lysozyme and protease inhibitors (Complete EDTA-free tablets, Roche). The cells were then lysed by sonication for 20min and centrifuged. After centrifugation (1h at 19,000 g), the clarified cell lysate was loaded on a His-trap FF Column (5mL) and the His-tagged Nucleolin (RBD1-2) was purified using GE ÄKTA FPLC™. Subsequently, protein fractions were collected, concentrated and further purified by size exclusion chromatography using superdex75 16/600 column in buffer B (Na₂HPO₄ 50mM, NaH₂PO₄ 8mM, NaCl 150mM, pH 7.6). The concentration of the protein was estimated by measuring absorbance at 280nm. SDS-polyacrylamide gel electrophoresis was used to assess the purity of the protein.

2.3.9 Ligand-binding NMR experiments

NMR spectra to detect ligand-binding were recorded on a 600 MHz Bruker Avance III-HD spectrometer equipped with a cryogenic (nitrogen-cooled) inverse probe-head. Samples were prepared in phosphate-buffered saline (PBS) at pH 7.6, to which 10 % v/v D₂O (Carlo Erba) was added for the NMR field-frequency lock. Final samples with a volume of ~500 uL were transferred to 5-mm-diameter NMR tubes for measurement. All spectra were recorded at a temperature of 278 K.³²

2.3.10 Saturation Transfer Difference NMR (STD-NMR) analysis

The STD pulse-sequence consists of an extended period of RF irradiation to saturate the protein resonances followed by a read-out element (in this work, the 3-9-19 WATERGATE sequence was used as the read-out element). Saturation of the protein resonances was achieved with an adiabatic pulse-

train; prior to acquiring the STD spectra, the parameters for the adiabatic pulse were first optimized on a sample of Nucleolin (RBD1-2) alone at a concentration of $\sim 150 \mu\text{M}$. The final optimized adiabatic pulse was a constant-adiabaticity WURST-2 pulse with a pulse-length of 25 ms, a sweep-width of 2 ppm and a B1 field-strength corresponding to an adiabaticity Q-factor of 3 ($v_{1,\text{max}} = 247 \text{ Hz}$). The saturation pulse-train was applied for the entire duration of the inter-scan recycle delay. STD spectra (256 scans with a recycle delay of 4 s and acquisition time of 1.3 s) were then recorded for samples of 14 ligands at a concentration of 1 mM in the presence of $10 \mu\text{M}$ Nucleolin (RBD1-2). Each final STD spectrum is calculated as the difference between two sub-spectra in which the protein is either saturated (the "on-resonance" sub-spectrum) or unsaturated (the "off-resonance" or reference sub-spectrum). The two sub-spectra for each ligand were recorded in an interleaved fashion with identical parameters except for the transmitter frequency of the saturation pulse-train, which was positioned at 8.6 and 100 ppm for the on- and off-resonance sub-spectra, respectively.³²

2.3.11 WaterLOGSY experiment

The water-LOGSY sequence consists of an initial e-PHOGSY element to destroy all non-water magnetization, a mixing period to allow magnetization-transfer, and final read-out element (in this work, the excitation-sculpting sequence was used as the read-out element; this read-out element was preceded by a water flip-down pulse in order to preserve the water magnetization). The water-selective refocusing pulse in the e-PHOGSY element was a 25-ms ReBURP pulse. Two broadband-inversion-pulses were applied during the mixing period (at \sim one-quarter and \sim three-quarters of the mixing-time) to improve suppression of auto-relaxed signals. Water-LOGSY spectra (512 scans with a mixing time of 1 s, a recycle delay of

3 s and an acquisition time of 1.3 s) were recorded for 14 samples (1 mM ligand in the presence of 10 μ M Nucleolin (RBD1-2)).^{33, 114}

2.3.12 Surface Plasmon Resonance (SPR)

SPR studies were performed using an optical biosensor BIACORE 3000 (GE Healthcare, Milano, Italy). Nucleolin (RBD 1-2) (6 mg/ml) was immobilized on a CM5 sensor chip using a 1 μ M protein solution in sodium acetate 50 mM, pH 4.16. using a standard amine-coupling protocol. All the compounds were dissolved in 100% DMSO to obtain 4 mM solutions, and diluted in PBS (10 mM NaH₂PO₄, 150 mM NaCl, pH 7.4) to a final DMSO concentration of 0.5%. The binding study was performed using a five-point concentration series (10, 100, 500, 1000 and 4000 nM) and triplicate aliquots of each compound concentration were dispensed into single-use vials. Binding experiments were performed at 25 °C, using a flow rate of 50 μ L/min, with 60 s of association and 300 s dissociation monitoring time. Simple interactions were adequately fit to a single-site bimolecular interaction model, yielding a single KD. Sensorgram elaboration was performed using the BIAevaluation software provided by GE Healthcare.

2.3.13 Western Blot analysis

Cell whole lysates (HeLa) immunoblot analysis were prepared according to the standard protocol. Protein concentration was determined by DC Protein Assay (Bio-Rad, Berkeley, CA, USA), using bovine serum albumin (BSA) as a standard. Proteins were fractionated on SDS-PAGE, transferred into nitrocellulose membranes, and immunoblotted with the appropriate primary antibody (1:1000). Signals were visualized with the appropriate horseradish peroxidase-conjugated secondary antibody and enhanced chemiluminescence (Amersham Biosciences-GE Healthcare, NY, USA). Densitometry of bands was performed with ImageJ software.

2.3.14 Reagents and Antibodies

Fetal bovine serum (FBS) was from GIBCO (Life Technologies, Grand Island, NY, USA). The anti-Nucleolin (rabbit polyclonal, ab22758) and anti-phospho T76-Nucleolin (rabbit monoclonal) were purchased from Abcam, Cambridge, UK. Anti-pAkt (rabbit polyclonal sc-7935-R), anti-Akt (rabbit polyclonal), anti-Bcl2 (mouse monoclonal sc-7382), anti- α -Tubulin (mouse monoclonal sc-32293), anti-GAPDH (rabbit polyclonal), anti-caveolin (rabbit polyclonal sc-894), were obtained from Santa Cruz Biotechnology (Santa Cruz Biotechnology, Inc., Delaware, CA, USA); anti-Lamin A (rabbit polyclonal, L1293) was purchased from Sigma-Aldrich (USA); appropriate peroxidase-conjugated secondary antibodies were from Jackson Immuno Research (Baltimore, PA, USA).

2.3.15 Cytosol and membrane extracts

After incubation of HeLa cells with oridonin (5 μ M) and **12** (20 μ M) for 4h at 37°C, the cells were washed twice with PBS, detached with trypsin-EDTA 1x in PBS (Euroclone), harvested in PBS and centrifuged for 5 minutes at 600 x g at 4°C. After that, the pellets were resuspended in 4 mL of lysis buffer (Tris HCl 20 mM, pH 7,4; sucrose 250 mM; DTT 1 mM; protease inhibitors, EDTA 1 mM in water), sonicated (5 seconds pulse - 9 seconds pause for 2 minutes, amplitude 42%) and then centrifuged at 4°C for 10 minutes, at 5000 x g. The obtained supernatants were ultra-centrifuged for 1 hour at 100000 x g at 4°C, until to get new supernatants that represent cytosol extracts. Each resulting pellet was resuspended in 4 mL of lysis buffer and ultra-centrifuged for 1 hour at 100000 x g at 4°C. The pellets were then resuspended in 250 μ L of solubilization buffer (Tris HCl 20 mM, pH 7,4; DTT 1 mM; EDTA 1 mM; Triton X-100 1%, in water) and left overnight on orbital shaker at 4°C. After that, the solution was centrifuged for 30 minutes at 50000 x g at 4°C: the supernatants represent the membrane extracts.

2.3.16 Nuclear extracts

HeLa cells were incubated with oridonin (5 μ M) and **12** (20 μ M) for 4h at 37°C, then washed twice with PBS, detached with trypsin-EDTA 1x in PBS (Euroclone), harvested in PBS and centrifuged for 5 minutes at 600 x g at 4°C. The pellets were resuspended in 500 μ L of buffer A (Hepes pH 7.9 10 mM, EDTA pH 8.0 1 mM, KCl 60 mM, N-P40 0.2%, DTT 1 mM, phenylmethylsulfonyl fluoride (PMSF) 1 mM, protease inhibitors) and then left on ice for 10 minutes. After that, the samples were centrifuged at 660 x g for 5 minutes at 4°C, resuspended in 50 μ L of buffer B (Tris HCl pH 7.8 250 mM, KCl 60 mM, DTT 1 mM, PMSF 2 mM, glycerol 20% v/v in PBS) and centrifuged again at 9500 x g for 15 minutes at 4°C. The obtained pellets were resuspended in 100 μ L of buffer C (Hepes pH 7.9 10 mM, EDTA pH 8.0 1 mM, KCl 60 mM, DTT 1 mM, PMSF 1 mM, protease inhibitors) and centrifuged at 660 x g for 5 minutes at 4°C. The samples were then washed twice with 1 mL of buffer C, resuspended in 50 μ L of buffer B and exposed to 3 cycles of freeze/thawing. Finally, the samples were centrifuged at 9500 x g for 15 minutes at 4°C: the supernatants represent the nuclear extracts.

2.3.17 Statistical analysis

Data are reported as the mean values \pm SD from at least three experiments, performed in duplicate ($n \geq 6$), showing similar results. Differences between treatment groups were analyzed by Student's t-test. Differences were considered significant when $p < 0.05$.

- Chapter 3 -

Introduction

3.1 Heat Shock Proteins (HSPs) family

Stress or heat shock proteins (HSPs) are a family of highly conserved proteins, induced in response to a wide range of physiological and environmental insults such as hypoxia, hyperoxia, exposure to UV light and chemicals, viral agents, heavy metals, surgical stress, nutritional deficiencies (e.g. glucose deprivation), emotional and mechanical stress, or other stresses. They maintain cellular homeostasis under stress or allow the cell survival to lethal conditions.^{115, 116} Mammalian HSPs have been classified into six families depending on their molecular size: Hsp100, Hsp90, Hsp70, Hsp60, Hsp40 and small HSPs (15 to 30 kDa) including Hsp27. Family members of HSPs are expressed either constitutively or inductively, and are localized in different subcellular compartments. HSPs with high molecular weight are ATP-dependent chaperones, whereas small HSPs act in an ATP-independent way. As molecular chaperones, the function of HSPs is to regulate protein folding, transport, translocation and assembly, especially helping in the refolding of misfolded proteins or assisting in their removal, if they are damaged after various stresses or environmental insults.¹¹⁷

Cancer cells, with higher metabolic requirements and more abundant signal transduction pathways than normal cells, need a higher amount of chaperones than normal cells in order to survive. Several studies have reported that overexpression of the HSPs increases tumor growth, metastatic potential, and resistance to chemotherapy in both human and animal models. Being involved in the folding and stabilization of relevant oncoproteins, HSPs stand at the crossroads of multiple oncogenic pathways. Therefore, inhibition of HSPs offers the unique advantage of depleting multiple oncoproteins affecting several pathways necessary for tumor progression.¹¹⁸ The most studied stress-

inducible HSPs are Hsp90, Hsp70 and Hsp27, whose expression and/or activity is abnormally high in cancer cells and increases after many different death stimuli.¹¹⁷ They are powerful anti-apoptotic proteins, associating with key apoptotic factors (Fig. 1), and thereby blocking this cell death process at different levels.¹¹⁹ The inhibition of Hsp90, Hsp70 and/or Hsp27 represents an interesting strategy for cancer therapy.

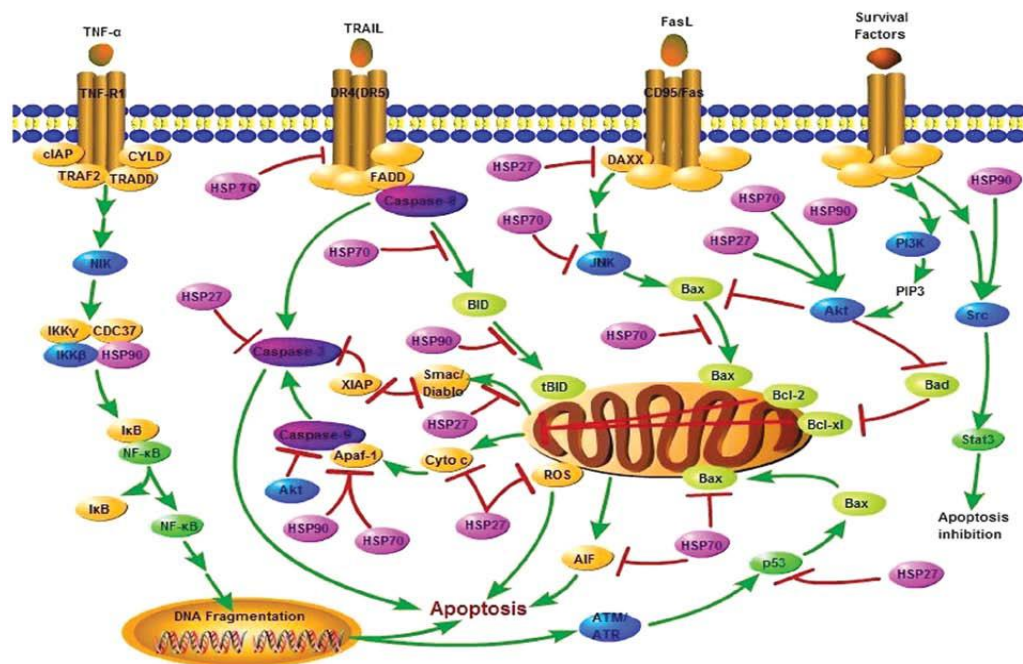


Figure 1. Hsp27, 70, 90 in the regulation of apoptosis and proliferation. Hsp27, 70 and 90 regulate apoptosis at different levels, from the death receptors signaling to executors of cell death program, affecting both upstream and downstream of the death-associated mitochondrial pathways. Induction of caspases activation determines proteasome activation. Moreover, HSPs facilitate the degradation of proteins by the ubiquitin/proteasome system. Adopted form: Wang X *et al.*, *Inter J Oncol.* 2014; 45: 18-3.

3.1.1 Heat Shock Protein 70 (Hsp70): structure, localizations and roles

The Hsp70 family of molecular chaperones plays central roles in all the aspects of proteostasis, from protein folding to disaggregation and degradation.¹²⁰ Hsp70 chaperones can interact with most proteins in their unfolded, misfolded or aggregated states, and can actively fold, solubilize, and

reactivate already formed, stable protein aggregates.¹²¹ With the help of its co-chaperones, some Hsp70s recognize a limited set of native proteins, and regulate or even redefine their activity.¹²² Although the prokaryotic system has a single Hsp70 (the archetypical DnaK), the number of genes has expanded in eukaryotes, which express distinct Hsp70 isoforms in different physiological conditions and subcellular locations (Table 1). The human genome encodes 13 Hsp70 isoforms; three are constitutively expressed, heat shock cognate protein (Hsc70 or HSPA8, which accumulates in cytosol and the nucleus), Bip (HSPA5 or 6RP78, endoplasmic reticulum) and mortalin (HSPA9 or 6RP75, mitochondrial). The expression of other Hsp70, particularly Hsp70-1 (HSPA1A/B), is inducible (after cell stress).

Table 1. Localization and isoforms of the Hsp70/Hsc70

Subcellular location	Protein	Expression/Tissue
Cytosol	HSPA1A (HSP70-1; HSP72; HSPA1); HSPA1B (HSP70-2); HSPA1L (hum70t; Hsp-hom); HSPA6 (HSP70B'); HSPA8 (HSC70; HSC71; HSP71; HSP73); HSPA9 (GRP75; HSPA98; MOT; MOT2; PBP74); HSPA14 (HSP70-4; HSP70L1; MCG131990);	Inducible/all tissues Inducible/all tissues Constitutive/spermatides Inducible/most tissues Constitutive/all tissues Constitutive/many tissues Undetermined/many tissues
Nucleus	HSPA1A (HSP70-1; HSP72; HSPA1); HSPA1B (HSP70-2); HSPA1L (hum70t; Hsp-hom); HSPA2 (Heat shock 70 kD protein-2); HSPA6 (hum70t; Hsp-hom); HSPA8 (HSC70; HSC71; HSP71; HSP73);	Inducible/all tissues Inducible/all tissues Constitutive/spermatides Constitutive/Variou tissues Inducible/most tissues Constitutive/All tissues
Endoplasmic Reticulum	HSPA5 (BIP; GRP78; MIF2); HSPA9 (GRP75; HSPA98; MOT; MOT2; PBP74);	Inducible/All tissues Constitutive/Many tissues
Mitochondrion	HSPA9 (GRP75; HSPA98; MOT; MOT2; PBP74);	Constitutive/Many tissues
Microsomes	HSPA13 (Stch);	Constitutive/All tissues

Apart from its intracellular localization, Hsp70 (also termed HSP70A1A) was found also on the plasma membrane, playing pivotal roles in eliciting anti-tumor immune response. Shevtsov *et al.* determined a tumorselective Hsp70 membrane expression, whereas a membrane Hsp70-positive tumour phenotype is associated with aggressiveness and therapy resistance. Therefore, membrane Hsp70 represents a recognition structure for targeted therapies,

allowing us to identify it as a target for novel therapies in the treatment of cancer.¹²³

Structurally, Hsp70 has two functional domains, connected by a short and highly conserved interdomain linker (Fig. 2):

- The N-terminal Nucleotide-Binding Domain (NBD; 45 kDa) structurally shows an actin/hexokinase fold, having a V-shaped structure composed of two subdomains that enclose the ATP-binding site (Fig 2a in blue).

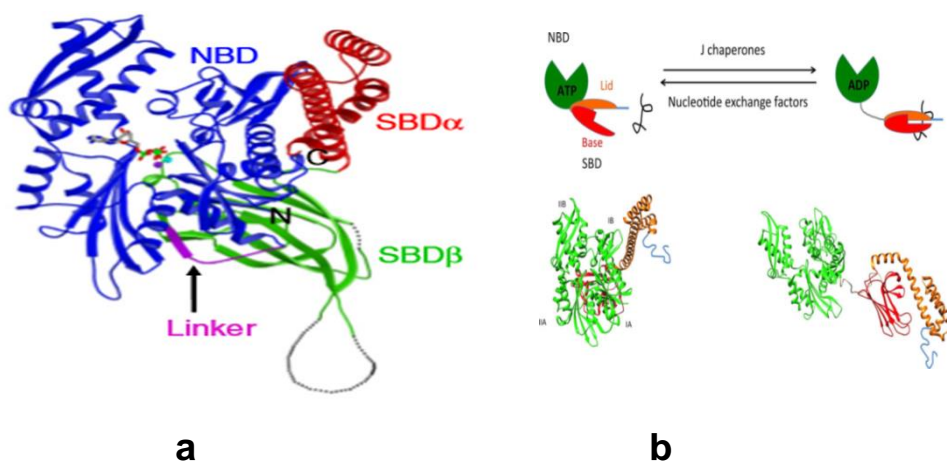


Figure 2. a) cristal structure of HSP70; b) different conformations of SBD; Adopted from Kumar DP *et al.* 2011; *J Mol Biol.* 411, 1099–1113.

Both NBD subdomains and the connecting helixes create the binding pocket for the nucleotide and Mg^{2+} and K^+ ions at the bottom of the cleft (Fig 3). The nucleotide is positioned into the active site by interactions with two phosphate-binding loops and a hydrophobic adenosine binding pocket, together with contacts with the Mg^{2+} ion, which is coordinated by several side chains of Hsp70. McKay and coworkers have proposed a mechanism for ATP hydrolysis: structural rearrangement of Hsp70 during ATP binding leads to adjustment of the position of the γ -phosphate so that a bidentate complex is formed between the β and γ -phosphate oxygens and Mg^{2+} , allowing the attack by a water (or OH^-) which is hydrogen bonded to Lys-71 (Fig 3). Precise

geometry of the nucleotide and the surrounding residue requires the correct positioning of the Mg^{2+} ion, established in part by the binding of two K^+ ions nearby.¹²⁴

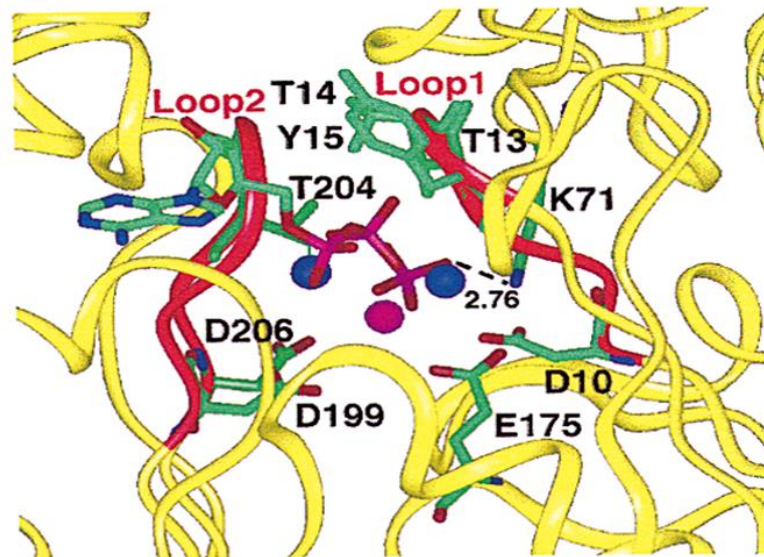


Figure 3. ATPase domain of Hsp70. Bound to it, ADP, Pi, Mg^{2+} (magenta), and two K^+ ions (blue) are indicated. The backbone of phosphate binding loops 1 (residues 10–15) and 2 (residues 199–206) is indicated in red, and the side chains involved in positioning the phosphates of bound nucleotide and Mg^{2+} (including Lys-71) are shown as green sticks. Adopted from Bukau B, Horwich AL. 1998; *Cell*. 92: 351–366.

- The C-terminal, Substrate-Binding Domain (SBD; 25 kDa), possesses two subdomains: a β -sheet domain (SBD β , fig 2a in green) or base, and a α -helical (SBD α , fig 2a in red) or Lid domain. The SBD recognizes and interacts with a motif present every 30–40 residues in several proteins; it is a five-residue motif enriched in hydrophobic amino acids and positively charged residues.¹²⁵ This type of hydrophobic region is usually found in the protein core, and its exposure signals a misfolded conformation. The SBD adopts two different conformations, the open and the closed ones; the switch between them is controlled by ATP binding to NBD (Fig. 2b). Indeed, the two functional domains have to be coupled to make a functional chaperone, which leads to modulation of the two intrinsic activities.¹²⁶

The crystal structure of the substrate binding domain of Hsp70 shows a β sandwich composed of two sheets of four strands each, followed in the primary structure by two α helices, A and B, which are positioned back over the sandwich (Fig. 4). The top sheet emanates four loops, two of which form the substrate binding pocket, a channel with a cross section of $5 \times 7 \text{ \AA}$. Along with loops at either side, they are stabilized by critical contacts with the overlying helix B, which may function as a lid in permitting entry and release of substrate (without directly contacting it). The most extensive contacts are hydrophobic side-chain interactions between the loops and three central leucines in the peptide. In order to obtain these contacts, the bound region of the polypeptide must be substantially unfolded.¹²⁷

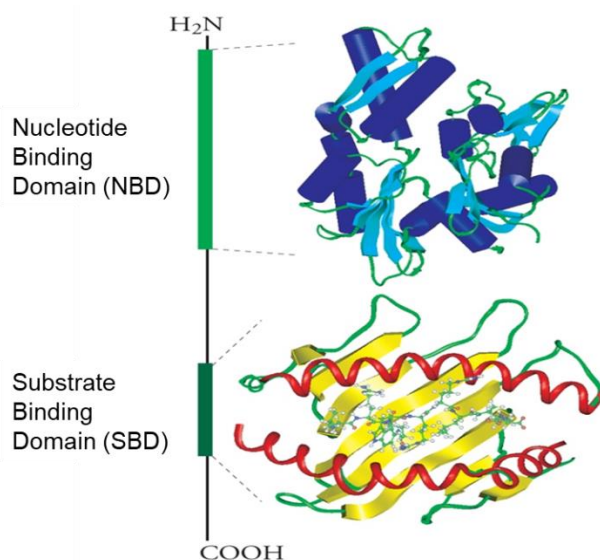


Figure 4. Crystal structure of NBD and SBD domains of Hsp70. Adopted from Bukau B, Horwich AL. 1998; *Cell*. 92: 351–366.

Hsp70 function is fine-tuned by the cooperation of a variety of cochaperones, which bind to Hsp70 and modulate its activity by increasing or decreasing the chaperone affinity for substrates, through the stabilization of the ADP or ATP bound state of Hsp70. They can be classified into three groups:

- The J-domain co-chaperones, like Hsp40, constitute a relatively large group of proteins that binds to the Hsp70 NBD and positively modulates the ATPase activity of this chaperone.
- The nucleotide exchange factor (NEF) co-chaperones catalyze the release of ADP, required for the completion of the ATPase cycle. Members of this group are BAG-1, BAG-3, Hsp110, or HspBP1.
- The TPR domain co-chaperones (Hop, CHIP) bind to the C-terminal EEVD motif presented in both Hsp70 and Hsp90. They are essential for combinational assembly of Hsp70 and Hsp90 complexes, required for the stabilization of Hsp90 client proteins.

The first two groups of these co-chaperones are required for the Hsp70 functional cycle.^{128, 129} J-proteins accelerate ATP hydrolysis and thus induce the achievement of the closed conformation, whereas NEFs promote ADP/ATP exchange and the open conformation. Both groups interact with Hsp70 through its NBD (Fig. 2b). The BAG proteins (Bcl-2-associated athanogene) are NEFs that use a conserved BAG domain to interact with the interface formed by NBD subdomains IB and IIB to promote nucleotide cycling.¹³⁰ The C-terminal-most Hsp70 domain (CTD) bears an EEVD amino acid motif that interacts with distinct cochaperones, which in turn guide Hsp70-bound substrate towards folding or degradation.¹³¹

Hsp70 has a prominent role in the ATP hydrolysis cycle (Fig. 5). When ATP is bound to the NBD, it induces the open conformation by separating the base and Lid subdomains. In this conformation, the SBD is in contact with the NBD and has low affinity for the substrate. The Hsp70 closed conformation is achieved after ATP hydrolysis; the NBD induces a change in the SBD such that the base and Lid subdomains come closer together and trap the substrate. SBD structural rearrangements are transmitted from the NBD via a flexible, conserved linker that contacts the NBD in the open state, and detaches in the

closed conformation. Two types of cofactors control the cycling of this ATPase between the two conformations: the J chaperones and the NEF. Through the intermediary of the J domain, Hsp40 binds to Hsp70 and promotes its ATPase activity, thus generating the ADP-bound Hsp70, which stably interacts with client protein. After the nucleotide exchange factor (NEF) intervention, the substrate is released from Hsp70 and leaves the cycle as a correctly folded protein.¹³¹

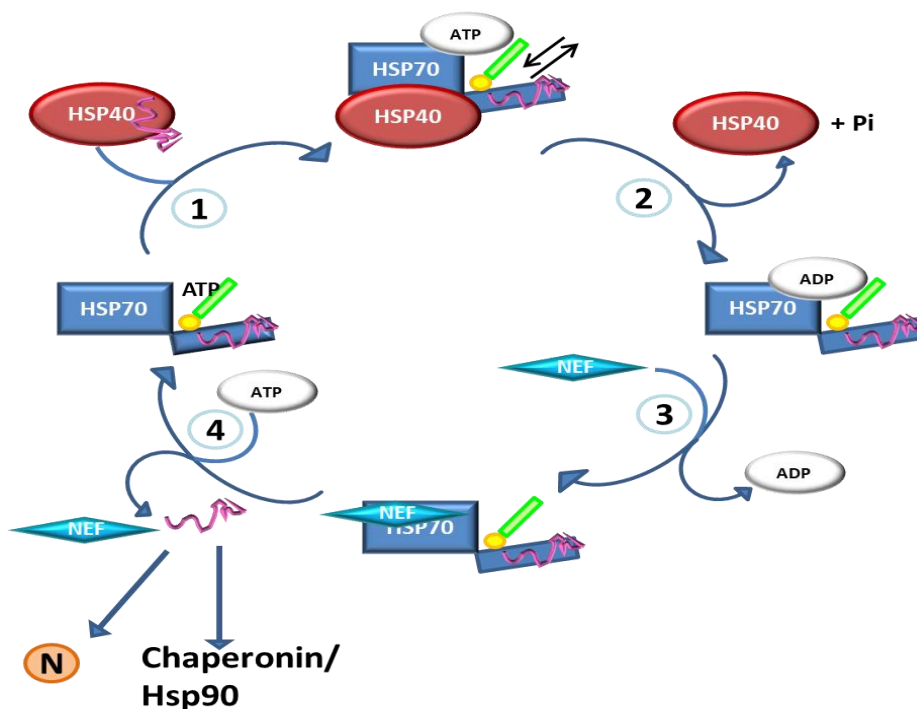


Figure 5. Hsp70/Hsp40 ATP hydrolysis cycle.

Heat Shock Protein 70 is involved in many physiological and pathological process,¹³² such as:

- preventing aggregation and assisting refolding of misfolded proteins;
- assisting folding of some newly translated proteins;
- guiding translocating proteins across organellar membranes acting at both the cis and trans sides;

- disassembling oligomeric protein structures;
- facilitating proteolytic degradation of unstable proteins;
- controlling the biological activity of folded regulatory proteins, including transcription factors;
- cancer, autophagy, neurodegenerative diseases and aging;

Hsp70 is abundantly expressed in many tumor types and it is accompanied by increased cell proliferation, metastases and poor response to chemotherapy. High expression of Hsp70 enhances the ability of the cancer cells to survive to a range of lethal conditions.¹³³ The cytotoxic effect of Hsp70 down-modulation is particularly strong in transformed cells, yet undetectable in normal, non-transformed cell lines or primary cells. This fact has been interpreted by assuming that tumor cells, as compared to their normal counterparts, exhibit a constitutively stressed phenotype with an enhanced dependency on the cytoprotective action of Hsp70. Hsp70 exerts the cytoprotective action probably through its ability to inhibit apoptosis. Gene ablation studies demonstrate that Hsp70 plays an important role in apoptosis. Indeed, Hsp70 suppresses apoptosis through inhibition of both intrinsic and extrinsic apoptotic pathways. Cells lacking *hsp70.1* and *hsp70.3*, the two genes that code for inducible Hsp70, are highly sensitive to apoptosis induced by a wide range of lethal stimuli.^{132, 133} Hsp70 can regulate apoptosis at different levels from death receptors signaling to executors of cell death program, affecting both upstream and downstream of the death-associated mitochondrial events. Hsp70 also negatively interferes with MAPK family kinase activity (Fig. 6), in particular, that of p38 and c-Jun N-terminal kinase (JNK).¹³⁴

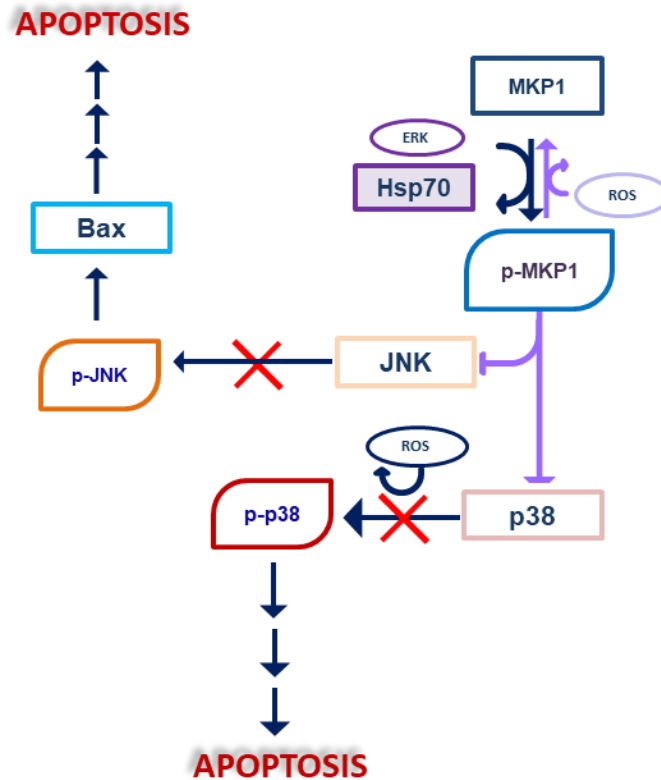


Figure 6. Hsp70 in apoptosis. Hsp70 plays a crucial role in the phosphorylation of MKP1, which avoids p38 and JNK1 phosphorylation. P-p38 and p-JNK1 lead to the activation of a cascade of signals which activate apoptosis.

Studies indicated that Hsp70 inhibits the apoptosis induced by hyperosmolarity modulating JNK and ERK phosphorylation.¹³⁵ Hsp70 contributes to the stabilization of the stress-activated kinases, such as AKT, binding to the non-phosphorylated kinase via the kinase carboxyl-terminus, priming the kinase for rephosphorylation and stabilizing the protein.¹³⁶ Several roles of Hsp70 in cancer initiation and progression are connected to its involvement in regulating cell signaling. Moreover, Hsp70 regulates multiple pathways in cancer cells via interaction with the co-chaperone BAG3, which may serve as a scaffold/mediator that transmits effects of Hsp70 to multiple signaling pathways which control cancer development.¹³⁷

3.1.2 Hsp70 inhibitors

Since the involvement of Hsp70 chaperones in human diseases such as cancer, neurodegeneration and aging, searching for compounds able to target Hsp70 has become a challenging goal in the last decades. Nowadays only a few modulators of Hsp70 activity have been identified.¹³⁸⁻¹⁴³

Hsp70 inhibitors can be classified in three basic categories:

- small molecule inhibitors:

A small molecule inhibitor called 2-phenylethylsulfonamide (PES) or pifithrin- μ interacts with the C-terminal SBD of Hsp70, disrupting the association between Hsp70 and cofactors such as Hsp40 and client proteins, including the pro-apoptotic proteins APAF-1, p53 and others. This takes to the aggregation of misfolded proteins, and to the destabilization of lysosome membranes, inducing cell death. PES has been proven as a potent antitumor agent.¹³⁸ 15-Deoxyspergualin (15-DSG Fig. 7), a natural immunosuppressive agent, disrupting Hsp70-ATP interaction through binding to Hsp70 and lowering its ATPase activity (25% of reduction), was the first compound described by Nadeau et al in 1994.¹³⁹

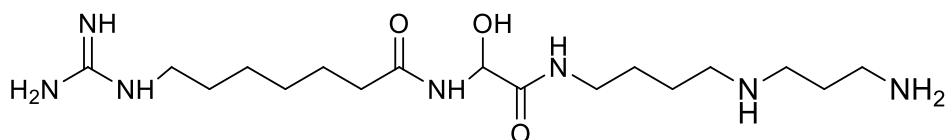


Figure 7. Structure of 15-DSG

VER-155008 is an adenosine-derived compound. It functions to inhibit the chaperone activity of Hsp70 and other family members by binding the ATPase domain. Azure C, methylene blue and myricetin have been identified as inhibitors of Hsp70 through a high-throughput screening for ATP turnover

mediated by human Hsp70, but their specificity for inducible Hsp70 family has not yet been analyzed.¹⁴⁰ MKT-077, a cationic rhodacyanine dye, Apoptozole, Sphingolipids can also bind to the NBD of Hsp70 and specifically inhibit Hsp70 ATPase activity.¹⁴¹

- protein aptamers: The most potent aptamer, A17, binds to the NBD of Hsp70, and was demonstrated to disrupts the function of Hsp70 in a biochemical assay *in vitro*. A17 increases the sensitivity to apoptosis induction by anticancer drugs (cisplatin and 5-fluorouracil) and, *in vivo*, has a strong antitumor effect.¹⁴²
- antibody treatments: The most promising strategy reported for developing Hsp70 inhibitors utilizes the immune system, and it is the only Hsp70-targeted therapy currently in clinical trials (clinicaltrials.gov). However, there are severe limitations due to the lack of tumor-specific markers related to Hsp70. However, a recently developed monoclonal antibody, cmHsp70.1, successfully recognizes the extracellular motif, TKDNNLLGRFELSG (TKD) of membrane bound Hsp70. Since only cancer cell moves Hsp70 to the membrane, while normal (non-transformed) cells do not, the TKD motif represents an excellent tumor-specific biomarker. CmHsp70.1 has successfully passed through a safety and efficacy phase I trial and it is currently in a phase II clinical trial for non-small cell lung cancer in combination with radio chemotherapy.¹⁴³

3.1.4 Aim of the project

The knowledge of the mechanism of action of promising plant molecules is a required starting point for many pharmaceutical and biochemical researches. In this field, biochemical and proteomic-based studies play a central role, allowing to describe the possible modulators of a selected protein target. In order to investigate the mechanism of action of our bioactive diterpenes, a

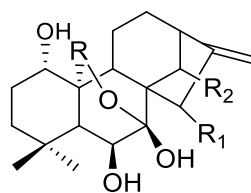
Reverse Chemical Genetics (RCG) approach was adopted. In this study we carried out:

- the screening of a library of bioactive kauranes and kaurane-derivatives against Hsp70, to identify the best ligand by Surface Plasmon Resonance (SPR).
- Hsp70/ligand interaction validation through:
 - * cell-free assays: LC/MS, peptide mapping, ATPase activity assay, molecular docking.
 - * cell-based assays: WB, MTT assay, Flow Cytometry, DARTS.

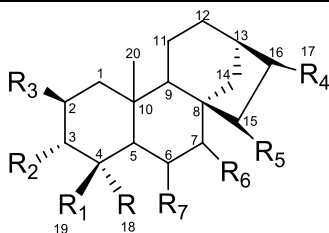
Results and discussion

3.2 Identification of Hsp70 ligands by Surface Plasmon Resonance

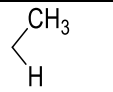
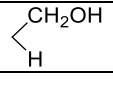
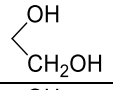
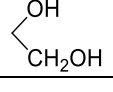
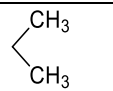
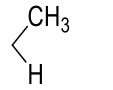
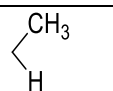
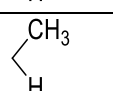
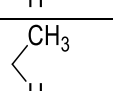
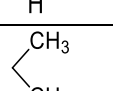
Our study started from the screening of a library of thirty-nine diterpenes (Fig. 8) for their affinity towards Hsp70. The screening was performed by Surface Plasmon Resonance (SPR).



Compound	R	R ₁	R ₂
Oridonin		=O	◀OH
1	H	◀OH	H
2	=O	◀OH	◀OH
3	OH	=O	H
4	H	=O	H



Compound	R	R ₁	R ₂	R ₃	R ₄	R ₅	R ₆	R ₇
5	-CH ₃	-COOH	H	H		H	H	H
6	-CH ₃	-CH ₂ OH	OH	H	-CH ₃	Δ15-16	◀OH	H
7	-CH ₂ OH	-CH ₂ OH	H	=O	==	H	H	H
8	-CH ₂ OH	-CH ₂ OH	H	OH		H	H	H
9	-CH ₂ OH	-CH ₃	H	OH	==	H	H	◀OH
10	-CH ₂ OH	-CH ₂ OH	H	OH	==	H	H	H
11	-CH ₃	-CH ₂ OH	H	=O	==	H	H	OH

12	-CH ₂ OH	-CH ₂ OH	H	H		Δ15-16	H	H
13	-CH ₂ OH	-CH ₂ OH	H	=O		Δ15-16	H	H
14	-CH ₂ OH	-CH ₂ OH	H	H	≡	H	H	OH
15	-CH ₃	-CH ₃	H	=O		H	H	H
16	-CH ₂ OH	-CH ₂ OH	H	H		H	H	H
17	-CH ₃	-CH ₂ OH	OH	H	≡	H	◄OH	H
18	-CH ₃	-CH ₂ OH	H	H		H ₂	⋯OH	H
19	-CH ₃	-CH ₂ OH	OH	H	≡	H ₂	H	H
20	-CH ₃	-CH ₃	OH	H	≡	H ₂	H	H
21	-CH ₃	-CH ₂ OAc	OH	H	≡	H ₂	◄OH	H
22	-CH ₂ OH	-CH ₂ OH	H	H		Δ15-16	⋯OH	H
23	-CH ₃	-CH ₂ OH	H	H		Δ15-16	OH	H
24	-CH ₃	-CH ₂ OH	H	H		Δ15-16	-OAc	H
25	-CH ₃	-CH ₂ OH	H	H		Δ15-16	=O	H
26	-CH ₃	-CH ₃	=O	H		H ₂	H	H

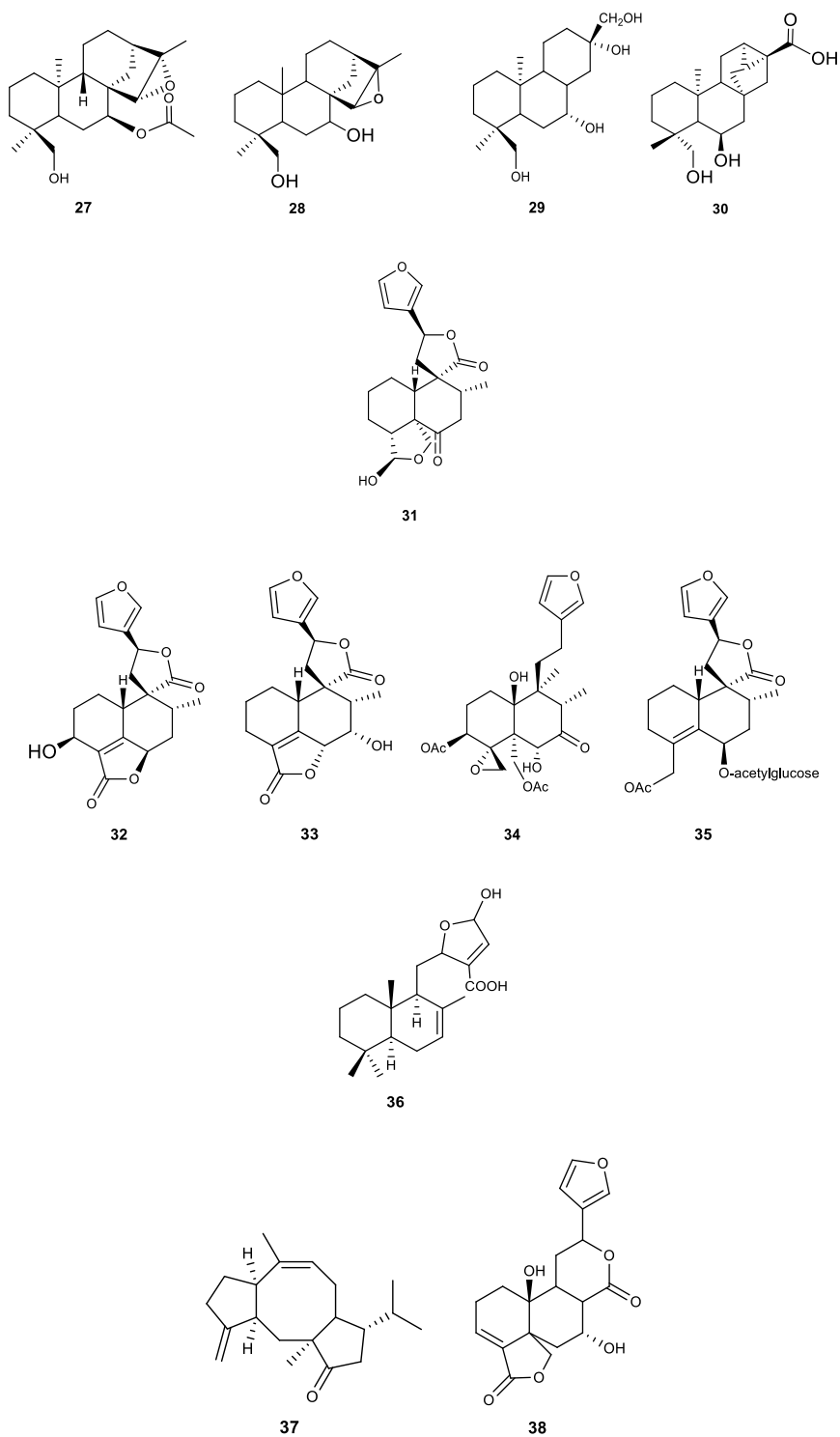


Figure 8. Structures of a library of plant compounds tested against Hsp70 by SPR screening.

Oridonin (Fig. 8) was used as positive control: previously published results indicated that this diterpene as ligand of Hsp70, exhibiting a thermodynamic K_D of 26 ± 1.2 nM and showing a covalent binding with Cys267 of Hsp70 mediated by its α,β -unsaturated carbonyl group in position 15. Oridonin/Hsp70 complex was proved by LC-MS/MS and molecular docking experiments.^{144,145} Therefore, all the analyzed compounds were selected based the importance of the carbonyl group in position 15 of oridonin. Our achieved SPR sensorgrams indicated that six compounds (**5**, **9**, **10**, **11**, **14** and **27**) were demonstrated to bind the chaperon, with thermodynamic constants ranging from 54 to 1000nM (Table 2). Compounds **9**, **10**, **11**, **14** share a $\Delta 16-17$ (in R₄) which probably could be responsible for an interaction with Hsp70.

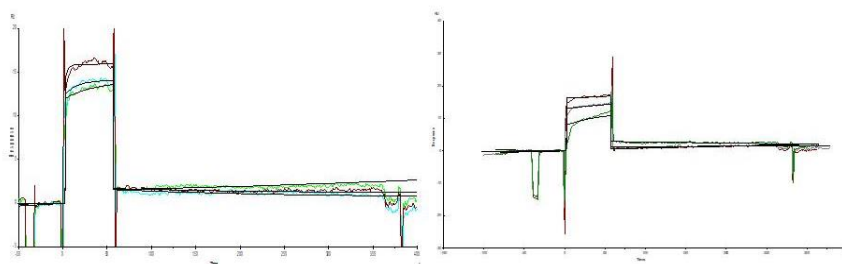


Figure 9. SPR Sensorgrams of oridonin (positive control, a) of epoxysiderol (b).

From our SPR results, the kaurane diterpene *ent*-7 β -acetoxy-18-hydroxy-15 α ,16 α -epoxsikaurane, also known as epoxysiderol (compound **27**), was the most active (Figure 10, sensorgram in figure 9b), showing higher affinity for Hsp70 ($K_D = 54.1 \pm 1.2$ nM; k_{on} (1/nMxs): 14.5 ± 1 ; k_{off} [(1/s) $\times 10^{-3}$]: 0.78 ± 0.1). This compound shows an epoxide group between C15 and C16, positions where we found the α,β -unsaturated carbonyl group in oridonin. Therefore, and epoxide group in that position could be very important for the interaction with Hsp70.

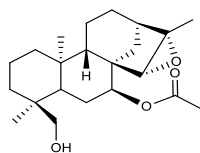


Figure 10. Structure of the *ent*-7 β -acetoxy-18-hydroxy-15 α ,16 α -epoxysikaurane (epoxysiderol).

Interestingly, also compound **28** presents an epoxide group, but the absence of binding activity for this compound could probably be explained by the different stereochemistry in comparison with the epoxide group of **27**.

Table 2. Thermodynamic constants measured by SPR of tested diterpenes on immobilized Hsp70.

Compound	KD (nM) \pm SD	Compound	KD (nM) \pm SD
Oridonin	26 \pm 1.2	20 SPU 10/7	No binding
1 Nervosanin B	No binding	21 SPU 15/11	No binding
2 IRU 9/10	No binding	22 Siderotriol	No binding
3 IRU 5/5	No binding	23 Compound y	No binding
4 Ponidonin	No binding	24 Compound e	No binding
5 Chetokauranic acid	400 \pm 1.5	25 Diterpene D	No binding
6 Isofoliol	No binding	26 EL 8/7	No binding
7 PPU 3/21	No binding	27 Epoxysiderol	54 \pm 1.2
8 PPU 18/31	No binding	28 Compound z	No binding
9 PPU 11/24	1180 \pm 5	29 SPU 19/5	No binding
10 PPU 7/44	100 \pm 3	30 PPU 11/31	No binding
11 PPU 3/10	1401 \pm 7.5	31 Teuscorodin	No binding
12 PAF 8/40	No binding	32 Teuflidin	No binding
13 PAF 8/3	No binding	33 Teucrin A	No binding
14 PAF 6/18	615 \pm 1.3	34 Teucrolivin B	No binding
15 PAF 7/7	No binding	35 Teuflavoside	No binding
16 PAF 9/11	No binding	36 PRE 1/11	No binding
17 SPU 10/11	No binding	37 HFR 5/9	No binding
18 SPU 11/7	No binding	38 SJ131	No binding
19 SPU 10/6	No binding		

3.2.1 Epoxysiderol

Epoxysiderol (Fig. 10) is a diterpene with *ent*-kauranic skeleton, isolated from plants of the genus *Sideritis*: *S. sicula*, *S. euboea*, *S. roeseri*, *S. distans*, *S. dichotoma* e *S. syriaca*.¹⁴⁶ The genus *Sideritis* (Lamiaceae) comprises more than 150 species widely distributed in temperate and tropical regions of the Northern Hemisphere. Most species are mainly found in the Mediterranean area, together with Canary and Madeira islands. This genus is characterized by a high number of hybridizations between species.¹⁴⁷ The aerial parts of *Sideritis* species, known as ‘mountain tea’, are used in Mediterranean countries folk medicine for gastrointestinal disorders such as stomach ache, indigestion, flatulence, to alleviate the symptoms of common colds, cough, rheumatism, and for tonic and diuretic effects.¹⁴⁸ Anti-inflammatory, antioxidant, antiulcerogenic, antimicrobial, antiherpetical activities of *Sideritis* spp. extracts have also been reported, and some pure compounds isolated from this genus have shown antiproliferative, anti-HIV or antifeedant activities. Moreover, it is known that diterpenoids isolated from this genus are responsible of antifeedant, antimicrobial, and anti-inflammatory activities.¹⁴⁷ Previous studies have shown the presence of mono-, sesqui-, di- and triterpenes, together with flavones, coumarins, phenylpropanoids and other aromatic derivatives in the *Sideritis* genus.¹⁴⁹ Epoxysiderol was isolated through chromatographic analyses and its structure was elucidated by spectroscopic methods (UV, NMR, MS).

Once identified epoxysiderol as ligand of Hsp70 by SPR, the next steps of our study were aimed at:

- 1) the validation of epoxysiderol as Hsp70 ligand;
- 2) the evaluation of epoxysiderol biological activity in cancer cells;
- 3) the characterization of epoxysiderol/Hsp70 complex;

3.2.2 MS-based studies on the epoxysiderol-Hsp70 interaction

According to the several reactive aminoacids of Hsp70, the chemical structure of epoxysiderol and the stability of Hsp70/epoxysiderol complex ($K_D = 54, 2 \pm 1.2 \times 10^{-9} M$), we investigated the characteristics of the interaction between the diterpene and the chaperone. To understand if the binding between epoxysiderol and Hsp70 was covalent or not, an LC-MS/MS-based *peptide mapping* analysis was implemented. To obtain an expedient *peptide mapping* for the coverage of Hsp70 sequence, we used Mascot Daemon (Matrix Science) software. Our analysis led to a *sequence coverage* of 43% for the control (recombinant Hsp70 treated with only DMSO for 3h, fig.11a) and 47% for the treated (Hsp70 with epoxysiderol in ratio 1:100, fig. 11b). These results were further investigated by conducting a manual analysis of LC-MS/MS spectra. The analysis was performed using Paws software, and allowed us to obtain a final *sequence coverage* of 84.5% for the control and the 86% for the treated sample.

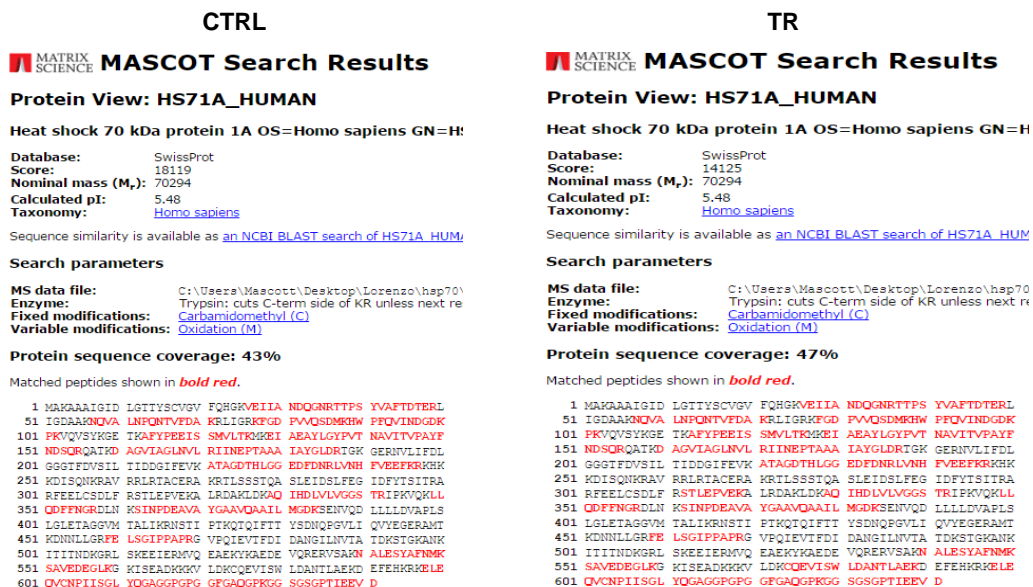


Figure 11. Mascot Research results. **a)** sequence coverage calculated for Hsp70 with only DMSO (control) **b)** sequence coverage for HSP70 with epoxysiderol (treated)

The manual analysis of the LC-MS/MS spectra also led us to investigate eventually modified peptides of Hsp70 involved in the interaction with epoxysiderol. In Figure 12 the HPLC spectra of control and treated samples are shown: except very small variations in the retention time between the control spectrum (in black) and the treated spectrum (in red), there was non significant difference between the two samples.

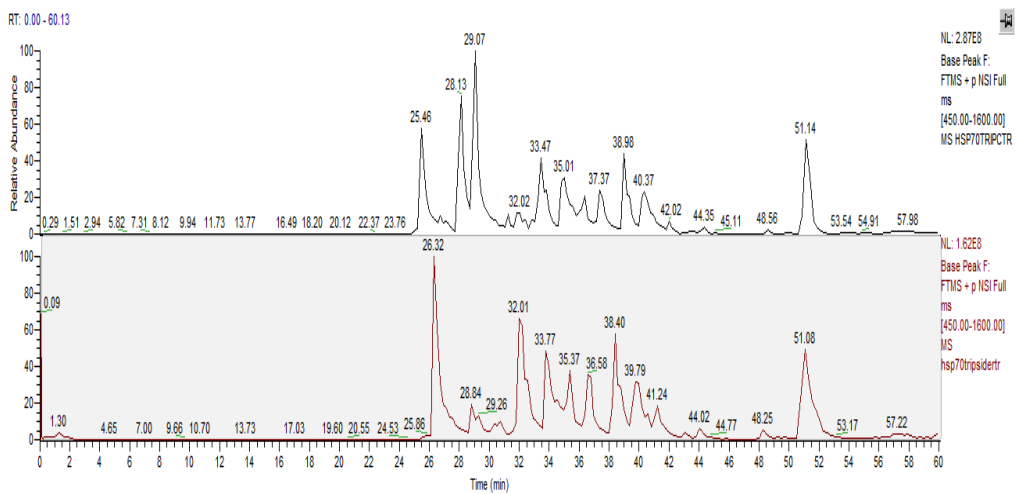


Figure 12. HPLC profiles of control and treated samples chromatograms. In black: control (Hsp70 with DMSO); in red: Hsp70 treated with epoxysiderol (1:100 v/v).

Analyzing MS/MS spectra, either way we could not find any m/z value that could match a covalent complex between epoxysiderol and Hsp70 (Fig. 13).

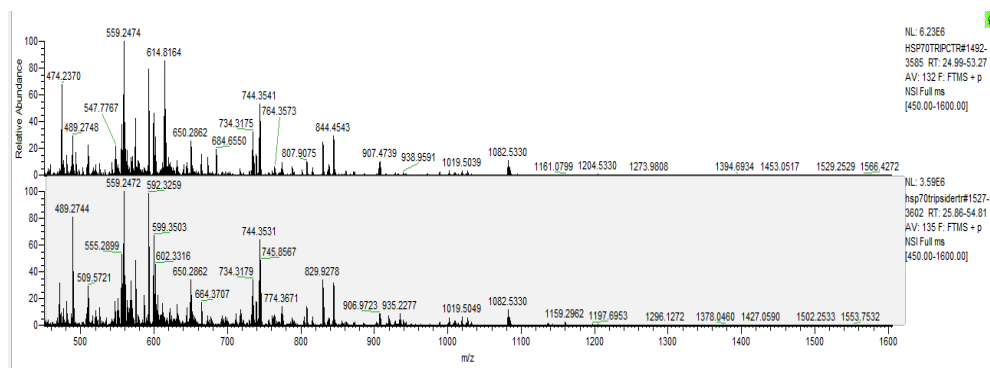


Figure 13. MS profiles of control and treated samples. above: control (Hsp70 with DMSO); below: Hsp70 treated with epoxysiderol (1:100 v/v).

These results suggested the occurrence of a non-covalent interaction between epoxysiderol and Hsp70.

3.2.3 Cytotoxic activity of epoxysiderol

The cytotoxic activity of epoxysiderol was evaluated by MTT assay on cancer cell lines such as HeLa (cervical carcinoma) and Jurkat (T-cell leukemia), and also on nontumor human peripheral blood mononuclear cell line (PBMC).

PBMC, Jurkat and HeLa cells were treated for 48h with DMSO (control) or epoxysiderol at different concentrations ranging from 5 μM up to 100 μM and the IC_{50} of the dose-effect curves was calculated (Table 3).

Table 3. IC_{50} (μM) by MTT assay.

Compound	Jurkat	HeLa	PBMC
Epoxysiderol	$30 \pm 1.5 \mu\text{M}$	$20 \pm 0.9 \mu\text{M}$	$>100 \mu\text{M}$

Data represent the mean \pm SD of 3 different experiments.

The obtained results show that epoxysiderol plays a moderate antiproliferative activity against these tumor cell lines, being more effective on HeLa cells ($\text{IC}_{50} = 20 \pm 0.9 \mu\text{M}$). On PBMC epoxysiderol did not show cytotoxic activity. Therefore, our next studies focused on this cell line, more susceptible to epoxysiderol.

3.2.4 Validation study of epoxysiderol/Hsp70 interaction by DARTS

In order to confirm Hsp70/epoxysiderol interaction in HeLa cells, we performed a cell-based assay by a *Drug Affinity Responsive Target Stability* (DARTS) approach, analyzing DARTS results by both WB and LC-MS/MS. HeLa cells (cervical carcinoma) were treated with epoxysiderol (15 μM) for 2h; after the incubation, the cells underwent lysis with RIPA buffer, and the resulting protein extract was subjected to the limited enzymatic digestion,

carried out by adding subtilisin (1:2000 w/w) for 20 minutes at 37°C. Subsequently, the partially digested proteins were fractionated by SDS-PAGE; each sample was divided in two aliquots, each loaded on a gel: in the first gel, the proteins were transferred into nitrocellulose membranes to perform a WB analysis. As shown in Figure 14, in the sample treated with subtilisin and epoxysiderol there was an enrichment of Hsp70 in comparison with the sample treated with only subtilisin: these data that epoxysiderol interacts with Hsp70 protecting the chaperone from the limited proteolysis by subtilisin.

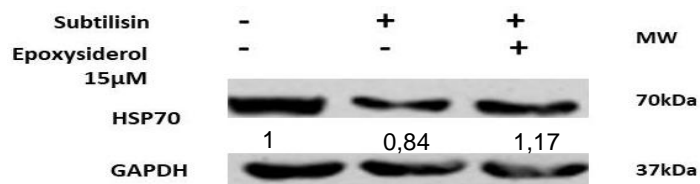


Figure 14. Effect of treatment with epoxysiderol, 15 µM for 2h on Hsp70 levels after treatment of HeLa cells with subtilisin (DARTS experiment). GAPDH was used as loading control. The blots are representative of three different experiments with similar results. Numbers below each lane represent the densitometric values. The blots are representative of at least three different experiments with similar results.

The second gel, on the other hand, was treated with Fixing Solution for 30 min, stained with Comassie Blue Colloidal overnight and washed with water. Afterwards, lanes of lysates treated with subtilisin was cut into five pieces (Figure 15, in blue), digested with trypsin and analyzed by LC-MS/MS.

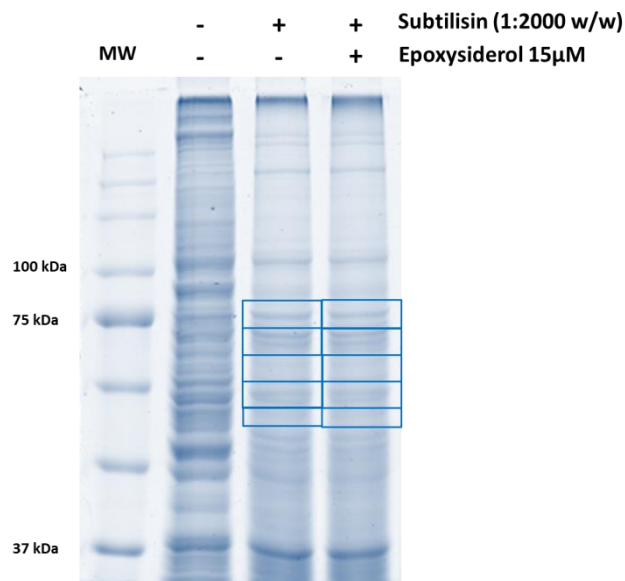


Figure 15. SDS Page carried on HeLa lysates. Each sample treated with subtilisin was split into five aliquots that underwent digestion with subtilisin, for 20 min at 37°C. Digestion was stopped by adding sample loading buffer and boiling immediately. Each sample was then loaded onto 10% SDS/PAGE gels and stained with Brilliant Blue G-Colloidal.

In order to evaluate the relative abundance of Hsp70 in treated and control samples, we carried out further data analyses using the Max Quant software. Each band of each lane underwent a digestion protocol with trypsin and then analyzed by LC-MS/MS. Each Raw file was then analyzed using Max Quant software, using a label-free quantification (LFQ) “within groups” method (each band of the same lane was united). In Table 4, Hsp70 intensities of samples treated with only DMSO (control) and with epoxyssiderol 15 μ M for 2h are shown.

Achieved results were in agreement with DARTS results analyzed by WB, since the LFQ total intensity of treated samples is higher than the LFQ total intensity of control samples

Table 4. Max Quant software analysis. Each sample of control and treated lanes underwent a label free quantification analysis within groups.

Protein name	Mr	LFQ intensity control (DMSO)	LFQ intensity treated (epoxysiderol)	mean	ratio
Heat shock 70 kDa protein	70730	2986200	115855000	$5.9 \cdot 10^{-7}$	38.8

Data are representative of at least two different experiments with similar results.

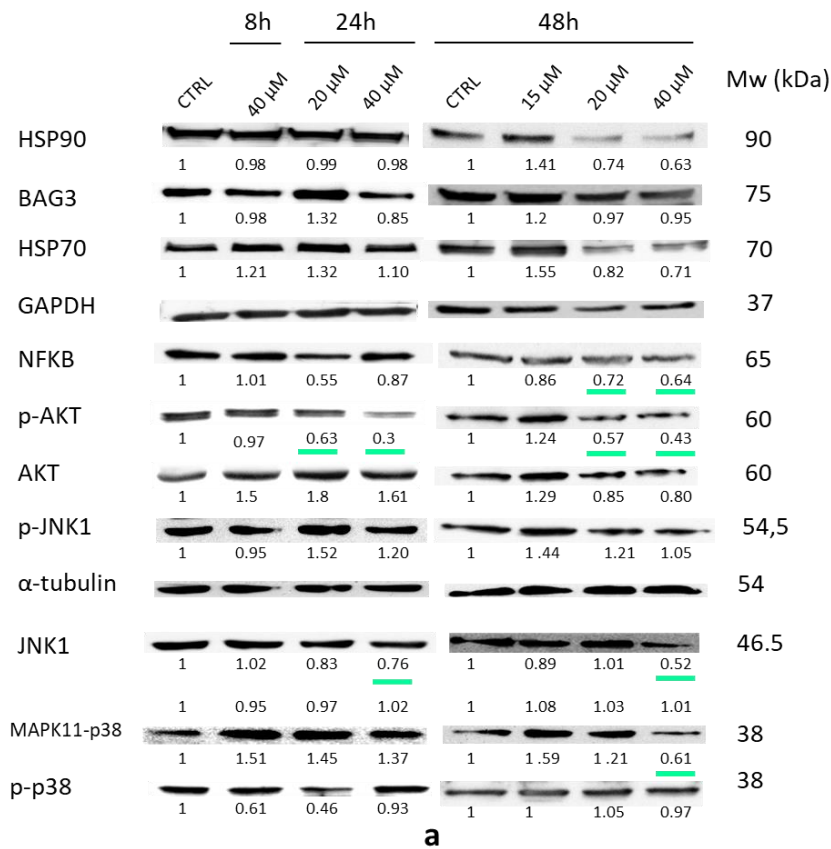
3.2.5 Western Blot of Hsp70, Hsp70 co-chaperones and client proteins

Once demonstrating epoxysiderol/Hsp70 interaction by cell-free and cell-based techniques, and epoxysiderol cytotoxicity in Jurkat and HeLa cells, the following step of our study aimed to investigate more in detail the biological activity of epoxysiderol, focusing on the cellular pathways involving Hsp70.

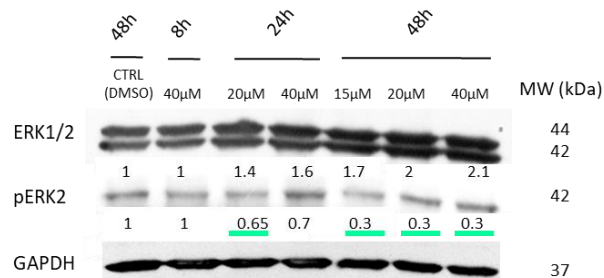
Firstly, we carried out WB in HeLa cells on Hsp70, in order to understand if epoxysiderol modulates Hsp70 levels. As shown in figure 16, Hsp70 levels decrease only after 48h at the highest concentrations of epoxysiderol (40 μ M). These results are in agreement with MTT data. About Hsp70 co-chaperones, also Hsp90 levels slightly decreased after 48h of incubation with epoxysiderol, whereas BAG3 levels did not show any consistent modulation.

We then focused on Hsp70 client proteins, particularly those involved in cell proliferation, apoptosis and cell cycle phases progression. WB results showed a dose and time-dependent reduction of NF-kB, p-Akt and p-ERK levels at 20 μ M and 40 μ M after 24h and 48h; a reduction of AKT1, p38 (MAPK11), p-p38, JNK1 (MAPK8) and p-JNK1 levels after 48h of incubation with epoxysiderol (Fig.16).

Based on these results, we can interestingly assert that epoxysiderol can modulate different cellular pathways involved in apoptosis, inflammation and cancer progression, where Hsp70 plays a crucial role.¹³³



a



b

Figure 16: a) and b) Effect of epoxysiderol 15 μM, 20 μM and 40 μM on Hsp70, Hsp70 client proteins and cochaperones levels in HeLa cells for 8h, 24h and 48h. Equal amounts (30 μg) of total protein lysate were separated on SDS-PAGE and client proteins were visualized by Western Blot analysis. α-tubulin and GAPDH were used as loading controls. The blots are representative of three different experiments with similar results. Numbers below each lane represent the densitometric values.

3.2.6 Evaluation of epoxysiderol biological activity in HeLa cells by flow cytometry and WB

In order to understand if the reduction of HeLa cells treated with epoxysiderol is due to an effect of the diterpene on cell cycle or cell death (hypodiploïdia), a flow cytometric analysis was implemented. HeLa cells were treated with epoxysiderol (15 μ M, 25 μ M e 40 μ M) for 24h and 48h. Achieved results indicated that the diterpene treatment induces a subG₀/G₁ and a more evident G₂/M cell cycle arrests after 48h of incubation (at 25 μ M and 40 μ M) (figure 17).

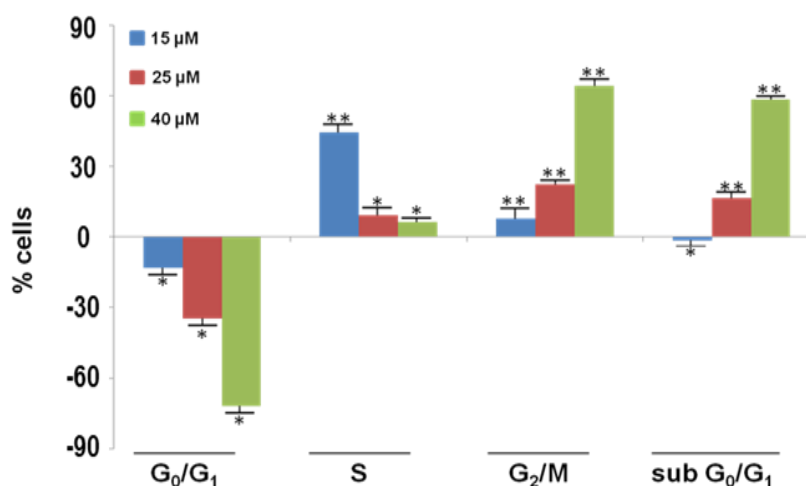


Figure 17. Effect of epoxysiderol on cell cycle progression. Flow cytometric evaluation of DNA content in HeLa cells treated with DMSO (control) or epoxysiderol (15 μ M, 25 μ M, 40 μ M) for 48h. On the Y axis: the percentages of cells in subG₀/G₁ (hypodiploïdia) and in each cell cycle phase of epoxysiderol-treated cells subtracted for the corresponding percentages of control cells. Results are expressed as means \pm SD of three experiment performed in duplicate (**p<0.005, *p<0.05).

The involvement of epoxysiderol in G₂/M cell cycle phase was validated by performing WB on cyclins Cdc2 and p-Cdc2, allowing us to discriminate the effect of epoxysiderol between the G₂ phase and the M phase. Infact, Cdc2 or also called cyclin B, is necessary for the progression of the cells in and out of the M phase of the cell cycle. Therefore, HeLa cells were treated with DMSO (ctrl) or epoxysiderol (15 μ M, 25 μ M and 40 μ M for 48h). After lysis, proteins

underwent SDS-page, transfer onto nitrocellulose membranes, and WB analysis. Figure 18 shows the effect of epoxysiderol on G2/M phase changes depending on the concentrations used: at 15 μ M we can observe an increase of p-Cdc2 levels compared to the control, thus suggesting an involvement in the M phase arrest of the cell cycle. On the contrary, at higher concentrations of epoxysiderol 25 μ M and 40 μ M of epoxysiderol, p-Cdc2 decreases, causing a G2 phase arrest of the cell cycle.

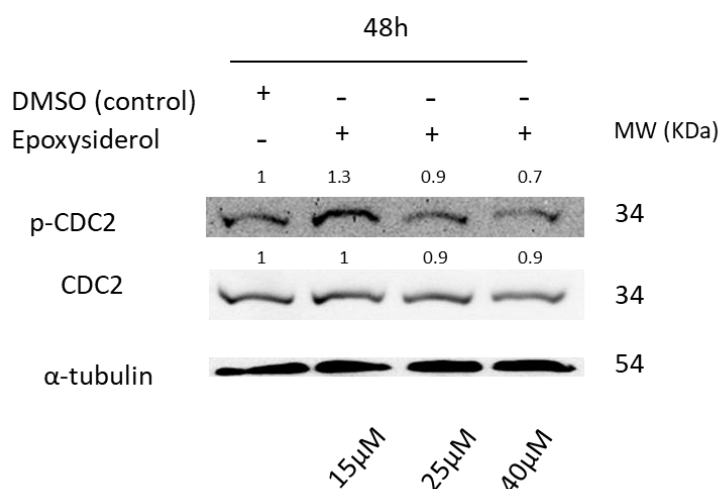


Figure 18. Effect of epoxysiderol on cell cycle regulatory protein levels. Western Blot analysis of Cdc2 and pCdc2 (Thr161) levels in HeLa cells treated with DMSO (ctrl) or epoxysiderol (15 μ M, 25 μ M and 40 μ M) for 48h. For each immunoblot, band intensity was quantified by densitometry (numbers above each lane). GAPDH was included as a loading control. The blots are representative of at least two different experiments with similar results.

In order to understand if the subG₀/G₁ cell cycle arrest was affecting apoptosis or necrosis events, an additional Flow Cytometry experiment, using Annexin V, FITC Coniugate/PI protocol, was implemented. Achieved results showed HeLa cells in late (10.85%) and early (7.11%) apoptosis after treatment of HeLa with epoxysiderol already at 15 μ M for 48h (Fig. 19). No significative necrosis effect was observed.

Therefore, the subG₀/G₁ cell cycle arrest caused by epoxysiderol was in agreement with WB results showed previously, according to the effect of

epoxysiderol on apoptosis pathways (reduction of pAkt, pERK2, JNK1 and p38).

In addition, PARP cleavage was observed by WB after treatment of HeLa cells with epoxysiderol 20 μ M and 40 μ M for 24h and 48h, confirming the involvement of epoxysiderol in apoptosis events mediated by PARP.

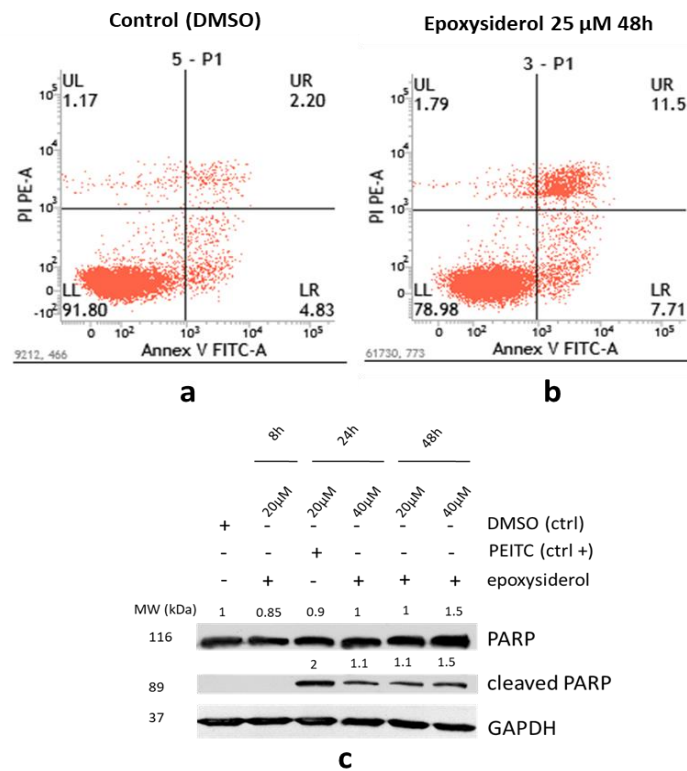


Figure 19. Flow Cytometry experiment using Annexin V-FITC/PI protocol. a) HeLa cells treated with DMSO (control) for 48h. b) HeLa cells treated with epoxysiderol 25 μ M for 48h. c) WB of HeLa cells treated with epoxysiderol 20 μ M and 40 μ M for 8h, 24h and 48h. For each immunoblot, band intensity was quantified by densitometry (numbers above each lane). Glyceraldehyde 3-phosphate dehydrogenase (GAPDH) was included as a loading control and phenetyl isothiocyanate (PEITC) as positive control. The blots are representative of at least two different experiments with similar results.

3.2.7 Epoxysiderol effect on Hsp70 levels in subcellular compartments

Hsp70 plays a crucial role in cancer progression. In particular, the Hsp70 located in cytoplasm and specially on the plasma membrane are considered tumor markers. Indeed, plasma membrane Hsp70 is overexpressed in cancer cells than normal cells.¹²³

In order to understand if epoxysiderol can modulate Hsp70 levels in different subcellular compartments in HeLa cells, a specific cell-based protocol was carried out. Our results were analyzed by WB. HeLa cells were incubated with oridonin 5 μ M and epoxysiderol 20 μ M for 4h at 37°C. After obtaining nucleus, cytosolic and plasma membrane extracts, each lysate was fractioned by SDS-PAGE and the proteins were immunoblotted on a nitrocellulose membrane with antibodies specific for each cell compartment.

As shown in figure 20, after 4h we can observe:

- no modulation of Hsp70 levels into the nucleus;
- reduction of Hsp70 levels into the cytoplasm (20% for oridonin and 40% for epoxysiderol);
- reduction of Hsp70 levels on the plasma membrane (40% for oridonin and 50% for epoxysiderol);

From these results, we could assert that epoxysiderol does not enter into the nucleus, whereas into the cytosol it does, modulating Hsp70 levels and its migration on the plasma membrane.

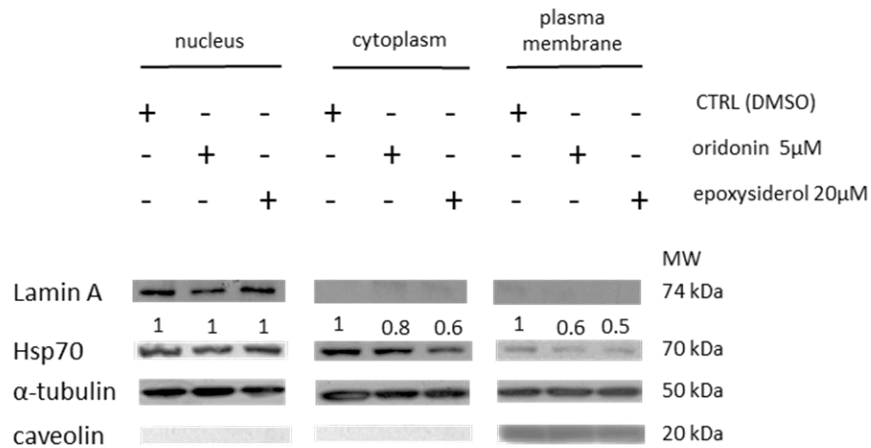


Figure 20. Effect of epoxysiderol on Hsp70 levels in nucleus, cytosol and plasma membrane. Western Blot analysis of Hsp70 levels in HeLa cells treated with DMSO (ctrl), oridonin 5 μ M and epoxysiderol 20 μ M for 4h. For each immunoblot, band intensity was quantified by densitometry (numbers above each lane). α -tubulin was included as a loading control for cytosol and plasma membrane, Lamin A for the nucleus. Caveolin was used as control for plasma membrane extracts. The blots are representative of at least two different experiments with similar results.

3.2.8 Inhibition of Hsp70 ATPase activity mediated by epoxysiderol

ATP hydrolysis and ADP/ATP exchange play a central role in Hsp70 chaperone activity. Therefore, disruption of Hsp70-ATP interaction could lead to the inability of Hsp70 to perform its functions. Thus, the effect of epoxysiderol on ATP-dependent Hsp70 (using also its cochaperon Hsp40) biochemical functions was studied. To evaluate the effect of epoxysiderol binding on Hsp70, the ATPase activity was measured in the presence of different amounts of epoxysiderol (1 μ M, 10 μ M and 50 μ M); oridonin was used as positive control.¹⁴⁵ Epoxysiderol was found to inhibit in a dose-

dependent manner the Hsp70 ATPase activity (Fig. 21).

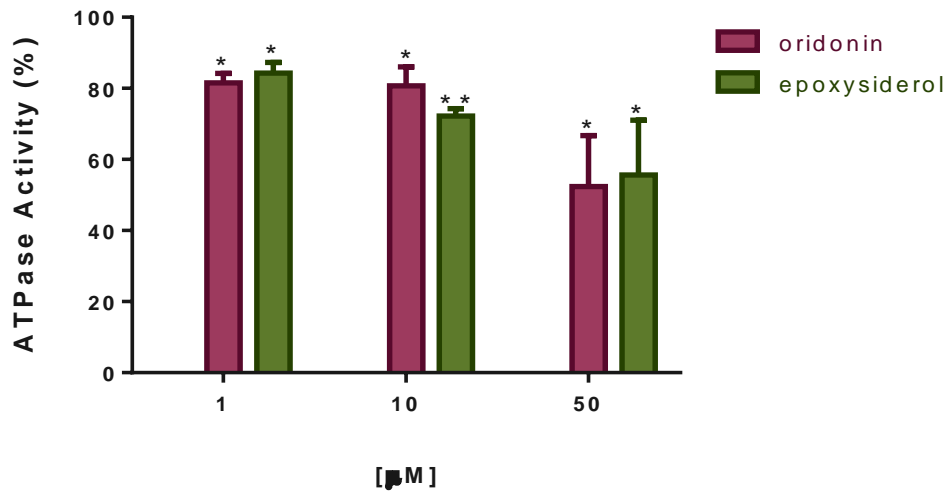


Figure 21. Epoxysiderol effect on Hsp70 ATPase activity. Inhibition of the ATPase activity of Hsp70 treated with DMSO (control) or different concentrations of epoxysiderol, oridonin (positive control). Data are the means \pm SD of two independent experiments performed in triplicate. *p<0.05, **p<0.005.

3.2.9 Molecular docking experiment

Presently, the knowledge of the structure and the dynamic of a small molecule/protein complex is crucial for drug discovery and for molecular bases studies of a pathological process. Thus, a characterization of epoxysiderol/Hsp70 complex was performed by molecular docking calculations. Particularly, the analyses were performed using the protein structure recently crystallized by van Montfort et al. (PDB code: 5AQX).¹⁵⁰ In this study the authors reported the discovery of novel Hsp70 inhibitors following a fragment-based approach, disclosing the binding mode of these compounds able to directly interact in the ATP binding site of the protein. Due to the similar dimensions of epoxysiderol and the fragments co-crystallized with the protein, a computational investigation hypothesizing a similar binding mode for the diterpene was performed. For these reasons, molecular docking experiments were focused in the ATP binding site of the protein and performed using Glide software; afterwards, a careful analysis of the binding poses and of the set of interactions established with the protein counterpart was done. In details, as shown in Fig. 22, the most energetically favoured docking poses of epoxysiderol in the ATP binding site of Hsp70 showed a large hydrogen bond network with polar residues due to the presence of hydrogen bond acceptor (HBA) and donor (HBD) chemical functions on epoxysiderol, that strengthened the good placement of the compound on the NBD (Nucleotide Binding Domain) of Hsp70.

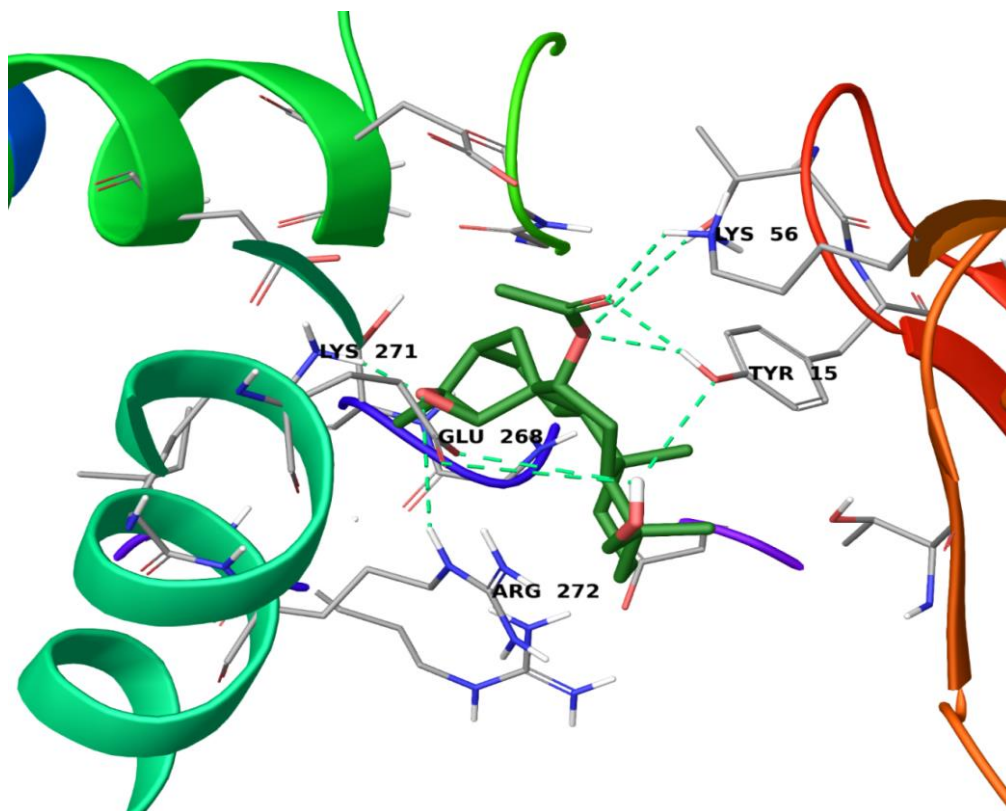


Figure 22. Epoxysiderol (represented in sticks and colored by atom types: C green, O red, polar H light grey) in docking with HSP70 ATP binding site (represented in ribbons, residues close to epoxysiderol are represented in sticks and colored by atom types: C grey, O red, N blue, polar H light grey). Hydrogen bond contacts are represented in dotted green lines.

Specifically, hydrogen bonds were established with Tyr15, Lys56, Glu268, Lys271, Arg272, the latter identified as a key residue for developing/optimizing putative Hsp70 inhibitors.

3.2.10 Conclusions

Epoxysiderol was identified as main ligand of Hsp70 from the screening by SPR. This diterpene has been shown to have multiple biological activities; the antitumor effects of epoxysiderol have been related to its ability to interfere with several pathways, such as cell proliferation, cell cycle arrest and apoptosis. In the present study, we identified epoxysiderol as a novel inhibitor of Hsp70 in HeLa

cells. Indeed, cell-free and cell-based assays were used as a tool to confirm the affinity of epoxysiderol towards Hsp70 and its ability to inhibit Hsp70 ATPase activity. Our biochemical cell-free studies demonstrated that Hsp70 showed a reduced ATPase activity after incubation with epoxysiderol. In addition, epoxysiderol affected the chaperone activity of Hsp70; this effect could be related to the ATPase activity inhibition, since Hsp70 client proteins strongly depend on its ATPase activity. Therefore, epoxysiderol may be considered as a new promising chemical scaffold to study the biology of this protein, and to develop new molecules for the inhibition of Hsp70 by medicinal chemistry approaches.

Materials and Methods

3.3 Surface Plasmon Resonance (SPR)

SPR analyses were carried out with a Biacore 3000 optical biosensor equipped with a research-grade CM5 sensor chip (GE Healthcare). Hsp70 1A (1.4 mg/ml, BPS Bioscience, 50287) $100\mu\text{g ml}^{-1}$ in 50 mM sodium acetate, pH 4.5., was immobilized on sensor chip surfaces at a flow rate of $5\mu\text{l ml}^{-1}$ by using a standard amine-coupling protocol. Forty compounds were dissolved in 100% DMSO to obtain 4mM solutions and diluted in 1:200 (v/v) in PBS (10mM NaH_2PO_4 , 137mM NaCl, 2.7mM KCl pH 7.4) containing variable amounts of DMSO, to achieve a final DMSO concentration of 0.1%. For each molecule a five point concentration series spanning 0.025-4 μM was set up. SPR experiments were carried out at 25°C, with a $50\mu\text{l ml}^{-1}$ flow rate. Association and dissociation times were set at 60s and 300s, respectively. Simple interactions were adequately fit to a single-site bimolecular interaction model to yield K_D . BIAevaluation software (GE Healthcare) was used for sensorgrams elaboration.

3.3.1 Drug Affinity Responsive Target Stability on HeLa cells

Human HeLa cells (cervical cancer cells), were treated with epoxysiderol 30mM for 2h (final concentration 15 μM in 10ml) and DMSO 100% (5% in 10mL), then lysed in RIPA buffer (10 mM Tris-Cl pH 7.6, 1 mM EDTA, 1% Triton X-100, 0.1% sodium deoxycholate, 140 mM NaCl, 1 mM Phenylmethanesulfonyl fluoride) supplemented with protease and phosphatase inhibitors (P8340, Sigma-Aldrich, St. Louis, MO, USA). Protein concentration was determined by Bradford assay (Bio-Rad, Hercules, CA, USA) using bovine albumin as standard. Subsequently, samples underwent proteolysis with Subtilisin (enzyme: lysate 1:2000 w/w) for 20 min at 37°C and then Laemmli buffer 4X (60 mM Tris HCl

pH 6.8, 2% sodium dodecylsulfate, 10% glycerol, 0.01% blue bromophenol, 5% β -mercaptoethanol) was added to each sample to stop the reaction. Finally, the samples were incubated at 100 °C for 5 min and loaded in duplicate in two 10% mono dimensional SDS-PAGE gels, in order to perform at the same time MS and WB analyses.

After performing SDS-Page, one gel was treated with Fixing solution (MEOH:CH₃COOH:H₂O 4:1:5) for 30min and then stained with Brilliant Blue G-Colloidal (Sigma-Aldrich) overnight. After washing with water, each band of the gel line from 70 kDa to 45 kDa was cut and underwent a digestion protocol by trypsin (Promega, Milano, Italy): after washing with 0.1M AMBIC (Sigma Aldrich) and 100% ACN Romil (ROMIL Ltd, Cambridge, UK), the bands were reduced by DTT, alkylated using iodoacetamide, and treated with trypsin (0.013 μ g/ μ l) overnight at 37°C. The resulting fragments were extracted and analyzed by LC/MS/MS.

3.3.2 Monodimensional electrophoresis SDS Page

Polyacrylamide gel electrophoresis of SDS-denatured proteins was performed on 10% acrylamide gel. Composition of a 10% gel is shown below:

	stacking gel	10%
H ₂ O	13.9 ml	15.4 ml
1 M Tris-HCl (pH 6.8)	2.5 ml	--
2 M Tris-HCl (pH 8.8)	--	7.5 ml
80% sucrose	--	2.4 ml
30% AA	3.34 ml	14.3 ml
10% SDS	200 μ l	0.4 ml
10% APS	160 μ l	160 μ l
TEMED	16 μ l	16 μ l
Total volume	20 ml	40 ml

Electrophoresis was performed for 1h at approx 30 mA, maximal power 100V, in denaturing conditions.

3.3.3 LC/MS/MS Analysis

The gel bands digested by trypsin, were subsequently analyzed by LC-MS/MS using a LTQ Orbitrap XL ESI-mass spectrometer (Thermo Fisher Scientific) equipped with a nano-ESI source, coupled with a nano-Aquity capillary UPLC (Waters): peptides separation was performed on a capillary BEH C18 column (0.075 mm × 100 mm, 1.7 μm, Waters) using aqueous 0.1% formic acid (A) and CH₃CN containing 0.1% formic acid (B) as mobile phases. Peptides were eluted by means of a linear gradient from 10 % to 40 % of B in 45 min and a 300 nl•min⁻¹ flow rate. Peptide fragmentation was achieved using helium as collision gas and a collision cell energy of 30 eV. Mass spectra were acquired in a *m/z* range from 400 to 1800, and MS/MS spectra in a *m/z* range from 25-2000. MS and MS/MS data were used by Mascot (Matrix Science) to interrogate the Swiss Prot non-redundant protein database. Settings were as follows: mass accuracy window for parent ion, 10 ppm; mass accuracy window for fragment ions, 50 millimass units; fixed modification, carbamidomethylation of cysteines; variable modifications, oxidation of methionine. Proteins with scores > 65 and identified by at least 2 significant sequences, were considered as reliable proteins. The quantitative analysis of the MS and MS/MS spectra was performed using Max Quant software, obtaining LFQ intensities of control and treated samples.

3.3.4 Hsp70 peptide mapping

Hsp701A (0.5 μg/μl) underwent incubation for 2h at 37°C with and without epoxysiderol (2mM) in ratio 100:1 ligand/protein. Subsequently, the samples were loaded in a 10% monodimensional SDSPage gel and digested with trypsin following the procedure described in paragraph 3.3.1. After digestion, the samples underwent a LC-MS/MS analysis as described in paragraph 3.3.3.

Peptide mapping was performed by Mascot Daemon (Matrix Science). The sequence coverage of the Hsp701A was further increased carrying out a manual analysis of the MS spectra by using the Paws software.

3.3.5 Cell culture and treatment

HeLa (cervical carcinoma) and Jurkat (T-cell leukemia) cell lines were purchased from the American Type Cell Culture (ATCC) (Rockville, MD, USA). The cells were maintained in DMEM (HeLa) or RPMI 1640 (Jurkat), supplemented with 10% FBS, 100 mg/L streptomycin and penicillin 100 IU/mL at 37 °C in a humidified atmosphere of 5% CO₂. To ensure logarithmic growth, cells were sub-cultured every 2 days. Under given experimental conditions, untreated cells were able to double in number in less than 24 hr. Stock solutions (50 mM) of purified compounds in DMSO were stored in the dark at 4 °C. Appropriate dilutions were prepared in culture medium immediately prior to use. In all experiments, the final concentration of DMSO did not exceed 0.1% (v/v).

3.3.6 Cell viability and cell cycle analyses

Cells were seeded in 96-well plates and incubated for the established times in the absence (vehicle only) and in the presence of different concentrations of compounds and Etoposide as positive control. The day before treatments, cells were seeded at a cell density of 1×10^4 cells/well. The number of viable cells was quantified by MTT ([3-(4,5-dimethylthiazol-2-yl)-2,5-diphenyl tetrazolium bromide]) assay. Absorption at 550 nm for each well was assessed using a microplate reader (LabSystems, Vienna, VA, USA). In some experiments cell viability was also checked by Trypan Blue (Lonza, USA) exclusion assay using a Bürker counting chamber. Half maximal inhibitory concentration (IC₅₀) values were calculated from cell viability dose–response curves and defined as the concentration resulting in 50% inhibition in cell survival as compared to controls.

Cell cycle was evaluated by propidium iodide (PI) staining of permeabilized cells, according to the available protocol, and flow cytometry (BD FACSCalibur *flow cytometer*, Becton Dickinson, San Jose, CA, USA). Data from 5000 events per sample were collected. The percentages of the elements in the hypodiploid region and in G₀/G₁, S and G₂/M phases of the cell cycle were calculated using the CellQuest and MODFIT software, respectively.

3.3.7 Determination of apoptosis

HeLa cells (3x10⁵ cells/well) were incubated with DMSO (control) and epoxysiderol 25μM for 48h in a cell culture incubator. Cells were then processed for detection of apoptosis according to the protocol described in the Annexin V, FITC Apoptosis Detection Kit (Dojindo EU GmbH, Munich (Germany)). Following incubation, HeLa pellets were suspended in 100μL of Annexin V Binding Solution; subsequently, 5μL of Annexin V, FITC conjugate and 5μL of PI Solution were added in each sample and incubated for 15 min at room temperature with protection from light. After adding 400μL of Annexin V Binding Solution, samples were detected by Flow Cytometry (BD FACSCalibur *flow cytometer*, Becton Dickinson, San Jose, CA, USA) using Cell-Quest software.

3.3.8 Western Blot analysis

Cell whole lysates (HeLa) immunoblot analysis were prepared according to the standard protocol. Protein concentration was determined by DC Protein Assay (Bio-Rad, Berkeley, CA, USA), using bovine serum albumin (BSA) as a standard. Proteins were fractionated on SDS-PAGE, transferred into nitrocellulose membranes, and immunoblotted with the appropriate primary antibody (1:1000). Signals were visualized with the appropriate horseradish peroxidase-conjugated secondary antibody and enhanced chemiluminescence (Amersham Biosciences-

GE Healthcare, NY, USA). Densitometry of bands was performed with ImageJ software.

3.3.9 Cytosol and membrane extracts

HeLa cells were washed twice with PBS, detached with trypsin-EDTA 1x in PBS (Euroclone), harvested in PBS and centrifuged for 5 minutes at 600 x g at 4°C. After that, the pellets were resuspended in 4 ml of lysis buffer (Tris HCl 20 mM, pH 7,4; sucrose 250 mM; DTT 1 mM; protease inhibitors, EDTA 1 mM in water), sonicated (5 seconds pulse - 9 seconds pause for 2 minutes, amplitude 42%) and then centrifuged at 4°C for 10 minutes, at 5000 x g. The obtained supernatants were ultra-centrifuged for 1 hour at 100000 x g at 4°C, until to get new supernatants that represent cytosol extracts. Each resulting pellet was resuspended in 4 ml of lysis buffer and ultra-centrifuged for 1 hour at 100000 x g at 4°C. The pellets were then resuspended in 250 µl of solubilization buffer (Tris HCl 20 mM, pH 7,4; DTT 1 mM; EDTA 1 mM; Triton X-100 1%, in water) and left overnight on orbital shaker at 4°C. After that, the solution was centrifuged for 30 minutes at 50000 x g at 4°C: the supernatants represent membrane extracts.

3.3.10 Nuclear extracts

HeLa cells were washed twice with PBS, detached with trypsin-EDTA 1x in PBS (Euroclone), harvested in PBS and centrifuged for 5 minutes at 600 x g at 4°C. The pellets were resuspended in 500 µl of buffer A (Hepes pH 7.9 10 mM, EDTA pH 8.0 1 mM, KCl 60 mM, N-P40 0.2%, DTT 1 mM, PMSF 1 mM, protease inhibitors) and then left on ice for 10 minutes. After that, the samples were centrifuged at 660 x g for 5 minutes at 4°C and the supernatants resuspended in 50 µl of buffer C (Tris HCl pH 7.8 250 mM, KCl 60 mM, DTT 1 mM, PMSF 2 mM, glycerol 20% v/v in PBS) and centrifuged again at 9500 x g for 15 minutes at 4°C. The obtained pellets were resuspended in 100 µl of buffer B (Hepes pH 7.9 10

mM, EDTA pH 8.0 1 mM, KCl 60 mM, DTT 1 mM, PMSF 1 mM, protease inhibitors) and centrifuged at 660 x g for 5 minutes at 4°C. The samples were then washed twice with 1 ml of buffer B, resuspended in 50 µl of buffer C and exposed to 3 cycles of freeze/thawing. Finally, the samples were centrifuged at 9500 x g for 15 minutes at 4°C: the pellets represent the nuclear extracts.

3.3.11 ATPase activity Assay

ATPase/GTPase Activity Assay Kit (MAK113-1KT) was from Sigma-Aldrich, performed by following the manufacturer's instructions. ATPase reactions were carried out for 3h at 37°C in Tris 40mM pH 7.4, NaCl 80mM, KCl 10mM, MgAc₂ 8mM, EDTA 1mM, using Hsp70 1A (1.4 mg/ml, BPS Bioscience, 50287, final concentration of 1µM in 20µL), Hsp40 (2,3 mg/ml, BPS-Bioscience, 90303) and different concentrations of epoxysiderol 10µM, 50 µM and 100µM in final volume 20µL). Oridonin was used as positive control. Subsequently, ATP 4mM was supplemented to each mixing solution for 40min at room temperature, before adding 80µL of malachite green reagent. ADP generation was measured after 30min with a Thermofisher UV Spectrophotometer (540 nm excitation and 620nm emission). Absorbance intensity values measured for Hsp70 without any testing compound was assumed as 100% of enzyme activity. The background reaction rate was measured in a reaction lacking enzyme or substrate and subtracted from the experimental rates.

3.3.12 Reagents and Antibodies

Fetal bovine serum (FBS) was from GIBCO (Life Technologies, Grand Island, NY, USA). The anti-HSP90α (mouse monoclonal SPA-835) was obtained from Stress-gen Bio-reagents Corporation (Victoria, Canada). Anti-BAG3 (rabbit polyclonal) was obtained from Biouniversa s.r.l (Montoro, AV, Italy). The antibodies anti-Hsp70 (mouse monoclonal sc-32239), anti-JNK1 (rabbit

polyclonal sc-571), anti-pJNK (mouse monoclonal sc-6254), anti-NFkB (mouse monoclonal sc-7386), anti-p-p38 (rabbit polyclonal sc-17852), anti p-38 (mouse monoclonal sc-7972), anti-pAkt (rabbit polyclonal sc-7935-R), anti-Akt (rabbit polyclonal), anti-Cdc2 (mouse monoclonal, sc-8395) and anti-phospho (Thr161)-Cdc2 p34 (rabbit polyclonal, sc-101654), anti-Erk1/2 (mouse monoclonal sc-1647), anti-pErk (mouse monoclonal sc-7383), anti- α -Tubulin (mouse monoclonal sc-32293), anti-GAPDH (rabbit polyclonal), anti-caveolin (rabbit polyclonal sc-894) were obtained from Santa Cruz Biotechnology (Santa Cruz Biotechnology, Inc., Delaware, CA, USA); anti-lamin A (L1293 rabbit polyclonal) was purchased from Sigma-Aldrich (USA); anti-PARP (#9542 rabbit polyclonal) was purchased from Cell-Signaling (USA); appropriate peroxidase-conjugated secondary antibodies were from Jackson Immuno Research (Baltimore, PA, USA).

3.3.13 Molecular Docking Studies

The 3D chemical structure of epoxysiderol was built using Maestro v. 10.7 (Schrödinger Suite). Afterwards, the generated structure was prepared using LigPrep software (Schrodinger Suite), and the structures were minimized using OPLS 2005 force field. Protein 3D model was prepared using the Schrödinger Protein Preparation Wizard, starting from the Hsp70 X-ray structure co-complexed with the inhibitor KC7 ((1*R*,2*S*,3*R*,5*R*)-3-((5-(benzyloxy)quinazolin-4-yl)amino)-5-(hydroxymethyl) cyclopentane-1,2-diol) (PDB code: 5AQX). Water molecules were removed, all hydrogen atoms were added, and bond orders were assigned. Docking calculations were performed after removal of the co-complexed compound KC7. Molecular docking experiments were performed using Glide software, using the Extra Precision scoring/sampling mode (XP), setting 20 maximum docking poses to be saved.

3.3.14 Statistical analysis

Data reported are the mean values \pm SD from at least three experiments, performed in duplicate, showing similar results. Differences between treatment groups were analyzed by Student's t-test. Differences were considered significant with $p < 0.05$.

- Chapter 4 -

Introduction

4.1 Heat Shock Protein 90: isoforms and localizations

Heat shock protein 90 (Hsp90) is one of the most abundant chaperones among the heat-related proteins. The "90" comes from its molecular weight, which is roughly 90 kDa. Heat shock protein 90 assists other proteins to their correct folding. It also stabilizes a number of proteins required for tumor growth (such as AKT, ERK, EGFR, Survivin and others), so Hsp90 modulators are investigated as anti-cancer drugs.

Hsp90 is highly conserved and expressed in a variety of different organisms, it is found in bacteria and all branches of eukaria, but it is absent in archaea.¹⁵¹ Whereas cytoplasmic Hsp90 is essential for viability under all conditions in eukaryotes, the bacterial homologue HtpG (high-temperature protein G, with 40% sequence identity and 55% similarity to the human protein) is dispensable under non-heat stress conditions. Several eukaryotes possess specialized mitochondrial (TRAP1) and endoplasmic reticulum (GRP94/GP96/endoplasmic) isoforms.¹⁵¹

Yeast Hsp90 is 60% identical to human Hsp90 α . In mammalian cells, there are two or more genes encoding cytosolic Hsp90 homologues, with the human Hsp90 α showing 85% sequence identity to Hsp90 β .^{152, 153} In table 1 the different isoforms of Hsp90 are showed.

Table 1. The five functional human genes encoding Hsp90 protein isoforms

family	subfamily	Gene	protein	subcellular location
HSP90A	HSP90AA (inducible)	HSP90AA1	Hsp90- α_1	cytosolic
		HSP90AA2	Hsp90- α_2	
	HSP90AB (constitutively expressed)	HSP90AB1	Hsp90- β	
HSP90B		HSP90B1	Endoplasmin/ GRP-94	endoplasmic reticulum
TRAP		TRAP1	TNF Receptor- Associated Protein 1	mitochondrial

4.1.1 Hsp90 structure

Hsp90 consists of four structural domains (Fig. 1):¹⁵⁴

- a highly conserved N-terminal domain (NTD) of ~25 kDa, with an adenosine triphosphate (ATP)-binding and hydrolyzing pocket, responsible for the ATPase activity of Hsp90;
- a "charged linker" region, that connects the N-terminus with the middle domain (MD);
- a middle domain (MD, divided in M₁ and M₂ domains) of ~40 kDa, involved in co-chaperones and client proteins recognition/binding;
- a C-terminal domain (CTD) of ~12 kDa, able to modulate Hsp90 dimerization. In addition, it contains the tetratricopeptide repeat-binding (TRP) motif, as well as its co-chaperones such as Hsp organizing protein (Hop). The TRP motif allows the binding to Hsp90 and the regulation of its ATPase functions.

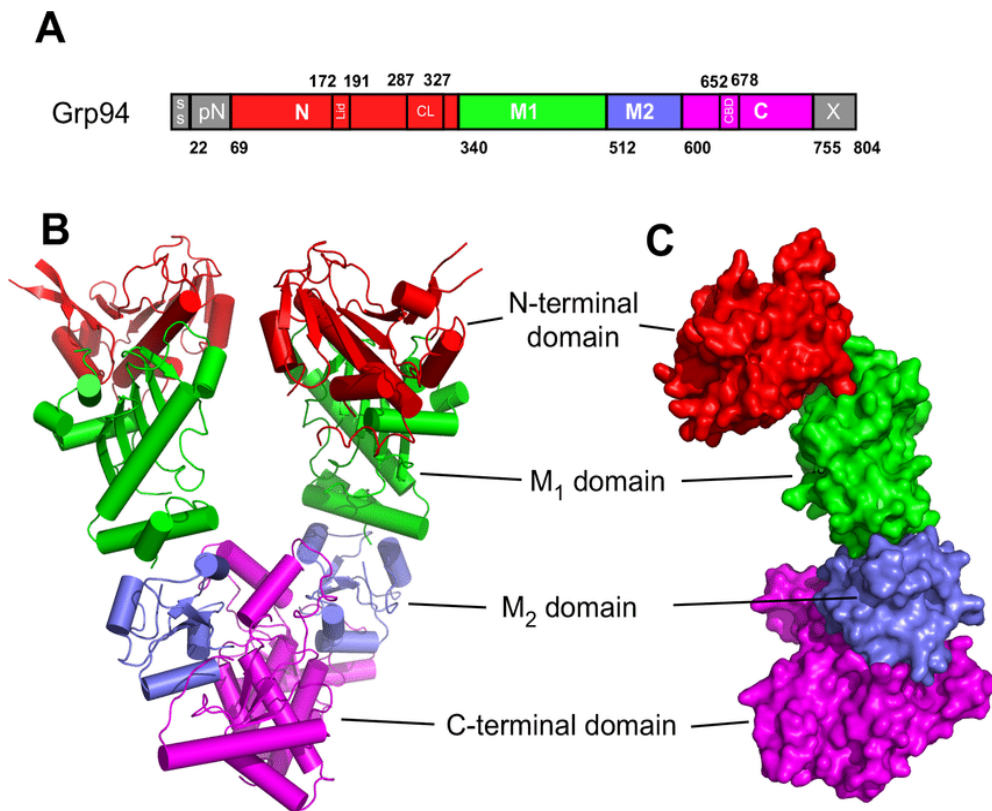


Figure 1. Domains and functional regions of Hsp90. The structure of Grp94 is shown. A) Schematic organization. B) Cartoon representation of the Grp94 dimer. C) surface representation of the Grp94 monomer. Adopted from: Maharaj KA et al. 2016; *PLoS ONE*.

The NTD shows homology not only among members of the Hsp90 chaperone family but also to members of the ATPase/kinase GHKL (Gyrase, Hsp90, Histidine Kinase, MutL) superfamily. This domain is responsible of ATP hydrolysis, required for the correct protein folding mediated by Hsp90.¹⁵⁵

The MD is divided into three regions:

- a 3-layer α - β - α sandwich;
- a 3-turn α -helix and irregular loops;
- a 6-turn α -helix;

The MD is also involved in client protein binding. For example, proteins known to interact with the Hsp90 MD include PKB/AKT1, ERK1/2, Raf1, cyclin A, eNOS.¹⁵⁶

The CTD possesses the dimerization region. The dimer formation is independent of nucleotide binding or client proteins or co-chaperones interactions. On the other hand, the dimerization of the N-terminal domains is dependent on binding. Residues in the MD and CTD are involved in interactions with the majority of clients, however residues in the NTD also participate in binding some specific clients.¹⁵⁷ Co-factors such as the immunophilins FKB (p51) and FKB (p52), the stress induced phosphoprotein 1 (Sti1/Hop), and many more proteins interact with the TRP motif recognition site (MEEVD pentapeptide).¹⁵⁸

4.1.2 Hsp90 ATPase activity and ATP binding site

As shown in Figure 2, a correct peptide folding includes Hsp40, Hsp70, HIP, HOP, Hsp90, immunophilin and p23 (Prostaglandin E synthase 3) proteins.¹⁵⁹ Just after translation, the unfolded peptide binds to Hsp40 and Hsp70 (top, left). Subsequently, HOP (composed of TPR domains) delivers it to Hsp90. HOP mediates interaction between Hsp70 and Hsp90 through their C-terminal domains. This transfer takes place only if ADP is bound to Hsp90. The exchange of ADP to ATP inside N-terminal pocket induces dissociation of Hsp70 and its co-chaperones from the complex that associates then with p23 (via N-terminal side of Hsp90 dimer) which prevents ATP hydrolysis, and immunophilins, which replaces HOP (right). The binding of ATP triggers the dimerization of the N-terminal domains and enables the client protein activation/binding. Hsp90-bound ATP is then hydrolyzed, and the energy released by ATP hydrolysis enables the client protein folding, leading to the dissociation of the complex Hsp90-peptide. ATP hydrolysis results in a conformational changing from an elongated

orientation in which the N-terminal domains dimerize to a wide, open V-shaped orientation releasing the client protein.¹⁵⁹

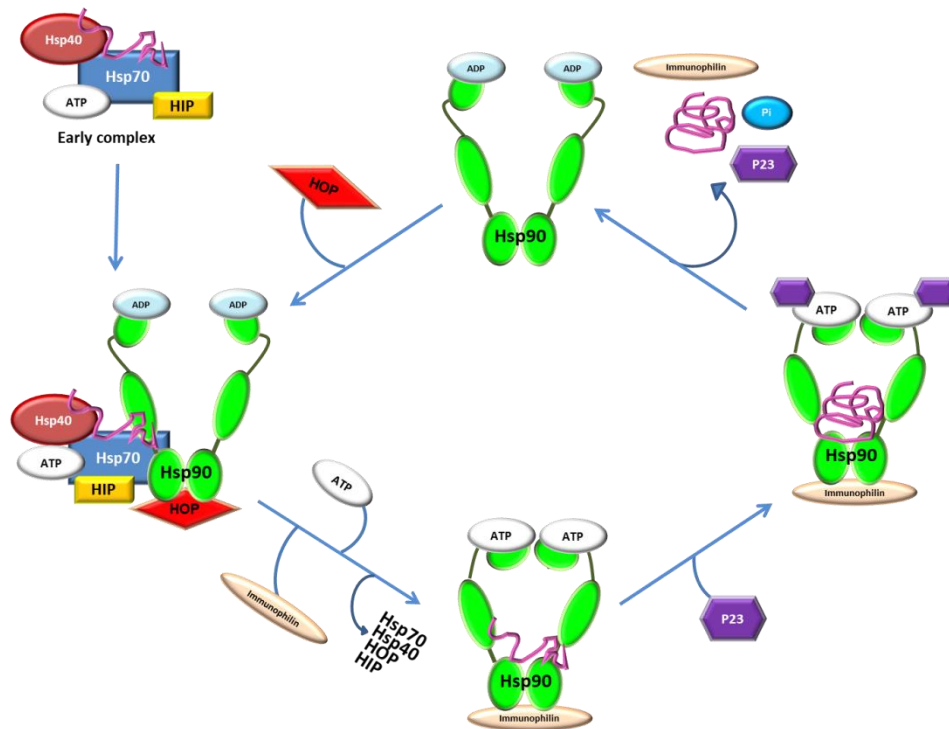


Figure 2. Hsp90-dependent ATP hydrolysis cycle of client proteins activation.

Amino acids that are directly involved in the interaction with ATP are Leu34, Asn37, Asp79, Asn92, Lys98, Gly121, and Phe124. In addition, Mg^{2+} and several water molecules form bridging electrostatic and hydrogen bonding interactions, respectively, between Hsp90 and ATP. In addition, Glu33 is required for ATP hydrolysis.¹⁶⁰

If the chaperone binds geldanamycin, a known Hsp90 inhibitor which mimics ADP binding, p23 and HOP dissociate and CHIP, an E3 ubiquitin ligase, is attached to the complex and the protein is degraded through the proteasome-mediated pathway. Immunophilins are responsible for transportation of Hsp90-peptide complex along the microtubule fibers (additionally, dynamin and dynein,

the microtubule-associated proteins are involved in this process). Therefore, a translocation of hormones, p53 and probably other Hsp90 substrate proteins within cytoplasm is fast and tightly controlled.¹⁵⁹

Hsp90 ATP-binding site is located in a pocket on the helical face of the N-domain. In the crystal structure the bound nucleotide interacts with hydrophobic residues of the pocket (Fig 3A and B), and with solvent molecules that mediate key polar interactions. Particularly, the ATP adenine base penetrates in the pocket with one face against hydrophobic side chains and makes one single hydrogen bond to the side chain of ASP79. Water molecules mediate other polar interactions, specially with the ribose sugar while the α and β phosphates of the ATP are coupled to the protein via an octahedrally coordinated Mg^{2+} ion (Fig 3C).¹⁶¹ Microbial antibiotics such as geldanamycin and radicicol are both able to bind Hsp90 in the same pocket of ATP (Fig. 3E and F). They possess anti-tumor activity and ability to interfere with protein kinase pathways,¹⁶² although their mechanism of action is not fully understood. Nevertheless, they can be identified as inhibitors of ATP-binding to Hsp90.¹⁶¹

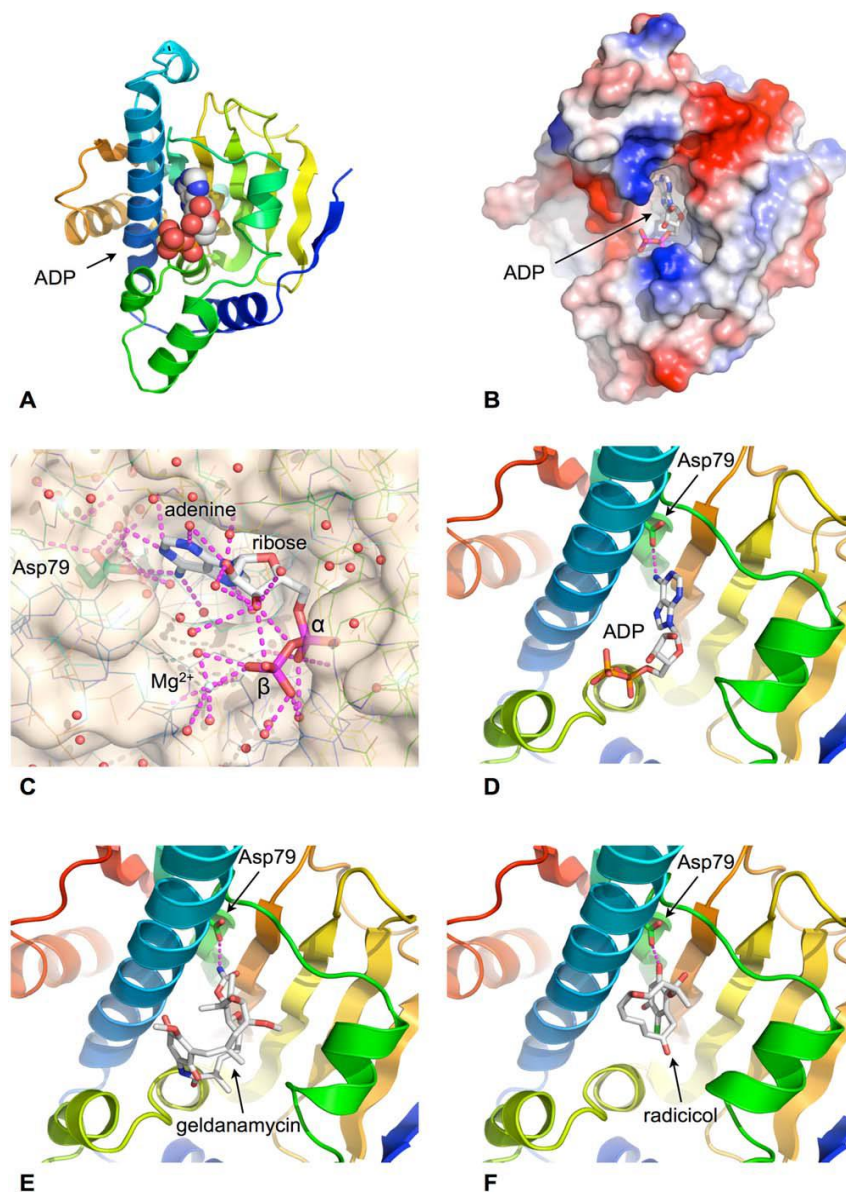


Figure 3. ATP-binding site of Hsp90. A) ATP/ADP binds into a pocket formed in the helical face of the N-terminal domain. B) Molecular surface of Hsp90 N-domain colored according to electrostatic potential blue:+ve, red:- ve. The adenine base is buried in the binding pocket with the phosphates exposed to solvent. C) Close up of the water-filled nucleotide-binding pocket. Polar interactions made by the bound ADP are shown as dashed lines. D) The adenine base makes only a single direct hydrogen bond with the protein, via the side chain of Asp 79. E) The natural product geldanamycin binds to the nucleotide binding pocket and is a competitive inhibitor of ATP binding

by Hsp90. F) The natural product radicicol binds to the nucleotide-binding pocket and is a competitive inhibitor of ATP binding by Hsp90. Adopted from: Pearl LH. 2016; *Biopolymers*.

4.1.3 Hsp90 client proteins

The Hsp90s are a family of molecular chaperones that function in the cellular stabilization, regulation, and activation of a variety of client proteins, such as oncogenic protein kinases and nuclear steroid hormone receptors, in order to obtain their active conformation. Many of these client proteins are involved in critical cellular functions that promote cell growth, proliferation and cell survival which are also important to maintain the cancer phenotype.¹⁶³

Hsp90 is also implicated in the assembly of RNA polymerases, PI3-kinase-like kinases such as mTOR and SMG1, snoRNPs8 and NLR innate immunity receptors.¹⁶⁴ Recent high-throughput screening experiments have also identified E3 ubiquitin ligase subunits interacting with Hsp90, but whether these are actually dependent as a class on Hsp90 for their function remains to be shown.¹⁶⁵ The ability of Hsp90 to engage with its client proteins (Fig. 4) is mediated by co-chaperones that act as adaptors and modulate the specificity and selectivity for client proteins. For the best of our knowledge, the simplest of these adaptor co-chaperones is Cdc37, which mediates recruitment of members of the eukaryotic Ser/Thr and Tyrosine kinase family and forms a stable ternary complex with Hsp90.

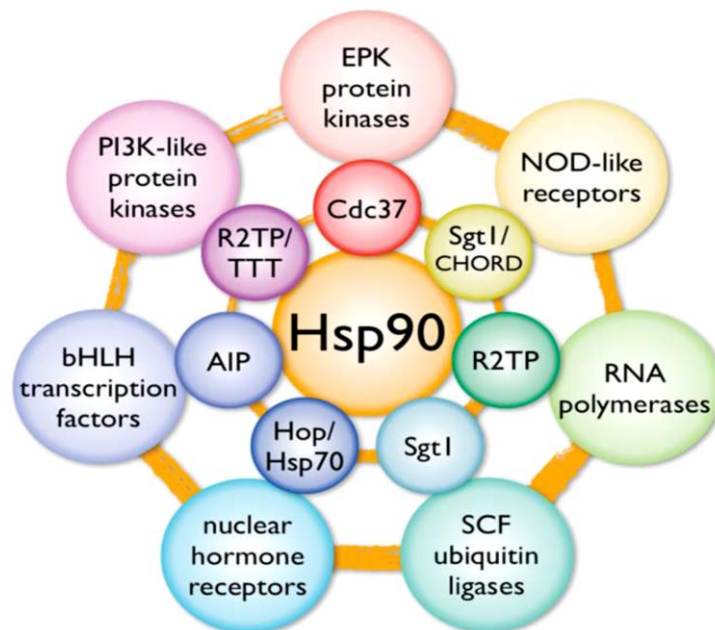


Figure 4. Hsp90 and its clients. Hsp90 engages with a range of ‘client’ protein classes (outer circle) via its interaction with various co-chaperone proteins or complexes (inner circle), that act as adaptors, simultaneously able to interact with the specific client and the central chaperone itself. Adopted from: Pearl LH. 2016; *Biopolymers*.

Steroid hormone receptors (estrogen and glucocorticoid receptors) are coupled to Hsp90 via the TPR-domain protein Hop.¹⁶⁶ Other TPR-domain co-chaperones such as AIP and FKB(p38) have been implicated in recruitment of such diverse proteins as aryl hydrocarbon receptor and hepatitis C NS5A to the Hsp90 system, but the mechanistic details of these process are not yet well understood.¹⁶⁷ The most complex Hsp90 co-chaperone system described to date, is the R2TP complex, a complex of four different proteins recruited to Hsp90 via the TPR-domain. R2TP couples Hsp90 to stabilization and assembly of snoRNPs, RNA Pol II and other proteins.¹⁶⁸

4.1.4 Functions of Hsp90 in cancer

Hsp90 is overexpressed in cancer cells and several of its client proteins are signaling oncoproteins (ERK1/ERK2, survivin, EGFR, AKT, Raf-1, mutate p53

and others) that represent nodal points in multiple oncogenic signaling pathways.¹⁶⁹ In addition, oncoproteins are often mutated and/or overexpressed in cancer cells, and maintenance of their malignancy requires higher Hsp90 activity than normal cells. Hsp90 client oncoproteins are also involved in other hallmark process of cancer, including induction of angiogenesis, mediation of apoptosis, and promotion of tissue invasion and metastasis. Hsp90 influences angiogenesis by chaperoning hypoxia-inducible factor-1 α (HIF-1 α) and vascular endothelial growth factor receptor (VEGFR) in addition to governing nitric oxide synthase upregulation. Hsp90 chaperones client proteins are also apoptotic mediators, including Bcl-2, Apaf-1, the serine-threonine protein kinase AKT/PKB and Survivin. Moreover, Hsp90 may promote tissue invasion and metastasis through MMP-2 activation, digesting extracellular matrix proteins. Other client proteins of Hsp90 that play a role in cell signaling processes include FAK (integrin pathway), IL6R (JAK/STAT3 pathway) and I κ B kinases (NF κ B pathway).¹⁷⁰ Based on this knowledge, the inhibition of the Hsp90 protein folding machinery can lead to the simultaneous disruption of multiple cellular pathways that are crucial for the growth and survival of cancer cells, which represents a multifaceted approach to tumor treatment.

4.1.6 Hsp90 inhibitors: therapeutic targeting of Hsp90 ATPase activity

The involvement of Hsp90 in the stabilization of many highly oncogenic protein kinase clients and the revelation of Hsp90 as an ATP-dependent protein with a ‘druggable’ nucleotide-binding site in its N-terminal domain, prompted a remarkable level of interest in Hsp90 as a therapeutic target in cancer. Progress was greatly assisted by the availability of natural compounds such as geldanamycin and radicicol.¹⁶² The approach was confirmed in early studies using modified versions of geldanamycin, such as 17-AAG, which showed

downregulation of key oncogenic client proteins such as ERBB2, CRAF, and AKT, and loss of signaling through critical cancer-driving signaling pathways in cell lines and in patients.¹⁷¹ Presently, there are more than a dozen Hsp90 ATP-competitive inhibitors in clinical trials at various stages, with promising activity against a range of tumors, such as radicicol (a macrocyclic antifungal antibiotic), geldanamycin (a benzquinoid ansamycin antibiotic) and other derivatives (Fig. 5).

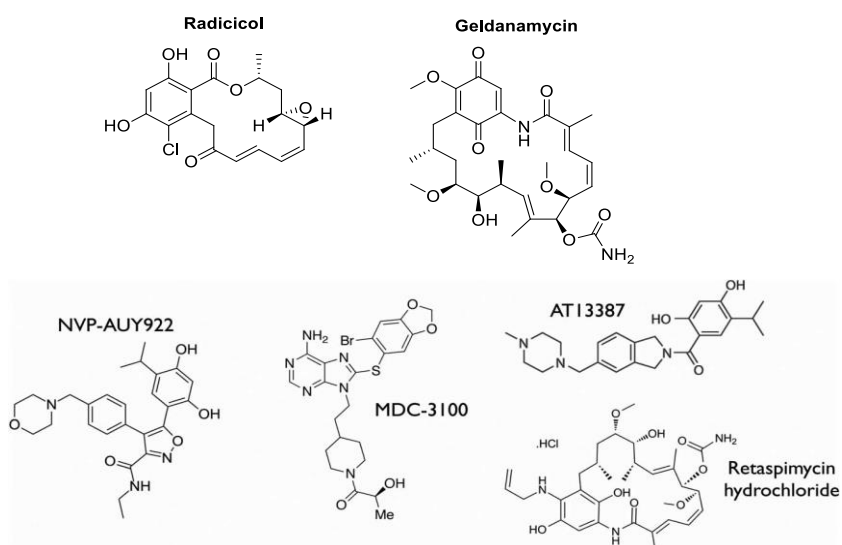


Figure 5. Hsp90 inhibitors. Structures of radicicol, geldanamycin and of a number of synthetic or semisynthetic ATP-competitive Hsp90 inhibitors currently in clinical development.

The multiple functions played by the molecular chaperone Hsp90, particularly in response to different type of stress, make this protein a promising target for several therapeutic approaches.¹⁷² The modulation of Hsp90 has indeed been proposed as an efficient strategy to face multiple cancer types.¹⁷³ Many plant metabolites, belonging to different classes, have been shown to efficiently interact with Hsp90, inhibiting its activity in cancer cell and exerting a significant antiproliferative and pro-apoptotic action.¹⁷⁴

Results and discussion

4.2 Screening of fusicoccane and abietane diterpenes by SPR

A SPR technology by Biacore was implemented to screen a collection of twenty-eight diterpenes with proven pharmacological activities to identify Hsp90 interactors. Particularly, sixteen diterpene fusicoccane skeletons from *Hypoestes forsskaolii* (Acanthaceae) and twelve abietanes from *Zhumeria majdae* (Lamiaceae) and different *Salvia* spp. (Lamiaceae) were tested in our studies (Fig. 6).

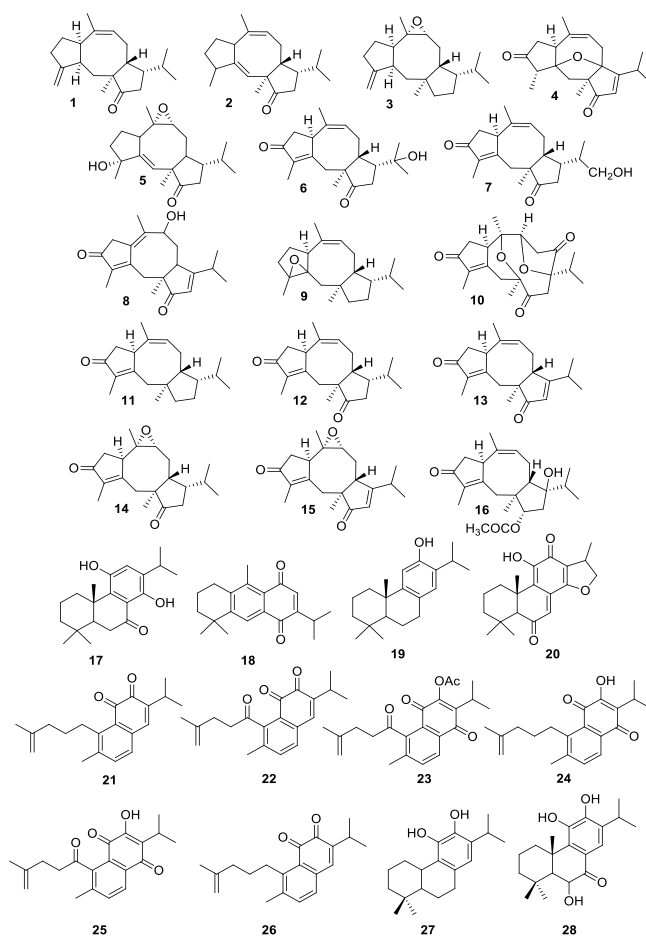


Figure 6. Structures of fusicoccanes and abietanes screened against Hsp90 α by SPR

The affinity towards the molecular chaperone Hsp90 was assayed by SPR for the isolated compounds (Table 2).

Table 2. Thermodynamic Constants Measured by Surface Plasmon Resonance for the Interaction between tested compounds and immobilized Hsp90 α

Compound	K_D (nM) ^a \pm SD
1	401 \pm 4
2	20.5 \pm 1.2
3	130 \pm 1
4	217 \pm 17
5	45 \pm 4
6	15.3 \pm 0.2
7	no binding
8	no binding
9	no binding
10	120 \pm 1
11	28 \pm 3
12	1000 \pm 25
13	1739 \pm 75
14	no binding
15	no binding
16	no binding
17	161 \pm 2
18	no binding
19	no binding
20	2.97 \pm 0.5
21	no binding
22	no binding
23	no binding
24	no binding

25	no binding
26	no binding
27	no binding
28	no binding
radicicol	1.2 ± 0.1
17-AAG	388 ± 89

^aResults were given mean ± standard deviation.

17-AAG and radicicol were used as positive controls ¹⁷⁴ SPR assay led us to obtain the thermodynamic and kinetic parameters of fusicoccanes/Hsp90 α complex formation. Nine (**2-6**, **10-11**, **17** and **20**), out of the twenty tested compounds interacted with the protein (Table 2): among them, compounds **2**, **6**, **11** and **20** showed higher affinity towards the chaperon, as inferred by the measured K_D values falling in the 3-30 nM range.

Due to the limited number of tested compounds and their structure variability, structure activity relationship study could not be attempted. Anyway, our data suggested that the interaction between fusicoccanes/abietanes and Hsp90 could involve multiple sites on their backbone.

4.2.1 Antiproliferative activity of fusicoccanes and abietanes tested by MTT on Jurkat, HeLa and MCF7 cell lines

On the basis of the ability of these compounds to bind Hsp90 α , we evaluated the potential antiproliferative or cytotoxic activity of the diterpenes on human HeLa (epithelial carcinoma), Jurkat (human T-cell lymphoma) and MCF7 (breast cancer) cell lines. The cells were incubated for 48h with increasing concentration of fusicoccanes and abietanes (10-150 μ M) and cell viability was determined by MTT assay.¹⁷⁵ Among tested fusicoccanes, **1**, **2**, **4**, **9**, **14-16**, were inactive, while **3** showed low activity on Jurkat cells, and **8** and **10** were not effective towards HeLa cells. Compounds **5**, **11-13** showed moderate activities on both cell lines.

Compound **6** demonstrated an interesting antiproliferative activity in HeLa cells, showing an IC₅₀ value of 18 ± 1 μM (Table 3).

Table 3. IC₅₀ (μM) Values of tested compounds against two cancer cell lines^a

compound	Jurkat ^b	HeLa ^c
1	>100	>100
2	66 ± 3	>100
3	44 ± 2	>100
4	70 ± 3	>100
5	45 ± 1	38 ± 1
6	45 ± 3	18 ± 1
7	>100	>100
8	>100	50 ± 4
9	>100	>100
10	>100	50 ± 2
11	49 ± 2	48 ± 2
12	65 ± 3	35 ± 2
13	47 ± 2	50 ± 3
14	>100	>100
15	>100	>100
16	>100	>100
etoposide	2.5 ± 0.4	4.0 ± 0.83

^aMean values ± SD from three experiments done in triplicate. ^bT-cell lymphoma. ^cCervical carcinoma.

Compounds **17-19** and **21-28** were not effective towards HeLa but showed moderate activity on MCF7. Compound **20** was found as the most active on MCF7 cells, showing an IC₅₀ of 20 ± 2 μM (Table 4). therefore, we decided to focus of the fusicoccane 18-hydroxyhypoestenone (**6**) and the abietan lanugon Q (**20**) for our further studies. Notably, compounds **6** and **20** did not show cytotoxic

activity on the nontumor human peripheral blood mononuclear cell line (PBMC) up to 100 μM .

Table 4. IC₅₀ (μM) Values of tested compounds against two cancer cell lines^a

compound	MCF7 ^b	HeLa ^c
17	>50	>50
18	45 \pm 2	>50
19	44 \pm 1	91 \pm 3
20	20 \pm 2	>50
21	>50	>50
22	>50	>50
23	>100	>100
24	>50	>50
25	>100	>100
26	>50	>100
27	>100	>50
28	>50	>50
etoposide	2.2 \pm 0.5	4.0 \pm 0.83

^aMean values \pm SD from three experiments done in triplicate. ^bBreast cancer. ^cCervical carcinoma.

4.2.2 Evaluation of the biological activity of the selected diterpenes by flow cytometry and WB

The mechanism of action of cancer cell viability inhibition exerted by **6** was investigated incubating HeLa cells for 48h with concentrations close to the IC₅₀ values of **6** (10 and 20 μM) and analyzed by flow cytometry. The treatment caused a G₂/M cell cycle arrest (Fig. 7A). Hsp90 α inhibition could induce G₂/M arrest by affecting, directly or indirectly, the levels and the phosphorylation state

of several cyclins and cyclin-dependent kinases (CDKs).^{176, 177} On this basis, the cell cycle arrest induced by **6** was studied evaluating the expression of these proteins. WB Results (Fig. 7B) indicated that the cell cycle arrest in G₂/M phase observed for the HeLa cells was accompanied by a significant decrease in the level of phosphorylated-Thr161 Cdc2/p34 protein.

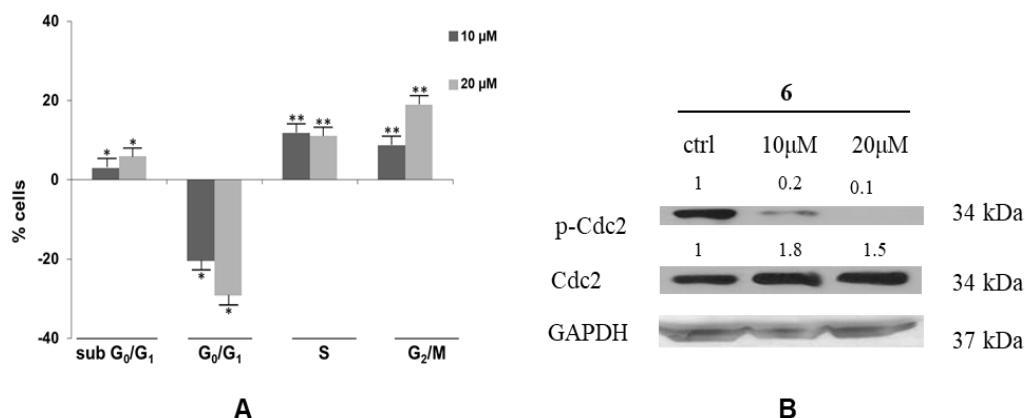


Figure 7. Effect of **6** on cell cycle progression and on cell cycle regulatory protein levels. A) Flow cytometric evaluation of DNA content in HeLa cells treated with DMSO (control) or **6** (10 and 20 μM) for 48 h. On the Y axis: the percentages of cells in subG₀G₁ (hypodiploiddia) and in each cell cycle phase of **6**-treated cells subtracted for the corresponding percentages of control cells. Results are expressed as means ± SD of three experiment performed in duplicate (**p<0.005, *p<0.05). B) Western Blot analysis of Cdc2 and pCdc2 (Thr161) levels in HeLa cells treated with DMSO (ctrl) or **6** (10 and 20 μM) for 48 h. For each immunoblot, band intensity was quantified by densitometry (numbers above each lane). GAPDH was included as a loading control. The blots are representative of at least two different experiments with similar results.

Subsequently, compound **6** (10 and 20 μM) was tested for its effect on some Hsp90 α client proteins level in the HeLa cells (Fig. 8); **6** was able to induce a strong depletion of p-Akt and p-ERK1 proteins (Fig. 8B), while the Hsp70 level was slightly affected after the treatment (Fig. 8A).

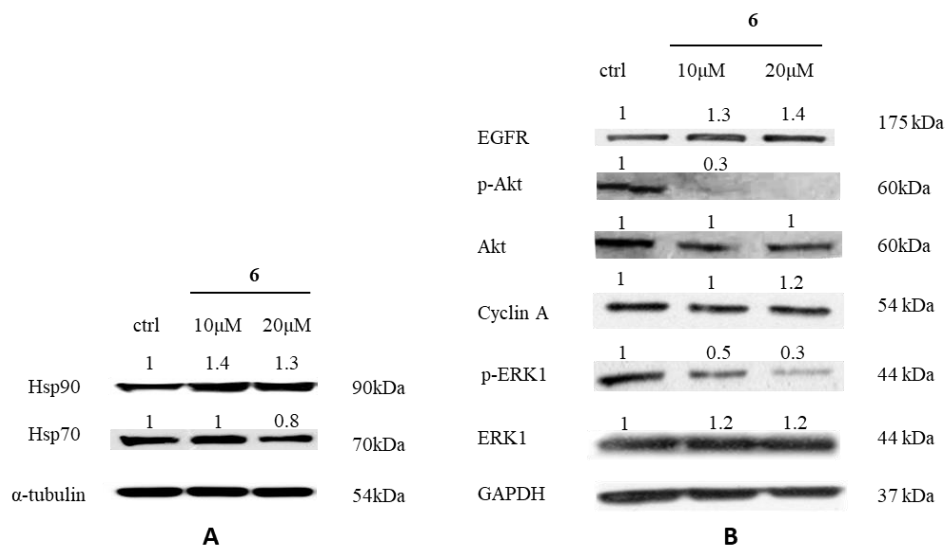


Figure 8. Effect of **6** on Hsp90α client proteins levels in HeLa cells after treatment with **6** (10 and 20 μM) for 48h. Equal amounts (30 μg) of total protein lysate were separated on SDS-PAGE and client proteins were visualized by Western Blot analysis. α-tubulin and GAPDH were used as loading controls. The blots are representative of three different experiments with similar results. Numbers above each lane represent the densitometric values.

Also compound **20** was investigated for its intracellular activity on Hsp90α client proteins by WB in MCF7 cells (Fig.9). After treatment of MCF7 with **20** (18 μM) for 48h, we observed:

- a moderate reduction of Hsp90 levels;
- strong decrease of p-Akt, p-ERK1 and cyclin A levels.
- slight increase of Hsp70 levels.

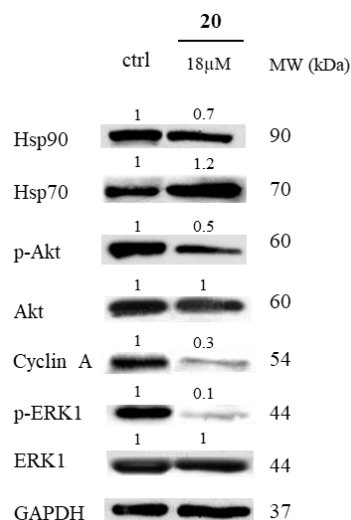
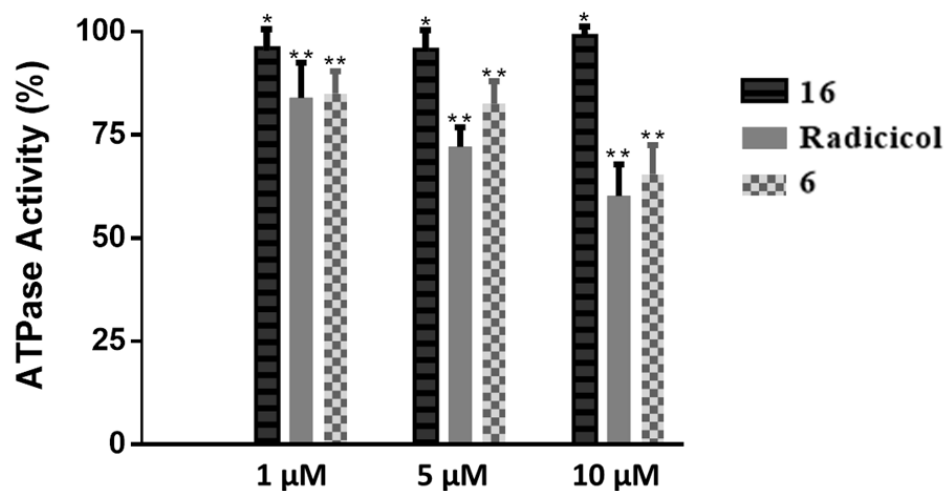


Figure 9. Effect of lanugon Q (**20**) on Hsp90 α client proteins levels in HeLa cells after treatment with **20** (18 μ M) for 48 h. Equal amounts (30 μ g) of total protein lysate were separated on SDS-PAGE and client proteins were visualized by Western Blot analysis. GAPDH was used as loading control. The blots are representative of three different experiments with similar results. Numbers above each lane represent the densitometric values.

From these these results we can assert that both **6** and **20** can, directly or indirectly, determine a decrease of some of Hsp90 α client proteins involved in anti-apoptotic and proliferative pathways in two different cell lines such as HeLa and MCF7.

4.2.3 Effect of **6** and **20** on Hsp90 α ATPase activity

To investigate the possible effects of compound **6** and **20** on Hsp90 α bioactivity, its ATPase enzymatic activity was investigated. Radicol and hypoestenonol B (**16**), showing no affinity towards the chaperone in the SPR studies, were selected as positive and negative control, respectively. ATPase activity of Hsp90 α was affected by **6** at 5 and 10 μ M (Fig. 10), showing an inhibition almost comparable to that of radicol. On the other hand, compound **20** did not show any ATPase activity inhibition. Therefore, we decided to focus our further studies on compound **6**.



Figure

10. Compound **6** effect on Hsp90 α ATPase activity. Inhibition of the ATPase activity of Hsp90 α treated with DMSO (control) or different concentrations of **6**, radicicol (positive control), and **16** (negative control). Data are the means \pm SD of two independent experiments performed in triplicate. * $p < 0.05$, ** $p < 0.005$.

4.2.4 Study of the interaction Hsp90 α /**6** by molecular docking

To rationalize the Hsp90 α ATPase activity inhibition and the biological effects of the selected fusicoccane diterpene in terms of interaction with Hsp90 α , molecular docking studies between **6** and Hsp90 α protein were performed. In more details, the ATP-bound active state of Hsp82, a yeast Hsp90 α homologue (PDB code: 2CG9), was used as a model receptor and its sequence alignment with the human protein, reported by Lee et al.,¹⁷⁸ was used as reference during the comparative experimental–computational analysis. We have used the Induced Fit docking protocol,¹⁷⁹ to account accurately for both ligand and receptor flexibility due to the high plasticity of the Hsp90 during its mechanism of action.

Starting from biological evaluation reported above, we have considered the region at interface between the C-terminal chains of Hsp90 homologue (Fig. 11) as the

area of pharmacologic interest. From the structural point of view, **6** interacts with chaperone structure by two hydrogen bonds between the CO group at C-5 and the OH group at C-18 with Leu676_{chainA} and Leu670_{chainB} respectively, and by hydrophobic interactions of fusicoccane diterpene skeleton with the side chains of chains A and B (Fig. 11). Therefore, the computational analysis of interaction pattern of Hsp90/6 complex suggests a C-terminal inhibition mode.



Figure 11. Three dimensional models of **6** (violet sticks) with the C-terminal domain of the HSP82 yeast analogue of Hsp90 α (chain A is depicted in green and chain B in cyan).

4.2.5 Conclusions

In the present study we identified 18-hydroxyhypoestenone (**6**) and Iqnugon Q (**20**) as novel modulators of Hsp90 by SPR. Moreover, from MTT, flow cytometry and WB experiments they showed cytotoxicity, cell cycle arrest and reduction of client proteins involved in cell proliferation and cancer progression (AKT, ERK) in HeLa and MCF7. Compound **6** also proved a strong dose-

dependent ATPase activity inhibition of the chaperone. In addition, molecular docking studies showed a possible interaction between **6** and the C-terminal domain of Hsp90. This domain plays a crucial role for Hsp90/co-chaperones interactions; therefore, a possible interaction with this domain could lead to the consequent inhibition of several protein client folding.

In conclusion, 18-hydroxyhypoestenone and lanugon Q may be considered as a new chemical hit compounds of this protein, and a starting point to obtain new bioactive products against Hsp90 by medicinal chemistry approaches.

Materials and methods

4.3 Reagents and Antibodies

Fetal bovine serum (FBS) was from GIBCO (Life Technologies, Grand Island, NY, USA). Hsp90 α was purchased from Tebu Bio Italy (Magenta, Milan, Italy) and bovine serum albumin (BSA) was from Sigma-Aldrich (Saint Louis, MO, USA). The antibody anti-Hsp90 α (mouse monoclonal SPA-835) was obtained from Stress-gen Bio-reagents Corporation (Victoria, Canada). The antibodies anti-Hsp70 (mouse monoclonal sc-32239), anti-cyclin A (rabbit polyclonal sc-596-G), anti-pAkt (rabbit polyclonal sc-7935-R), anti-Akt (rabbit polyclonal), anti-Cdc2 (mouse monoclonal, sc-8395) and anti-phospho (Thr161)-Cdc2 p34 (rabbit polyclonal, sc-101654), anti-Erk1/2 (mouse monoclonal sc-1647), anti-pErk (mouse monoclonal sc-7383), anti- α -tubulin (mouse monoclonal sc-32293), anti-GAPDH (rabbit polyclonal), were obtained from Santa Cruz Biotechnology (Santa Cruz Biotechnology, Inc., Delaware, CA, USA); anti-EGFR (rabbit polyclonal) were obtained from Cell Signaling Technologies, Danvers, USA; appropriate peroxidase-conjugated secondary antibodies were from Jackson Immuno Research (Baltimore, PA, USA).

4.3.1 Surface Plasmon Resonance Analyses

SPR analyses were performed using a Biacore 3000 optical biosensor, equipped with research-grade CM5 sensor chips (GE Healthcare, Milano, Italy). Recombinant human Hsp90 α (SPP-776, Stress-gen Bio-reagents Corporation, Victoria, Canada) was dissolved at 100 μ g/mL in CH₃COONa 50 mM, pH 5.0) and immobilized on a CM5 sensor chip surface using standard amine-coupling protocols and flow rate of 5 μ L/min, to obtain an optical density of 15 kRU. All the compounds, as well as 17-AAG and radicicol used as positive controls, were

dissolved in 100% DMSO to obtain 4 mM solutions, and diluted 1:200 (v/v) in PBS (10 mM NaH₂PO₄, 150 mM NaCl, pH 7.4) to a final DMSO concentration of 0.1%. For each molecule, a five-points concentration series were set up, spanning 25 nM–50 nM–250 nM–1 μM–4 μM, and for each sample the complete binding study was carried out using triplicate aliquots. SPR experiments were performed at 25 °C, using a flow rate of 50 μL/min, with 60 s monitoring of association and 300 s monitoring of dissociation. Changes in mass, due to the binding response, were recorded as resonance units (RU). To obtain the dissociation constant (K_D), these responses were fit to a 1:1 Langmuir binding model by nonlinear regression, using the BiaEvaluation software program provided by GE Healthcare. Simple interactions were suitably fitted to a single-site bimolecular interaction model (A + B = AB), yielding a single K_D.

4.3.2 ATP hydrolysis inhibition

The assay was performed using the ATPase/GTPase Activity Assay Kit (MAK113-1KT) from Sigma-Aldrich, and following the manufacturer's instructions. ATPase hydrolysis was carried out for 3 h at 37 °C in Tris 40 mM pH 7.4, NaCl 80 mM, KCl 10 mM, MgAc₂ 8 mM, EDTA 1 mM, using Hsp90α from Tebu Bio Italy (Magenta, Milan, Italy) 2.2 mg/mL (final concentration: 1 μM in 20 μL) and different concentrations of **6** (1 μM, 5 μM and 10 μM in 20 μL, final volume). Subsequently, ATP 4 mM was supplemented to each mixing solution for 40 min at room temperature, before adding 80 μL of malachite green reagent. ADP generation was measured after 30 min of incubation by a Thermofisher UV Spectrophotometer (540 nm excitation and 620 nm emission). Absorbance intensity value measured in the absence of compound **6** was assumed as 100% of Hsp90 α activity. The background reaction rate was measured in a reaction lacking enzyme or substrate and subtracted from the experimental rates.

4.3.3 Cell Culture and Treatment

HeLa (cervical carcinoma) and Jurkat (T-cell lymphoma) cell lines were purchased from the American Type Cell Culture (ATCC) (Rockville, MD, USA). The cells were maintained in DMEM (HeLa) or RPMI 1640 (Jurkat), supplemented with 10% FBS, 100 mg/L streptomycin and penicillin 100 IU/mL at 37 °C in a humidified atmosphere of 5% CO₂. To ensure logarithmic growth, cells were subcultured every two days. Stock solutions (50 mM) of purified compounds in DMSO were stored in the dark at 4 °C. Appropriate dilutions were prepared in culture medium immediately prior to use. In all experiments, the final concentration of DMSO did not exceed 0.15% (v/v).

4.3.4 Cell Viability and Cell Cycle

Cells were seeded in 96-well plates and incubated for 48 h in the absence (vehicle only) and in the presence of different concentrations of compounds (1 – 60 μM) and etoposide as positive control. The day before treatments, cells were seeded at a cell density of 1×10^4 cells/well. The number of viable cells was quantified by MTT ([3-(4,5-dimethylthiazol-2-yl)-2,5-diphenyl tetrazolium bromide]) assay. Absorption at 550 nm for each well was assessed using a microplate reader (LabSystems, Vienna, VA, USA). In some experiments cell viability was also checked by Trypan Blue exclusion assay using a Bürker counting chamber. Half maximal inhibitory concentration (IC₅₀) values were calculated from cell viability dose–response curves and defined as the concentration resulting in 50% inhibition of cell survival as compared to controls. Cell cycle was evaluated by propidium iodide (PI) staining of permeabilized cells, according to the available protocol, and flow cytometry (BD FACSCalibur flow cytometer, Becton Dickinson, San Jose, CA, USA) (Hernandez et al 2018). Data from 5000 events per sample were collected. The percentages of the elements in

the hypodiploid region and in G₀/G₁, S and G₂/M phases of the cell cycle were calculated using the CellQuest and MODFIT software, respectively.

4.3.5 Western Blot Analyses

Cell whole lysates (HeLa) for immunoblot analysis were prepared according to the standard protocol. Protein concentration was determined by DC Protein Assay (Bio-Rad, Berkeley, CA, USA), using bovine serum albumin (BSA) as a standard. Proteins were fractionated on SDS-PAGE, transferred into nitrocellulose membranes, and immunoblotted with the appropriate primary antibody. Signals were visualized with the appropriate horseradish peroxidase-conjugated secondary antibody and enhanced chemiluminescence (Amersham Biosciences-GE Healthcare, NY, USA). Densitometry of bands was performed with ImageJ software.

4.3.6 Statistical Analysis

Data reported are the mean values \pm SD from at least three experiments, performed in duplicate, showing similar results. Differences between treatment groups were analyzed by Student's *t*-test. Differences were considered significant when $p < 0.05$.

4.3.7 Molecular Docking Studies

Input Files Preparation for Docking. Protein 3D model of the ATP-bound active state of Hsp82, a yeast Hsp90 α homologue (PDB code: 2CG9) (Lee et al., 2011) was prepared using the Schrödinger Protein Preparation Wizard workflow (Maestro version 10.2, 2015). Briefly, water molecules that were found 5 Å or more away from heteroatom groups were removed and cap termini were included. Additionally, all hydrogen atoms were added, and bond orders were assigned. The resulting PDB files were converted to the MAE format. Chemical structure of **6**

was built with Maestro's Build Panel (Maestro version 10.2, 2015) and subsequently processed with LigPrep (LigPrep version 3.4, 2015) in order to generate all the possible tautomers and protonation states at a pH of 7.4 ± 1.0 ; the resulting ligands were finally minimized employing the OPLS 2005 force field.

4.3.8 Induced Fit Docking

Binding sites for the initial Glide docking phases (Glide Standard Precision Mode) of the Induced Fit Workflow (Induced Fit Docking, 2015; Shermann et al., 2006a; Sherman et al., 2006b) were calculated on the 2CG9 structure, (Lee et al., 2011) mapping onto a grid with dimensions of 36 Å (outer box) and 20 Å (inner box), centered on residues 628-630, 640-641, 670-675 (Hsp90 residues numbering as in the PDB entry 2CG9). Side chains of residues close to the docking outputs (within 8.0 Å of ligand poses) were reoriented using Prime (Prime version 3.7, Schrödinger 2015), and ligands were redocked into their corresponding low energy protein structures (Glide Extra Precision Mode), considering inner boxes dimensions of 5.0 Å (outer boxes automatically detected), with resulting complexes ranked according to GlideScore.

Bibliography

1. Banerjee, P.; Erehman, J.; Gohlke, B.-O.; Wilhelm, T.; Preissner, R.; Dunkel, M., Super Natural II—a database of natural products. *Nucleic Acids Research* **2014**, *43* (1), 935-939.
2. Cragg, G. M.; Newman, D. J., Natural products: a continuing source of novel drug leads. *Biochim Biophys Acta* **2013**, *1830* (6), 3670-3695.
3. Harvey, A. L.; Edrada-Ebel, R.; Quinn, R. J., The re-emergence of natural products for drug discovery in the genomics era. *Nature Rev Drug Discovery* **2015**, *14* (2), 111.
4. Blowman, K.; Magalhães, M.; Lemos, M.; Cabral, C.; Pires, I., Anticancer properties of essential oils and other natural products. *Evid Based Complement Alternat Med* **2018**, 2018.
5. Howitz, K. T.; Sinclair, D. A., Xenohormesis: sensing the chemical cues of other species. *Cell* **2008**, *133* (3), 387-391.
6. Koch, M. A.; Schuffenhauer, A.; Scheck, M.; Wetzal, S.; Casaulta, M.; Odermatt, A.; Ertl, P.; Waldmann, H., Charting biologically relevant chemical space: a structural classification of natural products (SCONP). *Proc Natl Acad Sci USA* **2005**, *102* (48), 17272-17277.
7. David, B.; Wolfender, J.-L.; Dias, D. A., The pharmaceutical industry and natural products: historical status and new trends. *Phytochemistry Rev* **2015**, *14* (2), 299-315.
8. Carlson, E. E., Natural products as chemical probes. *J ACS chemical biology* **2010**, *5* (7), 639-653.
9. Katz, L.; Baltz, R. H., Natural product discovery: past, present, and future. *J Ind Microbiol Biotechnol* **2016**, *43* (2-3), 155-176.

10. Basmadjian, C.; Zhao, Q.; Bentouhami, E.; Djehal, A.; Nebigil, C. G.; Johnson, R. A.; Serova, M.; De Gramont, A.; Faivre, S.; Raymond, E., Cancer wars: natural products strike back. *Front Chem* **2014**, *2*, 20.
11. Kunnumakkara, A. B.; Bordoloi, D.; Padmavathi, G.; Monisha, J.; Roy, N. K.; Prasad, S.; Aggarwal, B. B., Curcumin, the golden nutraceutical: multitargeting for multiple chronic diseases. *CA Cancer J Clin* **2017**, *174* (11), 1325-1348.
12. Baell, J. B., Feeling nature's PAINS: natural products, natural product drugs, and pan assay interference compounds (PAINS). *J Nat Prod* **2016**, *79* (3), 616-628.
13. Christianson, D. W., Structural and chemical biology of terpenoid cyclases. *Chem Rev* **2017**, *117* (17), 11570-11648.
14. Kumari, I.; Ahmed, M.; Akhter, Y., Evolution of catalytic microenvironment governs substrate and product diversity in trichodiene synthase and other terpene fold enzymes. *Biochimie* **2018**, *144*, 9-20.
15. Tholl, D., Biosynthesis and biological functions of terpenoids in plants. In *Biotechnology of isoprenoids*, Springer: 2015; pp 63-106.
16. Coll, J.; Tandron, Y. A.; Zeng, X., New phytoecdysteroids from cultured plants of *Ajuga nipponensis* Makino. *Steroids* **2007**, *72* (3), 270-277.
17. Islam, M. T.; da Mata, A. M. O. F.; de Aguiar, R. P. S.; Paz, M. F. C. J.; de Alencar, M. V. O. B.; Ferreira, P. M. P.; de Carvalho Melo-Cavalcante, A. A., Therapeutic potential of essential oils focusing on diterpenes. *Phytother Res* **2016**, *30* (9), 1420-1444.
18. Weaver, B. A., How Taxol/paclitaxel kills cancer cells. *J Mol Biol Cell* **2014**, *25* (18), 2677-2681.
19. Vasaturo, M.; Cotugno, R.; Fiengo, L.; Vinegoni, C.; Dal Piaz, F.; De Tommasi, N., The anti-tumor diterpene oridonin is a direct inhibitor of Nucleolin in cancer cells. *Scient Rep* **2018**, *8* (1), 16735.

20. Islam, M. T., Andrographolide, an up-coming multi-edged plant-derived sword in cancers. *Asian J Ethnopharmacol Med Foods* **2016**, *2*, 1-3.
21. Lee, K.-A.; Chae, J.-I.; Shim, J.-H., Natural diterpenes from coffee, cafestol and kahweol induce apoptosis through regulation of specificity protein 1 expression in human malignant pleural mesothelioma. *J Biomed Sci* **2012**, *19* (1), 60.
22. Siegel, R. L.; Miller, K. D.; Jemal, A., Cancer statistics, 2016. *CA Cancer J Clin* **2016**, *66* (1), 7-30.
23. Islam, M. T., Diterpenes and their derivatives as potential anticancer agents. *Phytother Res* **2017**, *31* (5), 691-712.
24. Ares, J. M. B.; Durán-Peña, M. J.; Hernández-Galán, R.; Collado, I. G., Chemical genetics strategies for identification of molecular targets. *Phytochem Rev* **2013**, *12* (4), 895-914.
25. Schenone, M.; Dančík, V.; Wagner, B. K.; Clemons, P. A., Target identification and mechanism of action in chemical biology and drug discovery. *Nat Chem Biol* **2013**, *9* (4), 232.
26. Hübel, K.; Lessmann, T.; Waldmann, H., Chemical biology—identification of small molecule modulators of cellular activity by natural product inspired synthesis. *Chem Soc Rev* **2008**, *37* (7), 1361-1374.
27. Neumann, G.; Hatta, M.; Kawaoka, Y., Reverse genetics for the control of avian influenza. *Avian Dis* **2003**, *47* (s3), 882-887.
28. Jafari, R.; Almqvist, H.; Axelsson, H.; Ignatushchenko, M.; Lundbäck, T.; Nordlund, P.; Molina, D. M., The cellular thermal shift assay for evaluating drug target interactions in cells. *Nature* **2014**, *9* (9), 2100.
29. Lomenick, B.; Hao, R.; Jonai, N.; Chin, R. M.; Aghajan, M.; Warburton, S.; Wang, J.; Wu, R. P.; Gomez, F.; Loo, J. A., Target identification using drug affinity responsive target stability (DARTS). *Proc Natl Acad Sci U S A* **2009**, *106* (51), 21984-21989.

30. Patching, S. G., Surface plasmon resonance spectroscopy for characterisation of membrane protein–ligand interactions and its potential for drug discovery. *Biochim Biophys Acta* **2014**, *1838* (1), 43-55.
31. Dal Piaz, F.; Vassallo, A.; Lepore, L.; Tosco, A.; Bader, A.; De Tommasi, N., Sesterterpenes as Tubulin Tyrosine Ligase Inhibitors. First Insight of Structure– Activity Relationships and Discovery of New Lead. *J Med Chem* **2009**, *52* (12), 3814-3828.
32. Orts, J.; Gossert, A. D., Structure determination of protein-ligand complexes by NMR in solution. *Methods* **2018**, *138*, 3-25.
33. Huang, R.; Bonnichon, A.; Claridge, T. D.; Leung, I. K., Protein-ligand binding affinity determination by the waterLOGSY method: an optimised approach considering ligand rebinding. *Scient Rep* **2017**, *7*, 43727.
34. Srivastava, M.; McBride, O.; Fleming, P.; Pollard, H.; Burns, A., Genomic organization and chromosomal localization of the human nucleolin gene. *J Biol Chem* **1990**, *265* (25), 14922-14931.
35. Prestayko, A. W.; Klomp, G. R.; Schmoll, D. J.; Busch, H., Comparison of proteins of ribosomal subunits and nucleolar preribosomal particles from Novikoff hepatoma ascites cells by two-dimensional polyacrylamide gel electrophoresis. *Biochemistry* **1974**, *13* (9), 1945-1951.
36. Bugler, B.; Caizergues-Ferrer, M.; Bouche, G.; Bourbon, H.; Amalric, F., Detection and localization of a class of proteins immunologically related to a 100-KDa nucleolar protein. *The FEBS Journal* **1982**, *128* (2-3), 475-480.
37. Lapeyre, B.; Bourbon, H.; Amalric, F., Nucleolin, the major nucleolar protein of growing eukaryotic cells: an unusual protein structure revealed by the nucleotide sequence. *J Proceedings of the National Academy of Sciences* **1987**, *84* (6), 1472-1476.

38. Bourbon, H.-M.; Amalric, F., Nucleolin gene organization in rodents: highly conserved sequenced within three of the 13 introns. *Gene* **1990**, 88 (2), 187-196.
39. Rao, S.; Mamrack, M.; Olson, M., Localization of phosphorylated highly acidic regions in the NH₂-terminal half of nucleolar protein C23. *Journal of Biological Chemistry* **1982**, 257 (24), 15035-15041.
40. Leitinger, N.; Wesierska-Gadek, J., ADP-ribosylation of nucleolar proteins in HeLa tumor cells. *Journal of Cellular Biochemistry* **1993**, 52 (2), 153-158.
41. Lischwe, M. A.; Cook, R. G.; Ahn, Y. S.; Yeoman, L. C.; Busch, H., Clustering of glycine and NG, NG-dimethylarginine in nucleolar protein C23. *Biochemistry* **1985**, 24 (22), 6025-6028.
42. Erard, M.; Lakhdar-Ghazal, F.; Amalric, F., Repeat peptide motifs which contain β -turns and modulate DNA condensation in chromatin. *European journal of biochemistry* **1990**, 191 (1), 19-26.
43. Bouvet, P.; Diaz, J.-J.; Kindbeiter, K.; Madjar, J.-J.; Amalric, F., Nucleolin interacts with several ribosomal proteins through its RGG domain. *Journal of Biological Chemistry* **1998**, 273 (30), 19025-19029.
44. Caizergues-Ferrer, M.; Belenguer, P.; Lapeyre, B.; Amalric, F.; Wallace, M. O.; Olson, M. O., Phosphorylation of nucleolin by a nucleolar type NII protein kinase. *Biochemistry* **1987**, 26 (24), 7876-7883.
45. Belenguer, P.; Baldin, V.; Mathieu, C.; Prats, H.; Bensaid, M.; Bouche, G.; Amalric, F., Protein kinase NII and the regulation of rDNA transcription in mammalian cells. *Nucleic Acids Research* **1989**, 17 (16), 6625-6636.
46. Zhou, G.; Seibenhener, M. L.; Wooten, M. W., Nucleolin is a protein kinase C-zeta substrate. Connection between cell surface signaling and nucleus in PC12 cells. *Journal of Biological Chemistry* **1997**, 272 (49), 31130-31137.
47. Nagai, K., RNA—protein complexes. *Current opinion in structural biology* **1996**, 6 (1), 53-61.

48. Herrera, A. H.; Olson, M. O., Association of protein C23 with rapidly labeled nucleolar RNA. *Biochemistry* **1986**, *25* (20), 6258-6264.
49. Ghisolfi-Nieto, L.; Joseph, G.; Puvion-Dutilleul, F.; Amalric, F.; Bouvet, P., Nucleolin is a sequence-specific RNA-binding protein: characterization of targets on pre-ribosomal RNA. *Journal of molecular biology* **1996**, *260* (1), 34-53.
50. Serin, G.; Joseph, G.; Ghisolfi, L.; Bauzan, M.; Erard, M.; Amalric, F.; Bouvet, P., Two RNA-binding domains determine the RNA-binding specificity of nucleolin. *Journal of Biological Chemistry* **1997**, *272* (20), 13109-13116.
51. Bögre, L.; Jonak, C.; Mink, M.; Meskiene, I.; Traas, J.; Ha, D.; Swoboda, I.; Plank, C.; Wagner, E.; Heberle-Bors, E., Developmental and cell cycle regulation of alfalfa nucMs1, a plant homolog of the yeast Nsr1 and mammalian nucleolin. *The Plant Cell* **1996**, *8* (3), 417-428.
52. Martin, M.; Garcia-Fernandez, L. F.; de la Espina, S. M. D.; Noaillac-Depeyre, J.; Gas, N.; Medina, F. J., Identification and localization of a nucleolin homologue in onion nucleoli. *Experimental cell research* **1992**, *199* (1), 74-84.
53. Léger-Silvestre, I.; Gulli, M.-P.; Noaillac-Depeyre, J.; Faubladiet, M.; Sicard, H.; Caizergues-Ferrer, M.; Gas, N., Ultrastructural changes in the *Schizosaccharomyces pombe* nucleolus following the disruption of the *gar2+* gene, which encodes a nucleolar protein structurally related to nucleolin. *Chromosoma* **1997**, *105* (7-8), 542-552.
54. Borer, R.; Lehner, C.; Eppenberger, H.; Nigg, E., Major nucleolar proteins shuttle between nucleus and cytoplasm. *Cell* **1989**, *56* (3), 379-390.
55. Semenkovich, C. F.; Ostlund Jr, R. E.; Olson, M. O.; Yang, J. W., A protein partially expressed on the surface of HepG2 cells that binds lipoproteins specifically is nucleolin. *Biochemistry* **1990**, *29* (41), 9708-9713.

56. Scherl, A.; Couté, Y.; Déon, C.; Callé, A.; Kindbeiter, K.; Sanchez, J.-C.; Greco, A.; Hochstrasser, D.; Diaz, J.-J., Functional proteomic analysis of human nucleolus. *Molecular biology of the cell* **2002**, *13* (11), 4100-4109.
57. Gaume, X.; Tassin, A.-M.; Ugrinova, I.; Mongelard, F.; Monier, K.; Bouvet, P., Centrosomal nucleolin is required for microtubule network organization. *Cell Cycle* **2015**, *14* (6), 902-919.
58. Nisole, S.; Krust, B.; Callebaut, C.; Guichard, G.; Muller, S.; Briand, J.-P.; Hovanessian, A. G., The anti-HIV pseudopeptide HB-19 forms a complex with the cell-surface-expressed nucleolin independent of heparan sulfate proteoglycans. *Journal of Biological Chemistry* **1999**, *274* (39), 27875-27884.
59. Ugrinova, I.; Monier, K.; Ivaldi, C.; Thiry, M.; Storck, S.; Mongelard, F.; Bouvet, P., Inactivation of nucleolin leads to nucleolar disruption, cell cycle arrest and defects in centrosome duplication. *BMC molecular biology* **2007**, *8* (1), 66.
60. Gaume, X.; Monier, K.; Argoul, F.; Mongelard, F.; Bouvet, P., In vivo study of the histone chaperone activity of nucleolin by FRAP. *Biochemistry research international* **2011**, *2011*.
61. Escande, M.; Gas, N.; Stevens, B., Immunolocalization of the 100 K nucleolar protein in CHO cells. *Biology of the Cell* **1985**, *53* (2), 99-109.
62. Creancier, L.; Prats, H.; Zanibellato, C.; Amalric, F.; Bugler, B., Determination of the functional domains involved in nucleolar targeting of nucleolin. *Molecular biology of the cell* **1993**, *4* (12), 1239-1250.
63. Schwab, M.; Dreyer, C., Protein phosphorylation sites regulate the function of the bipartite NLS of nucleolin. *European journal of cell biology* **1997**, *73* (4), 287-297.
64. Deng, J.-S.; Ballou, B.; Hofmeister, J. K., Internalization of anti-nucleolin antibody into viable HEp-2 cells. *Molecular biology reports* **1996**, *23* (3-4), 191-195.

65. Ding, Y.; Song, N.; Liu, C.; He, T.; Zhuo, W.; He, X.; Chen, Y.; Song, X.; Fu, Y.; Luo, Y., Heat shock cognate 70 regulates the translocation and angiogenic function of nucleolin. *Arteriosclerosis, thrombosis, vascular biology* **2012**, *32* (9), e126-e134.
66. Cong, R.; Das, S.; Ugrinova, I.; Kumar, S.; Mongelard, F.; Wong, J.; Bouvet, P., Interaction of nucleolin with ribosomal RNA genes and its role in RNA polymerase I transcription. *Nucleic acids research* **2012**, *40* (19), 9441-9454.
67. Angelov, D.; Bondarenko, V. A.; Almagro, S.; Menoni, H.; Mongelard, F.; Hans, F.; Mietton, F.; Studitsky, V. M.; Hamiche, A.; Dimitrov, S., Nucleolin is a histone chaperone with FACT-like activity and assists remodeling of nucleosomes. *The EMBO journal* **2006**, *25* (8), 1669-1679.
68. Abdelmohsen, K.; Gorospe, M., RNA-binding protein nucleolin in disease. *RNA biology* **2012**, *9* (6), 799-808.
69. Lee, J. H.; Lee, Y. S.; Jeong, S. A.; Khadka, P.; Roth, J.; Chung, I. K., Catalytically active telomerase holoenzyme is assembled in the dense fibrillar component of the nucleolus during S phase. *Histochemistry cell biology* **2014**, *141* (2), 137-152.
70. Daniely, Y.; Dimitrova, D. D.; Borowiec, J. A., Stress-dependent nucleolin mobilization mediated by p53-nucleolin complex formation. *Molecular cellular biology* **2002**, *22* (16), 6014-6022.
71. Abdelmohsen, K.; Tominaga, K.; Lee, E. K.; Srikantan, S.; Kang, M.-J.; Kim, M. M.; Selimyan, R.; Martindale, J. L.; Yang, X.; Carrier, F., Enhanced translation by Nucleolin via G-rich elements in coding and non-coding regions of target mRNAs. *Nucleic acids research* **2011**, *39* (19), 8513-8530.

72. Takagi, M.; Absalon, M. J.; McLure, K. G.; Kastan, M. B., Regulation of p53 translation and induction after DNA damage by ribosomal protein L26 and nucleolin. *Cell* **2005**, *123* (1), 49-63.
73. Soundararajan, S.; Wang, L.; Sridharan, V.; Chen, W.; Courtenay-Luck, N.; Jones, D.; Spicer, E. K.; Fernandes, D. J., Plasma membrane nucleolin is a receptor for the anticancer aptamer AS1411 in MV4-11 leukemia cells. *Molecular pharmacology* **2009**, *76* (5), 984-991.
74. Bhatia, S.; Reister, S.; Mahotka, C.; Meisel, R.; Borkhardt, A.; Grinstein, E., Control of AC133/CD133 and impact on human hematopoietic progenitor cells through nucleolin. *Leukemia* **2015**, *29* (11), 2208.
75. Fujiki, H.; Watanabe, T.; Suganuma, M., Cell-surface nucleolin acts as a central mediator for carcinogenic, anti-carcinogenic, and disease-related ligands. *Journal of cancer research clinical oncology* **2014**, *140* (5), 689-699.
76. Kireeva, M. L.; Walter, W.; Tchernajenko, V.; Bondarenko, V.; Kashlev, M.; Studitsky, V. M., Nucleosome remodeling induced by RNA polymerase II: loss of the H2A/H2B dimer during transcription. *Molecular cellular biology* **2002**, *9* (3), 541-552.
77. Ginisty, H.; Amalric, F.; Bouvet, P., Nucleolin functions in the first step of ribosomal RNA processing. *The EMBO journal* **1998**, *17* (5), 1476-1486.
78. Belotserkovskaya, R.; Oh, S.; Bondarenko, V. A.; Orphanides, G.; Studitsky, V. M.; Reinberg, D., FACT facilitates transcription-dependent nucleosome alteration. *Science* **2003**, *301* (5636), 1090-1093.
79. Escande-Geraud, M.; Azum, M.; Tichadou, J.; Gas, N., Correlation between rDNA transcription and distribution of a 100 kD nucleolar protein in CHO cells. *Experimental cell research* **1985**, *161* (2), 353-363.

80. Bouche, G.; Caizergues-Ferrer, M.; Bugler, B.; Amalric, F., Interrelations between the maturation of a 100 kDa nucleolar protein and pre rRNA synthesis in CHO cells. *Nucleic acids research* **1984**, *12* (7), 3025-3035.
81. Sipos, K.; Olson, M. O., Nucleolin promotes secondary structure in ribosomal RNA. *Biochemical biophysical research communications* **1991**, *177* (2), 673-678.
82. Bourbon, H.; Bugler, B.; Caizergues-Ferrer, M.; Amalric, F.; Zalta, J., Maturation of a 100 kDa protein associated with preribosomes in Chinese hamster ovary cells. *Molecular biology reports* **1983**, *9* (1-2), 39-47.
83. Schmidt-Zachmann, M.; Nigg, E., Protein localization to the nucleolus: a search for targeting domains in nucleolin. *Journal of Cell Science* **1993**, *105* (3), 799-806.
84. Hovanessian, A. G.; Puvion-Dutilleul, F.; Nisole, S.; Svab, J.; Perret, E.; Deng, J.-S.; Krust, B., The cell-surface-expressed nucleolin is associated with the actin cytoskeleton. *Experimental cell research* **2000**, *261* (2), 312-328.
85. Galzio, R.; Rosati, F.; Benedetti, E.; Cristiano, L.; Aldi, S.; Mei, S.; D'Angelo, B.; Gentile, R.; Laurenti, G.; Cifone, M., Glycosilated nucleolin as marker for human gliomas. *Journal of cellular biochemistry* **2012**, *113* (2), 571-579.
86. Christian, S.; Pilch, J.; Akerman, M. E.; Porkka, K.; Laakkonen, P.; Ruoslahti, E., Nucleolin expressed at the cell surface is a marker of endothelial cells in angiogenic blood vessels. *The Journal of cell biology* **2003**, *163* (4), 871-878.
87. Hammoudi, A.; Song, F.; Reed, K. R.; Jenkins, R. E.; Meniel, V. S.; Watson, A. J.; Pritchard, D. M.; Clarke, A. R.; Jenkins, J. R., Proteomic profiling of a mouse model of acute intestinal Apc deletion leads to identification of

potential novel biomarkers of human colorectal cancer (CRC). *Biochemical biophysical research communications* **2013**, *440* (3), 364-370.

88. Qiu, W.; Zhou, F.; Zhang, Q.; Sun, X.; Shi, X.; Liang, Y.; Wang, X.; Yue, L., Overexpression of nucleolin and different expression sites both related to the prognosis of gastric cancer. *Apmis* **2013**, *121* (10), 919-925.

89. Pichiorri, F.; Palmieri, D.; De Luca, L.; Consiglio, J.; You, J.; Rocci, A.; Talabere, T.; Piovan, C.; Lagana, A.; Cascione, L., In vivo NCL targeting affects breast cancer aggressiveness through miRNA regulation. *Journal of Experimental Medicine* **2013**, *210* (5), 951-968.

90. Shen, N.; Yan, F.; Pang, J.; Wu, L.-C.; Al-Kali, A.; Litzow, M. R.; Liu, S., A nucleolin-DNMT1 regulatory axis in acute myeloid leukemogenesis. *Oncotarget* **2014**, *5* (14), 5494.

91. Zhao, H.; Huang, Y.; Xue, C.; Chen, Y.; Hou, X.; Guo, Y.; Zhao, L.; huang Hu, Z.; Huang, Y.; Luo, Y., Prognostic significance of the combined score of endothelial expression of nucleolin and CD31 in surgically resected non-small cell lung cancer. *PloS one* **2013**, *8* (1), e54674.

92. El Khoury, D.; Destouches, D.; Lengagne, R.; Krust, B.; Hamma-Kourbali, Y.; Garcette, M.; Niro, S.; Kato, M.; Briand, J.-P.; Courty, J., Targeting surface nucleolin with a multivalent pseudopeptide delays development of spontaneous melanoma in RET transgenic mice. *BMC cancer* **2010**, *10* (1), 325.

93. Grinstein, E.; Wernet, P.; Snijders, P. J.; Rösl, F.; Weinert, I.; Jia, W.; Kraft, R.; Schewe, C.; Schwabe, M.; Hauptmann, S., Nucleolin as activator of human papillomavirus type 18 oncogene transcription in cervical cancer. *Journal of Experimental Medicine* **2002**, *196* (8), 1067-1078.

94. Wise, J. F.; Berkova, Z.; Mathur, R.; Zhu, H.; Braun, F. K.; Tao, R.-H.; Sabichi, A. L.; Ao, X.; Maeng, H.; Samaniego, F., Nucleolin inhibits Fas ligand

binding and suppresses Fas-mediated apoptosis in vivo via a surface nucleolin-Fas complex. *Blood* **2013**, *121* (23), 4729-4739.

95. Di Segni, A.; Farin, K.; Pinkas-Kramarski, R., Identification of nucleolin as new ErbB receptors-interacting protein. *PLoS one* **2008**, *3* (6), e2310.

96. Farin, K.; Schokoroy, S.; Haklai, R.; Cohen-Or, I.; Elad-Sfadia, G.; Reyes-Reyes, M. E.; Bates, P. J.; Cox, A. D.; Kloog, Y.; Pinkas-Kramarski, R., Oncogenic synergism between ErbB1, nucleolin, and mutant Ras. *Cancer research* **2011**, *71* (6), 2140-2151.

97. Said, E. A.; Courty, J.; Svab, J.; Delbé, J.; Krust, B.; Hovanessian, A. G., Pleiotrophin inhibits HIV infection by binding the cell surface-expressed nucleolin. *The FEBS journal* **2005**, *272* (18), 4646-4659.

98. Shibata, Y.; Muramatsu, T.; Hirai, M.; Inui, T.; Kimura, T.; Saito, H.; McCormick, L. M.; Bu, G.; Kadomatsu, K., Nuclear targeting by the growth factor midkine. *Molecular cellular biology* **2002**, *22* (19), 6788-6796.

99. Tate, A.; Isotani, S.; Bradley, M. J.; Sikes, R. A.; Davis, R.; Chung, L. W.; Edlund, M., Met-Independent Hepatocyte Growth Factor-mediated regulation of cell adhesion in human prostate cancer cells. *BMC cancer* **2006**, *6* (1), 197.

100. Huang, Y.; Shi, H.; Zhou, H.; Song, X.; Yuan, S.; Luo, Y., The angiogenic function of nucleolin is mediated by vascular endothelial growth factor and nonmuscle myosin. *Blood* **2006**, *107* (9), 3564-3571.

101. Watanabe, T.; Tsuge, H.; Imagawa, T.; Kise, D.; Hirano, K.; Beppu, M.; Takahashi, A.; Yamaguchi, K.; Fujiki, H.; Suganuma, M., Nucleolin as cell surface receptor for tumor necrosis factor- α inducing protein: a carcinogenic factor of *Helicobacter pylori*. *Journal of cancer research clinical oncology* **2010**, *136* (6), 911-921.

102. Mongelard, F.; Bouvet, P., AS-1411, a guanosine-rich oligonucleotide aptamer targeting nucleolin for the potential treatment of cancer, including acute

myeloid leukemia. *Current opinion in molecular therapeutics* **2010**, *12* (1), 107-114.

103. Teng, Y.; Girvan, A. C.; Casson, L. K.; Pierce, W. M.; Qian, M.; Thomas, S. D.; Bates, P. J., AS1411 alters the localization of a complex containing protein arginine methyltransferase 5 and nucleolin. *Cancer research* **2007**, *67* (21), 10491-10500.

104. Pichiorri, F.; Palmieri, D.; De Luca, L.; Consiglio, J.; You, J.; Rocci, A.; Talabere, T.; Piovan, C.; Lagana, A.; Cascione, L., In vivo NCL targeting affects breast cancer aggressiveness through miRNA regulation. *Journal of Experimental Medicine* **2013**, *210* (5), 951-968.

105. Drygin, D.; Siddiqui-Jain, A.; O'Brien, S.; Schwaebe, M.; Lin, A.; Bliesath, J.; Ho, C. B.; Proffitt, C.; Trent, K.; Whitten, J. P., Anticancer activity of CX-3543: a direct inhibitor of rRNA biogenesis. *Cancer research* **2009**, *69* (19), 7653-7661.

106. Hovanessian, A. G.; Soundaramourty, C.; El Khoury, D.; Nondier, I.; Svab, J.; Krust, B., Surface expressed nucleolin is constantly induced in tumor cells to mediate calcium-dependent ligand internalization. *PloS one* **2010**, *5* (12), e15787.

107. Zhao, Z.; Chen, Y., Oridonin, a promising antitumor natural product in the chemotherapy of hematological malignancies. *Current pharmaceutical biotechnology* **2014**, *15* (11), 1083-1092.

108. Wang, K.; Deng, G.; Chen, G.; Liu, M.; Yi, Y.; Yang, T.; McMillan, D. R.; Xiao, X., Heat shock protein 70 inhibits hydrogen peroxide-induced nucleolar fragmentation via suppressing cleavage and down-regulation of nucleolin. *Cell Stress Chaperones* **2012**, *17* (1), 121-130.

109. Nicoletti, I.; Migliorati, G.; Pagliacci, M.; Grignani, F.; Riccardi, C., A rapid and simple method for measuring thymocyte apoptosis by propidium iodide

staining and flow cytometry. *Journal of immunological methods* **1991**, *139* (2), 271-279.

110. Choi, S. D., Ezrin is an essential marker for metastasis of gynecologic cancer. *The Journal of Korean Society of Menopause* **2012**, *18* (2), 81-93.

111. Chen, Z.; Xu, X., Roles of nucleolin: Focus on cancer and anti-cancer therapy. *Saudi medical journal* **2016**, *37* (12), 1312.

112. Serin, G.; Joseph, G.; Ghisolfi, L.; Bauzan, M.; Erard, M.; Amalric, F.; Bouvet, P., Two RNA-binding domains determine the RNA-binding specificity of nucleolin. *Journal of Biological Chemistry* **1997**, *272* (20), 13109-13116.

113. Allain, F. H.-T.; Gilbert, D. E.; Bouvet, P.; Feigon, J., Solution structure of the two N-terminal RNA-binding domains of nucleolin and NMR study of the interaction with its RNA target. *Journal of molecular biology* **2000**, *303* (2), 227-241.

114. Canales, A.; Nieto, L.; Rodríguez-Salarichs, J.; Sánchez-Murcia, P. A.; Coderch, C.; Cortés-Cabrera, A.; Paterson, I.; Carlomagno, T.; Gago, F.; Andreu, J. M., Molecular recognition of epothilones by microtubules and tubulin dimers revealed by biochemical and NMR approaches. *ACS chemical biology* **2014**, *9* (4), 1033-1043.

115. Young, J. C.; Agashe, V. R.; Siegers, K.; Hartl, F. U., Pathways of chaperone-mediated protein folding in the cytosol. *Nature reviews Molecular cell biology* **2004**, *5* (10), 781.

116. Khalil, A. A.; Kabapy, N. F.; Deraz, S. F.; Smith, C., Heat shock proteins in oncology: diagnostic biomarkers or therapeutic targets? *Biochimica et Biophysica Acta -Reviews on Cancer* **2011**, *1816* (2), 89-104.

117. Jego, G.; Hazoumé, A.; Seigneuric, R.; Garrido, C., Targeting heat shock proteins in cancer. *Cancer letters* **2013**, *332* (2), 275-285.

118. Xia, Y.; Rocchi, P.; Iovanna, J. L.; Peng, L., Targeting heat shock response pathways to treat pancreatic cancer. *Drug discovery today* **2012**, *17* (1-2), 35-43.
119. Joly, A.-L.; Wettstein, G.; Mignot, G.; Ghiringhelli, F.; Garrido, C., Dual role of heat shock proteins as regulators of apoptosis and innate immunity. *Journal of innate immunity* **2010**, *2* (3), 238-247.
120. Mayer, M.; Bukau, B., Hsp70 chaperones: cellular functions and molecular mechanism. *Cellular molecular life sciences* **2005**, *62* (6), 670.
121. Mayer, M. P., Hsp70 chaperone dynamics and molecular mechanism. *Trends in biochemical sciences* **2013**, *38* (10), 507-514.
122. Cuéllar, J.; Perales-Calvo, J.; Muga, A.; Valpuesta, J. M.; Moro, F., Structural Insights into the Chaperone Activity of the 40-kDa Heat Shock Protein DnaJ binding and remodeling of a native substrate *Journal of Biological Chemistry* **2013**, *288* (21), 15065-15074.
123. Shevtsov, M.; Huile, G.; Multhoff, G., Membrane heat shock protein 70: a theranostic target for cancer therapy. *Philosophical Transactions of the Royal Society; Biological Sciences* **2017**, *373* (1738), 20160526.
124. Flaherty, K. M.; Wilbanks, S. M.; DeLuca-Flaherty, C.; McKay, D. B., Structural basis of the 70-kilodalton heat shock cognate protein ATP hydrolytic activity. II. Structure of the active site with ADP or ATP bound to wild type and mutant ATPase fragment. *Journal of Biological Chemistry* **1994**, *269* (17), 12899-12907.
125. Rüdiger, S.; Germeroth, L.; Schneider-Mergener, J.; Bukau, B., Substrate specificity of the DnaK chaperone determined by screening cellulose-bound peptide libraries. *The EMBO journal* **1997**, *16* (7), 1501-1507.
126. Kumar, D. P.; Vorvis, C.; Sarbeng, E. B.; Ledesma, V. C. C.; Willis, J. E.; Liu, Q., The four hydrophobic residues on the Hsp70 inter-domain linker have two distinct roles. *Journal of molecular biology* **2011**, *411* (5), 1099-1113.

127. Bukau, B.; Horwich, A. L., The Hsp70 and Hsp60 chaperone machines. *Cell* **1998**, *92* (3), 351-366.
128. Kampinga, H. H.; Craig, E. A., The HSP70 chaperone machinery: J proteins as drivers of functional specificity. *Nature reviews Molecular cell biology* **2010**, *11* (8), 579.
129. Harrison, C., GrpE, a nucleotide exchange factor for DnaK. *Cell stress chaperones* **2003**, *8* (3), 218.
130. Gamerding, M.; Hajieva, P.; Kaya, A. M.; Wolfrum, U.; Hartl, F. U.; Behl, C., Protein quality control during aging involves recruitment of the macroautophagy pathway by BAG3. *The EMBO journal* **2009**, *28* (7), 889-901.
131. Alvira, S.; Cuéllar, J.; Röhl, A.; Yamamoto, S.; Itoh, H.; Alfonso, C.; Rivas, G.; Buchner, J.; Valpuesta, J. M., Structural characterization of the substrate transfer mechanism in Hsp70/Hsp90 folding machinery mediated by Hop. *Nature communications* **2014**, *5*, 5484.
132. Schmitt, E.; Parcellier, A.; Gurbuxani, S.; Cande, C.; Hammann, A.; Morales, M. C.; Hunt, C. R.; Dix, D. J.; Kroemer, R. T.; Giordanetto, F., Chemosensitization by a non-apoptogenic heat shock protein 70-binding apoptosis-inducing factor mutant. *Cancer research* **2003**, *63* (23), 8233-8240.
133. Chatterjee, S.; Burns, T., Targeting heat shock proteins in cancer: a promising therapeutic approach. *International journal of molecular sciences* **2017**, *18* (9), 1978.
134. Proctor, C. J.; Lorimer, I. A., Modelling the role of the Hsp70/Hsp90 system in the maintenance of protein homeostasis. *PloS one* **2011**, *6* (7), e22038.
135. Lee, J.-S.; Lee, J.-J.; Seo, J.-S., HSP70 deficiency results in activation of c-Jun N-terminal Kinase, extracellular signal-regulated kinase, and caspase-3 in hyperosmolarity-induced apoptosis. *Journal of Biological Chemistry* **2005**, *280* (8), 6634-6641.

136. Gao, T.; Newton, A. C., The turn motif is a phosphorylation switch that regulates the binding of Hsp70 to protein kinase C. *Journal of Biological Chemistry* **2002**, 277 (35), 31585-31592.
137. Sherman, M. Y.; Gabai, V. L., Hsp70 in cancer: back to the future. *Oncogene* **2015**, 34 (32), 4153.
138. Leu, J.-J.; Pimkina, J.; Frank, A.; Murphy, M. E.; George, D. L., A small molecule inhibitor of inducible heat shock protein 70. *Molecular cellular biology* **2009**, 36 (1), 15-27.
139. Nadeau, K.; Nadler, S. G.; Saulnier, M.; Walsh, C. T.; Tepper, M. A., Quantitation of the interaction of the immunosuppressant deoxyspergualin and analogs with Hsc70 and Hsp90. *Biochemistry* **1994**, 33 (9), 2561-2567.
140. Jinwal, U. K.; Miyata, Y.; Koren, J.; Jones, J. R.; Trotter, J. H.; Chang, L.; O'Leary, J.; Morgan, D.; Lee, D. C.; Shults, C. L., Chemical manipulation of hsp70 ATPase activity regulates tau stability. *Journal of Neuroscience* **2009**, 29 (39), 12079-12088.
141. Powers, M. V.; Jones, K.; Barillari, C.; Westwood, I.; Montfort, R. L. v.; Workman, P., Targeting HSP70: the second potentially druggable heat shock protein and molecular chaperone? *Cell Cycle* **2010**, 9 (8), 1542-1550.
142. Chatterjee, M.; Andrulis, M.; Stühmer, T.; Müller, E.; Hofmann, C.; Steinbrunn, T.; Heimberger, T.; Schraud, H.; Kressmann, S.; Einsele, H., The PI3K/Akt signaling pathway regulates the expression of Hsp70, which critically contributes to Hsp90-chaperone function and tumor cell survival in multiple myeloma. *Haematologica* **2013**, 98 (7), 1132-1141.
143. Multhoff, G.; Radons, J., Radiation, inflammation, and immune responses in cancer. *Frontiers in oncology* **2012**, 2, 58.
144. Zhang, T., Recent studies on the antitumor activity of rabdosia rubescences. *Chin J Oncol* **1982**, 4, 322-3.

145. Dal Piaz, F.; Cotugno, R.; Lepore, L.; Vassallo, A.; Malafronte, N.; Lauro, G.; Bifulco, G.; Belisario, M. A.; De Tommasi, N., Chemical proteomics reveals HSP70 1A as a target for the anticancer diterpene oridonin in Jurkat cells. *Journal of proteomics* **2013**, *82*, 14-26.
146. Venturella, P.; Bellino, A.; Piozzi, F., Diterpenes from *Sideritis theezans*. *Phytochemistry Rev* **1975**.
147. González-Burgos, E.; Carretero, M.; Gómez-Serranillos, M., *Sideritis* spp.: uses, chemical composition and pharmacological activities—a review. *Journal of ethnopharmacology* **2011**, *135* (2), 209-225.
148. Erkan, N.; Cetin, H.; Ayranci, E., Antioxidant activities of *Sideritis congesta* Davis et Huber-Morath and *Sideritis arguta* Boiss et Heldr: Identification of free flavonoids and cinnamic acid derivatives. *Food Research International* **2011**, *44* (1), 297-303.
149. Fraga, B. M., Phytochemistry and chemotaxonomy of *Sideritis* species from the Mediterranean region. *Phytochemistry Rev* **2012**, *76*, 7-24.
150. Jones, A. M.; Westwood, I. M.; Osborne, J. D.; Matthews, T. P.; Cheeseman, M. D.; Rowlands, M. G.; Jeganathan, F.; Burke, R.; Lee, D.; Kadi, N., A fragment-based approach applied to a highly flexible target: Insights and challenges towards the inhibition of HSP70 isoforms. *Scientific reports* **2016**, *6*, 34701.
151. Chen, B.; Zhong, D.; Monteiro, A., Comparative genomics and evolution of the HSP90 family of genes across all kingdoms of organisms. *BMC genomics* **2006**, *7* (1), 156.
152. Chen, B.; Piel, W. H.; Gui, L.; Bruford, E.; Monteiro, A., The HSP90 family of genes in the human genome: insights into their divergence and evolution. *Genomics* **2005**, *86* (6), 627-637.

153. Maharaj, K. A.; Que, N. L.; Hong, F.; Huck, J. D.; Gill, S. K.; Wu, S.; Li, Z.; Gewirth, D. T., Exploring the functional complementation between Grp94 and Hsp90. *PloS one* **2016**, *11* (11), e0166271.
154. Mayer, M. P., Gymnastics of molecular chaperones. *Molecular cellular biology* **2010**, *39* (3), 321-331.
155. Wandinger, S. K.; Richter, K.; Buchner, J., The Hsp90 chaperone machinery. *Journal of Biological Chemistry* **2008**, *283* (27), 18473-18477.
156. Söti, C.; Rácz, A.; Csermely, P., A nucleotide-dependent molecular switch controls ATP binding at the C-Terminal domain of Hsp90 N-terminal nucleotide binding unmask a C-Terminal binding pocket. *Journal of Biological Chemistry* **2002**, *277* (9), 7066-7075.
157. Dahiya, V.; Buchner, J., Functional principles and regulation of molecular chaperones. *Advances in protein chemistry structural biology* **2019**, *114*, 1-60.
158. Jackson, S. E., Hsp90: structure and function. In *Molecular chaperones*, Springer: 2012; pp 155-240.
159. Prodromou, C.; Pearl, L. H., Structure and functional relationships of Hsp90. *Current cancer drug targets* **2003**, *3* (5), 301-323.
160. Pearl, L. H., The HSP90 molecular chaperone—an enigmatic ATPase. *Biopolymers* **2016**, *105* (8), 594-607.
161. Haque, A.; Alam, Q.; Zubair Alam, M.; I Azhar, E.; Hussain Wali Sait, K.; Anfinan, N.; Mushtaq, G.; Amjad Kamal, M.; Rasool, M., Current understanding of HSP90 as a novel therapeutic target: An emerging approach for the treatment of cancer. *Current pharmaceutical design* **2016**, *22* (20), 2947-2959.
162. Karagöz, G. E.; Rüdiger, S. G., Hsp90 interaction with clients. *Trends in biochemical sciences* **2015**, *40* (2), 117-125.
163. Kadota, Y.; Shirasu, K.; Guerois, R., NLR sensors meet at the SGT1–HSP90 crossroad. *Trends in biochemical sciences* **2010**, *35* (4), 199-207.

164. Taipale, M.; Tucker, G.; Peng, J.; Krykbaeva, I.; Lin, Z.-Y.; Larsen, B.; Choi, H.; Berger, B.; Gingras, A.-C.; Lindquist, S., A quantitative chaperone interaction network reveals the architecture of cellular protein homeostasis pathways. *Cell* **2014**, *158* (2), 434-448.
165. Vaughan, C. K.; Gohlke, U.; Sobott, F.; Good, V. M.; Ali, M. M.; Prodromou, C.; Robinson, C. V.; Saibil, H. R.; Pearl, L. H., Structure of an hsp90-cdc37-cdk4 complex. *Molecular cellular biology* **2006**, *23* (5), 697-707.
166. Morgan, R. M.; Hernández-Ramírez, L. C.; Trivellin, G.; Zhou, L.; Roe, S. M.; Korbonits, M.; Prodromou, C., Structure of the TPR domain of AIP: lack of client protein interaction with the C-terminal α -7 helix of the TPR domain of AIP is sufficient for pituitary adenoma predisposition. *PloS one* **2012**, *7* (12), e53339.
167. Kakihara, Y.; Houry, W. A., The R2TP complex: discovery and functions. *Biochimica et Biophysica Acta -Molecular Cell Research* **2012**, *1823* (1), 101-107.
168. Neckers, L.; Workman, P., Hsp90 molecular chaperone inhibitors: are we there yet? *Clinical cancer research* **2012**, *18* (1), 64-76.
169. Hanahan, D.; Weinberg, R. A., Hallmarks of cancer: the next generation. *Cell* **2011**, *144* (5), 646-674.
170. Banerji, U.; O'Donnell, A.; Scurr, M.; Pacey, S.; Stapleton, S.; Asad, Y.; Simmons, L.; Maloney, A.; Raynaud, F.; Campbell, M., Phase I pharmacokinetic and pharmacodynamic study of 17-allylamino, 17-demethoxygeldanamycin in patients with advanced malignancies. *Journal of Clinical Oncology* **2005**, *23* (18), 4152-4161.
171. Tatokoro, M.; Koga, F.; Yoshida, S.; Kihara, K., Heat shock protein 90 targeting therapy: state of the art and future perspective. *EXCLI journal* **2015**, *14*, 48.

172. Dal Piaz, F.; Terracciano, S.; De Tommasi, N.; Braca, A., Hsp90 activity modulation by plant secondary metabolites. *Planta Medica* **2015**, *81* (14), 1223-1239.
173. Dal Piaz, F.; Vassallo, A.; Chini, M. G.; Cordero, F. M.; Cardona, F.; Pisano, C.; Bifulco, G.; De Tommasi, N.; Brandi, A., Natural iminosugar (+)-lentiginosine inhibits ATPase and chaperone activity of hsp90. *PLoS One* **2012**, *7* (8), e43316.
174. Oliver, M. H.; Harrison, N. K.; Bishop, J. E.; Cole, P. J.; Laurent, G. J., A rapid and convenient assay for counting cells cultured in microwell plates: application for assessment of growth factors. *Journal of cell science* **1989**, *92* (3), 513-518.
175. Suzuki, R.; Hideshima, T.; Mimura, N.; Minami, J.; Ohguchi, H.; Kikuchi, S.; Yoshida, Y.; Gorgun, G.; Cirstea, D.; Cottini, F., Anti-tumor activities of selective HSP90 α/β inhibitor, TAS-116, in combination with bortezomib in multiple myeloma. *Leukemia* **2015**, *29* (2), 510.
176. Karkoulis, P. K.; Stravopodis, D. J.; Konstantakou, E. G.; Voutsinas, G. E., Targeted inhibition of heat shock protein 90 disrupts multiple oncogenic signaling pathways, thus inducing cell cycle arrest and programmed cell death in human urinary bladder cancer cell lines. *Cancer cell international* **2013**, *13* (1), 11.
177. Lee, C.-C.; Lin, T.-W.; Ko, T.-P.; Wang, A. H.-J., The hexameric structures of human heat shock protein 90. *PloS one* **2011**, *6* (5), e19961.
178. Chini, M. G.; Malafrente, N.; Vaccaro, M. C.; Gualtieri, M. J.; Vassallo, A.; Vasaturo, M.; Castellano, S.; Milite, C.; Leone, A.; Bifulco, G., Identification of limonol derivatives as heat shock protein 90 (Hsp90) inhibitors through a multidisciplinary approach. *Chemistry—A European Journal* **2016**, *22* (37), 13236-13250.

179. Terracciano, S.; Russo, A.; Chini, M. G.; Vaccaro, M. C.; Potenza, M.; Vassallo, A.; Riccio, R.; Bifulco, G.; Bruno, I., Discovery of new molecular entities able to strongly interfere with Hsp90 C-terminal domain. *Scientific reports* **2018**, 8 (1), 1709.

Publications

- D'Ambola, M.[#], Fiengo, L.[#], Chini, M.G., Cotugno, R., Bader, A., Bifulco, G., Braca, A., De Tommasi, N. and Dal Piaz, F. Fusicoccane diterpenes from *Hypoestes forsskaolii* as Heat Shock Protein 90 (Hsp90) modulators. *Journal of Natural Products* **2019**, 82, 539-549.
- Vasaturo, M., Cotugno, R., Fiengo, L., Vinegoni, C., Dal Piaz, F., De Tommasi, N., the anti-tumor diterpene oridonin is a direct inhibitor of Nucleolin in cancer cells. *Scientific Reports* **2018**, 8, 16735.
- Virelli, M., Moroni, E., Colombo, G., Fiengo, L., Porta, A., Ackermann, L., Zanoni, G., expedient access to 2-Benzazepines by palladium-catalyzed C–H activation: identification of a unique Hsp90 inhibitor scaffold. *Chemistry – a European Journal* **2018**, 24(62), 16516-16520.
- Vasaturo, M., Fiengo, L., De Tommasi, N., Sabatino, L., Ziccardi, P., Colantuoni, V., Bruno, M., Cerchia, C., Novellino, E., Lupo, A., Lavecchia, A., Dal Piaz, F., a compound-based proteomic approach discloses 15-ketoatractyligenin methyl ester as a new PPAR γ partial agonist with anti-proliferative ability. *Scientific Reports* **2017**, 7, 41273.

Poster and oral presentations at international meetings

- 30th International Congress of Chemistry of Natural products (IUPAC), Athens, Greece. Fiengo L, Vassallo A, Cotugno R, De Tommasi N, Dal Piaz F, Bader A, chemical-biological study of *ent*-kaurane and *ent*-trachylobane diterpenes from *Psiadia punctulata* (Vatke). (24-30 November 2018)
- GA Young Researcher Workshop, Shanghai, China. D'Ambola M, Bader A, Fiengo L, Dal Piaz F, Vassallo A, Cotugno R, De Tommasi N, fusicoccane diterpenes from *Hypoestes forskalii* (Vahl) R.P.r. natural products research. (26-29 August 2018)
- 113th Congress of the Italian Botanical Society (SBI), Fisciano, Italy. Fiengo L, D'Ambola M, De Tommasi N, Dal Piaz F, Omran Z, Halawani M, Bader A, phytochemical study of *Calotropis Procera* (Ait.) R.Br. leaves, fruits, stems and latex extracts and evaluation of their cytotoxic activity. (12-15 September 2018)
- 2nd Sino-Italian symposium on Bioactive Natural Products, Naples, Italy. Fiengo L, Vassallo A, Cotugno R, Vasaturo M, De Tommasi N, Dal Piaz F, study of the interaction between Nucleolin and 6,19-dihydroxy-*ent*-trachiloban-17-oic acid. (24-25 November 2016)